An Empirical Study of Compliant Assembly In Three Dimensions

by

José A. Rivero

Submitted to the Department of
Mechanical Engineering in
Partial Fulfillment of the
Requirements for the Degrees of

Bachelor Of Science
In Mechanical Engineering
And
Master Of Science

at the

Massachusetts Institute Of Technology
June 1987

Signature of Author_____

Department of Mechanical Engineering
May 8, 1987

Certified by_____

Professor Warren P. Seering
Associate Professor of Mechanical Engineering
Thesis Supervisor

Accepted by_____

Ain A. Sonin
Chairman, Departmental Graduate Committee

An Empirical Study of Compliant Assembly in Three Dimensions

by

José A. Rivero

Submitted to the Department of Mechanical Engineering on June 3, 1987 in partial fulfillment of the requirements for the degrees of Bachelor of Science in Mechanical Engineering and Master of Science.

Abstract

Automated assembly processes require parts to be assembled in three dimensions in the presence of errors. These errors arise from uncertainties in the location of the parts being assembled and from performance limitations of the machine conducting the assembly.

This thesis presents an empirical study of compliant assembly in three dimensions. Experiments were conducted using a five degree-of-freedom compliant parts mating machine (PMM). This apparatus can mate two parts together, regardless of shape, and measure insertion forces, lateral forces, and moments during the assembly. The PMM also measures insertion depths, and the displacement and rotations of the parts during assembly.

Experiments were conducted in three dimensions to investigate the effects of positional errors, angular errors, axes compliance, and location of the center of rotation. The effects of these parameters on maximum insertion forces during assembly are plotted and discussed.

Criteria for determining the location of the center of rotation and the ratio of rotary to linear stiffness are discussed for four assembly initial conditions in three dimensions. Combinations of location of center of rotation and stiffness ratio that minimize insertion forces are presented.

Thesis Supervisor: Warren P. Seering
Title: Associate Professor of Mechanical Engineering

Acknowledgments

First of all I would like to thank my thesis advisor, Professor Warren P. Seering, for his input, encouragement, and support throughout this research. This thesis is made possible thanks to his guidance.

I would also like to thank the members of Professor's Seering Design Group who helped throughout my research: especially Michael Caine, Steve Eppinger, Steve Gordon, Fred Martin, Ken Pasch, Neil Singer, Karl Ulrich, and Erik Vaaler. All of them played an important role in my research. I would also like to thank my friends Gregory Hammel, Toshiki Masaki, and Karim Salamé.

I must also thank the Advanced Manufacturing Technology Department of Digital Equipment Corporation in Colorado Springs. Their support throughout my involvement in the Engineering Internship Program in Colorado helped complete this research. I would like to thank Edward Chojin, Keith Glick, Kent McNaughton, Steve Mendell, and Ian Stokes.

The Office of Naval Research is greatly appreciated for their financial support. Their fellowship has made this research possible.

I am also very grateful to my parents for their love and support throughout my graduate and undergraduate studies.

To my parents:

José Antonio and Ada Rivero

Contents

1 Introduction **11**

1.1 Problem Statement 11
1.2 Background 12
1.2.1 The Assembly Process 13
1.2.2 Ideal Assembly Phases 14
1.2.3 Using Passive Compliance to Aid Assembly 15
1.2.4 Assembly Parameters 18
1.3 Outline of The Thesis 20

2 A Parts Mating Machine (PMM) **21**

2.1 Introduction 21
2.2 Apparatus Description 23
2.2.1 Components of the PMM 23
2.2.2 Compliance 28
2.2.3 Measurements 28
2.2.4 Specifications 31
2.3 Operation 31
2.4 Data Acquisition and Processing 33
2.5 Calibration Procedure 35
2.5.1 Calibration of LVDTs 35
2.5.2 Calibration of Strain Gage 36
2.5.3 Calibration of Linear Springs 36
2.5.4 Calibration of Rotary Springs 39
2.5.5 Dimensions 41
2.6 Apparatus Verification 41
2.6.1 CSDL Experiment 42

2.6.2 Results Using the PMM 46
2.6.3 Conclusion 53

3 Experimental Results **56**
3.1 Introduction 56
3.2 Parts Analyzed 58
3.3 Experimental Procedure 58
3.3.1 Assembly Parameters 58
3.3.2 Notation 59
3.3.3 Procedure 60
3.3.4 Graphical Techniques 62
3.4 Experimental Results and Discussion 62
3.4.1 Effect of Positional Errors 62
3.4.2 Effect of Axes Stiffness 65
3.4.3 Effect of Angular Errors 70
3.4.4 Effect of Location of the Center of Rotation. 78
3.5 Conclusion 83

4 Criteria for Determining γ and L_g **85**
4.1 Initial Conditions Considered 86
4.2 Selection Criteria 87
4.2.1 Experimental Results and Discussion 89
4.3 Conclusion 98

5 Conclusion **100**
5.1 Recommendations 100
5.2 Suggestions for Future Work 101

A Determination of the Coefficient of Friction **103**

B Data Acquisition Software **107**

References **140**

List of Figures

1.1 Ideal assembly phases for the two dimensional assembly of a peg and a hole. 16
1.2 Force history during each of the assembly phases. 17
1.3 An analitical model for a compliant support. 18

2.1 Photograph of the parts mating machine. 22
2.2 Hole support and slides of the parts mating machine. 25
2.3 Gimbal assembly of the PMM which holds the peg. 27
2.4 Trajectory mechanism of the parts mating machine. 29
2.5 Compliance generation using a spring. 30
2.6 Data acquisition hardware. 34
2.7 Calibration of strain gage using a force gage. 37
2.8 Calibration of linear springs. 39
2.9 Insertion force vs. insertion depth for CSDL experiment: insertion of a 12.672 mm peg and a 12.705 mm hole; center of compliance 45 mm from assembly interface; 1.35 mm x-axis offset. 43
2.10 Lateral force vs. insertion depth for CSDL experiment. 44
2.11 Mathematical representation for a compliant support. 45
2.12 A two dimensional model for the parts mating machine 49
2.13 Reproduction of CSDL experiment using the PMM: insertion force vs. insertion depth. 50
2.14 Experimental setup used to determine the coefficient of friction. 52
2.15 Reproduction of CSDL experiment using the PMM: lateral force vs. insertion depth. 54

3.1 Typical insertion force vs insertion depth plot showing maximum insertion forces. 57

3.2 Peg and hole used to conduct the experiments. 58
3.3 Notation used for positional and angular errors. 61
3.4 Effect of positional errors on maximum insertion forces (MIF) *after* chamfer crossing for a stiffness ratio equal to one. 64
3.5 Effect of positional errors on maximum insertion forces (MIF) *during* chamfer crossing for a stiffness ratio of one. 64
3.6 Effect of positional errors on MIF after chamfer crossing for stiffness ratios of 1, 2, and 4.8. 65
3.7 Effect of positional errors on MIF during chamfer crossing for stiffness ratios of 1, 2, and 4.8. 66
3.8 Effect of changing the stiffness ratio for a positional error of 50 thousanths. 67
3.9 Effect of changing the axes stiffness on MIF during chamfer crossing for three positional errors and a γ of 2. 68
3.10 Effect of changing the axes stiffness on MIF after chamfer crossing for three positional errors and a γ of 2. 69
3.11 Effect of changing the axes stiffness for a γ of 1. 69
3.12 Effect of two stiffness ratios of 1 and 2 on MIF during chamfer crossing. 70
3.13 Effect of stiffness ratios of 1 and 2 on MIF after chamfer crossing. . . 71
3.14 Effect of angular errors on MIF during chamfer crossing for a stiffness ratio of one. 72
3.15 Plot of MIF during chamfer crossing vs angular errors in X and Y for a stiffness ratio of one. 73
3.16 Effect on angular errors on MIF after chamfer crossing for a stiffness ratio of one. 74
3.17 Plot of MIF after chamfer crossing vs angular errors in X and Y for a stiffness ratio of one. 74
3.18 Effect of angular errors on MIF for a stiffness ratio of one. 75
3.19 Effect of angular errors on MIF during chamfer crossing for different stiffness with a ratio of two. 76
3.20 MIF during chamfer crossing vs angular errors for different stiffnesses with a ratio of two. 76
3.21 Effect of angular errors on MIF after chamfer crossing for different stiffnesses with a ratio of two. 77
3.22 MIF after chamfer crossing vs angular errors for different stiffnesses with a ratio of two. 77
3.23 Effect of angular errors on MIF for a stiffness ratio of one. 78
3.24 Effect of the location of the center of rotation (COR) on MIF during chamfer crossing for stiffnesses with a ratio of one. 80

3.25 Effect of the location of the COR on MIF after chamfer crossing for stiffnesses with a ratio of one. 80
3.26 Effect of the location of the center of rotation (COR) on MIF during chamfer crossing for stiffnesses with a ratio of two. 81
3.27 Effect of the location of the center of rotation (COR) on MIF after chamfer crossing for stiffnesses with a ratio of two. 82

4.1 Drawing showing, in two dimensions, the four assembly initial conditions considered. 88
4.2 Effect of L_g and γ on MIF for a positional error of 20 thousanths. . . . 91
4.3 Effect of L_g and γ on MIF for a positional error of 50 thousanths. . . . 92
4.4 Effect of L_g and γ on MIF for an angular error of 0.54°. 94
4.5 Effect of L_g and γ on MIF for an angular error of 1.54°. 95
4.6 Effect of L_g and γ on MIF for a positional error of 50 thousanths and an angular error of 0.54°. 96
4.7 Effect of L_g and γ on MIF for a positional error of -50 thousanths and an angular error of 0.54°. 97

A.1 Forces acting on the hole during chamfer crossing. 104
A.2 Forces acting on the peg during chamfer crossing. 105

List of Tables

2.1 Specifications for the parts mating machine. 32
2.2 Calibration factors for LVDT's. 36
2.3 Calibration factors for linear springs. 38
2.4 Calibration factors for rotary springs. 40
2.5 Stiffer calibration factors for rotary springs. 40
2.6 Stiffness conversion factors from metric to SI units. 41
2.7 Symbol description. 47
2.8 Effect of some assembly parameters on the location where 2-pt contact starts. 53

3.1 Notation description. 60
3.2 Experiments conducted to investigate the effects of positional errors . . 63
3.3 Experiments conducted to investigate the effects of the axes stiffness. . 67
3.4 Experiments conducted to investigate the effects of angular errors. . . 71
3.5 Experiments conducted to investigate the effects of the location of the center of rotation with respect to the tip of the peg (L_g). 79

4.1 Initial assembly conditions investigated assuming symmetry. 87
4.2 Experiments conducted to develop criteria for determining γ and L_g. . . 89

Introduction

Chapter 1

1.1 Problem Statement

Robots are increasingly being used in assembly applications. Therefore, it is necessary to improve the productivity of robots in performing these tasks. To do so, the assembly process must be studied. In particular, three dimensional assembly processes must be analyzed since real or industrial applications occur in three dimensions. One area which must be researched is the effect of parameters on three dimensional assembly.

Most real assembly operations take place in the presence of uncertainties, mainly positional and angular errors. Error-free assembly, where the location of the parts is exactly known, is rare due to the high costs of fixturing and tolerancing, and also due to limitations of the assembly machine. One solution to the problem of assembling parts in the presence of errors is to use passive compliance. Passive compliance, which will be described later, involves using a compliant device that absorbs the initial misalignments and permits the parts to mate successfully. An example of such a device is a remote center of compliance (RCC).

Significant research has been conducted in the area of compliant assembly. However, most of this research has been limited to the analysis of the two dimensional case, and not to the significantly more complicated three dimensional case.

On the other hand, research has already been conducted in the area of three dimensional assembly. However, the models developed have not been tested empirically, or can not be used readily to investigate the effects of parameters on assembly processes using passive compliance.

This research attempts to provide information on the three dimensional compliant assembly of parts. More concretely, the goal of this research is to determine the effects of parameters on the assembly process and to develop criteria for selecting these parameters. To achieve this goal, an empirical approach was used, and not an analytical one. The empirical approach was chosen for several reasons. First, the complexity of three dimensional assembly makes an analytical approach difficult to solve. Second, empirical data on three dimensional assembly is scarce. Third, information of three dimensional assembly can be readily obtained using a test apparatus developed at the MIT Artificial Intelligence Laboratory.

1.2 Background

As pointed out in the previous section, much research has been conducted in the area of compliant assembly in two dimensions. For example, Arai [1] investigates the forces that arise when using a worktable with compliance. In this research, the compliance was located in the worktable and not in the end-effector of the assembly machine, as it is commonly done. Several reports by the Charles Stark Draper Laboratory staff also describe research conducted in assembly. The sixth report in industrial modular

assembly [6] describes research conducted in interference fits, high-speed insertions, the remote center of compliance device, and other areas. Drake [7] investigates different compliance systems. Simunovic [16,17] investigates the information available during assembly, and the form and use of this information to help the assembly process. Models are presented to investigate the interaction of parts during assembly. Whitney [19] describes what the remote center of compliance device is and how it works. Also, Whitney [20] provides an encompassing and thorough study of two dimensional assembly of compliantly supported rigid parts; that is, of parts that do not deform substantially during assembly. Models are developed and verified experimentally, the functioning of the remote center of compliance (RCC) device is explained, and guidelines for choosing RCC parameters are presented. Research has also been conducted in the are of two dimensional assembly of compliant parts. Compliant parts deform considerable during assembly. Hennessey [10] developed models of compliantly supported rigid pegs entering compliant holes and minimum energy chamfer designs

Research has also been conducted in the area of three dimensional assembly. Caine [3] investigates the three dimensional assembly of chamferless rectangular parts in the presence of friction. Models are developed and implemented to assemble a rectangular peg and hole using force control. Gustavson [9] describes the requirements for a compliant device for three dimensional assembly, such that at the end of chamfer crossing there would be zero tilt angle of the peg.

1.2.1 The Assembly Process

The assembly process is purely a positioning problem. If there was exact knowledge of the location of the parts, assembly would be trivial. However, misalignments between the parts are present. These errors occur due to errors in fixturing, tolerances in

the geometry of the parts, and also due to performance limitations of the machines conducting the assembly.

The assembly process can be divided into two stages (Simunovic [16.17]): transition from transport to mating, and part mating. The transition from transport to mating involves bringing the parts together to the point where they can start to be mated. Parts mating occurs when the parts are actually touching each other.

This thesis concentrates with the parts mating process. To analyze parts mating, three ideal assembly phases can be used (Whitney [20]): chamfer crossing, one point contact, and two point contact. These three ideal phases will be described next.

1.2.2 Ideal Assembly Phases

Figure 1.1 shows the three ideal assembly phases in two dimensions for the case of a peg and a hole. As the names imply, chamfer crossing happens when the peg is within the chamfer of the hole and is moving downward, one-point contact occurs after the peg crosses the chamfer and is touching the hole at only one point, and two point contact occurs as the peg moves farther downward and touches the hole at two points. Eventually, when the peg is sufficiently down the hole one-point contact will then occur again.

Figure 1.2 shows a typical force history plot during each of the ideal assembly phases. These plots are for the compliant assembly of a rigid peg and hole. The plots to the right of each of the ideal phases show insertion force along the insertion axis vs insertion depth (labeled in the figure). As can be seen, forces during chamfer crossing increase rapidly, then decrease significantly and stay roughly constant during one-point contact, and then increase again as two-point contact occurs. As seen in Figure 1.2, it is desirable to force the assembly to maintain the one-point contact

situation to minimize insertion forces.

1.2.3 Using Passive Compliance to Aid Assembly

As pointed out before, errors are present when assembling parts. To mate the parts, the initial error must be smaller than the chamfer so that the parts engage. After the parts engage, a passive compliance device can be used to absorb the errors present and allow the parts to mate successfully. A device called a remote center of compliance (RCC) is an example of using passive compliance.

References [5,6,7,16,19,20] describe the functioning of the RCC. Briefly, the RCC is a device that absorbs independently the positional and angular errors present in the assembly. It also projects the center of compliance to a determined point. The center of compliance is the point at which an applied force results in pure translation and about which an applied torque results in pure rotation. By placing the center of compliance close to the tip of the peg, the RCC can minimize the angular errors created when absorbing the initial positional errors. Therefore, two point contact can be avoided in many situations and the insertion forces can be minimized.

An RCC can be thought of as consisting of a linear stiffness and a rotary stiffness. The linear stiffness helps absorb the linear errors, and the rotary helps absorb the rotary errors or tilt of the peg. They are located in such a way that they project the center of compliance to a known determined distance. Figure 1.3 shows an analitical model for a compliant support or RCC. This method of representing supports was first developed by Simunovic [16]. The center of compliance is labeled by •, the linear stiffness by K_x, the rotary stiffness by K_θ, and the distance from the tip of the peg to the location of the center of compliance by L_g. Altogether, three parameters are necessary to characterize an RCC: (1) the linear stiffness, (2) the rotary stiffness, and

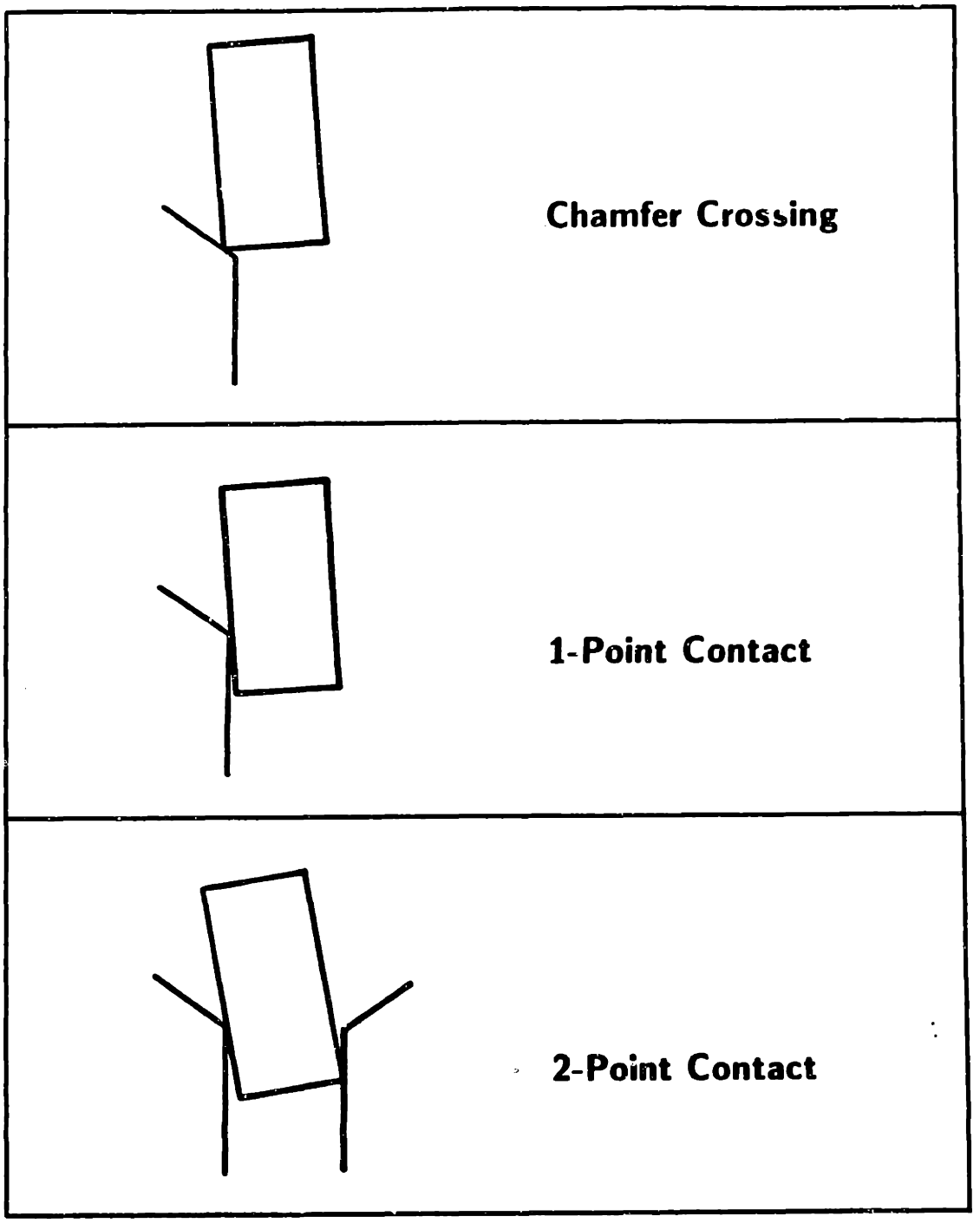

Figure 1.1: Ideal assembly phases for the two dimensional assembly of a peg and a hole.

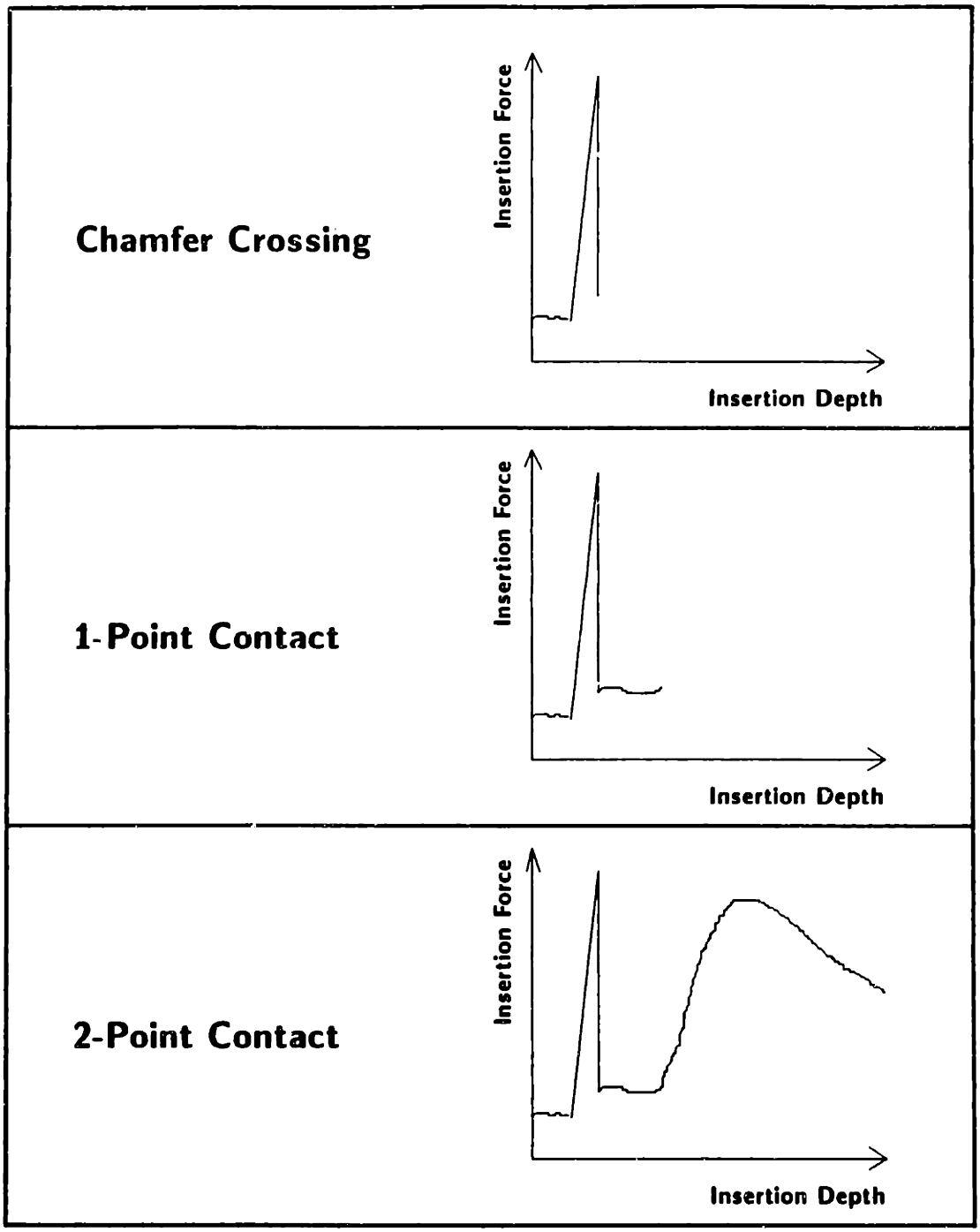

Figure 1.2: Force history during each of the assembly phases.

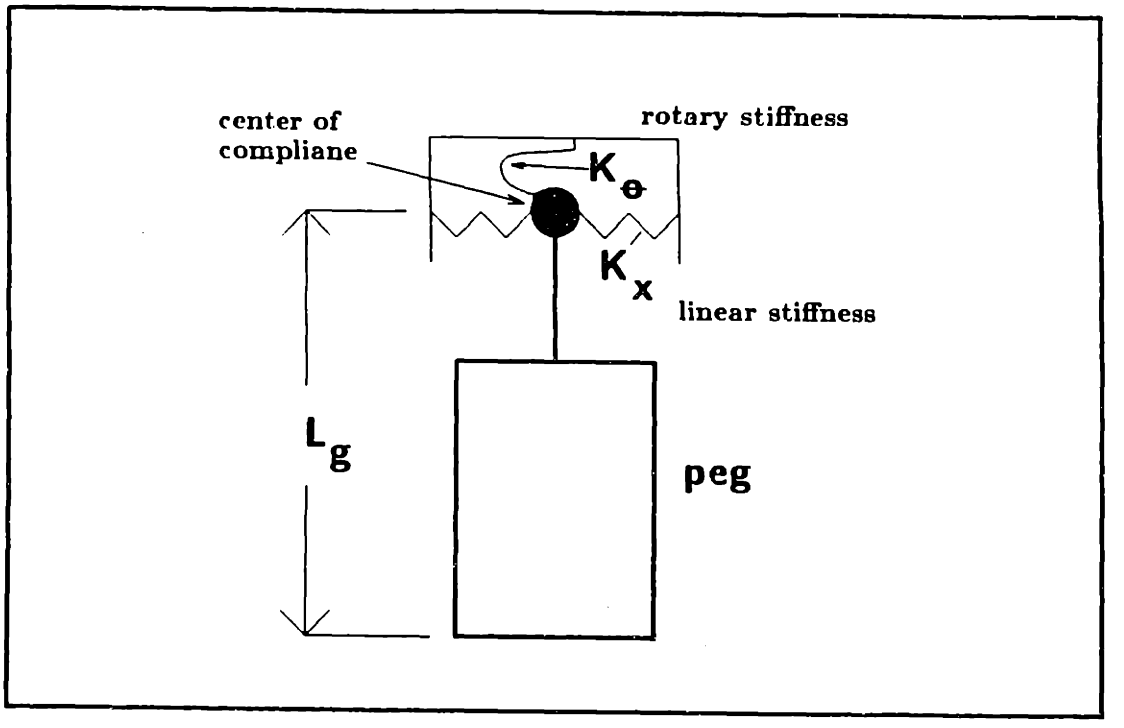

Figure 1.3: An analitical model for a compliant support.

(3) the location of the center of compliance or L_g if the part length is known.

The RCC is commonly used in many applications and has become a "standard" in many industries. Due to the importance of RCC's, this thesis will investigate the effects of parameters associated with this device, such as the linear stiffness, rotary stiffness, and location of the center of rotation.

1.2.4 Assembly Parameters

As just pointed out, three parameters are necessary to describe the compliant device used for assembling parts:

- linear stiffness

- rotary stiffness
- location of center of compliance, or L_y

Furthermore, two parameters are also necessary to describe the initial conditions of the assembly:

- positional errors prior to assembly
- angular errors prior to assembly

Also, to describe the parts to be mated, several parameters can be used:

- geometry (size and shape) of the parts
- clearance between the parts
- surface finish

Overall, if we are given a set of parts to be assembled compliantly, five parameters can be used to describe the assembly process:

1. linear stiffness
2. rotary stiffness
3. location of center of compliance, or L_y
4. positional errors
5. angular errors

Throughout this thesis, this set of five parameters will be referred to as the *assembly parameters* and will be used to characterize an assembly process.

1.3 Outline of The Thesis

This thesis investigates the effects of the assembly parameters on the insertion forces that occur in the three dimensional assembly of a peg and a hole. The thesis also presents criteria for selecting the adjustable parameters. Chapter 2 describes in detail the test apparatus that was used to obtain all the empirical information. Chapter 3 presents a major portion of the experimental results and investigates the effect of four parameters on maximum insertion forces: (1) positional errors, (2) angular errors, (3) stiffness (linear and rotary), (4) and L_g. Chapter 4 provides criteria for selecting the ratio of rotary to linear stiffness and L_g. Finally, Chapter 5 presents recommendations and suggestions for future work. The appendices include some derivations and a listing of the data acquisition software. The references used are also included.

A Parts Mating Machine (PMM)

Chapter 2

2.1 Introduction

The following chapter describes a five degree-of-freedom (dof) compliant parts mating machine. All the experimental results presented in this thesis were obtained using this test apparatus.

The parts mating machine, or PMM, was designed and built by Steve Potter, Muhammad Rifai, and Karl Ulrich in 1985. Further hardware and software was then developed to make the machine fully operational and take advantage of its data acquisition capabilities.

The PMM, which is shown in Figure 2.1, is a test apparatus capable of analyzing assembly processes in three dimensions. The PMM allows the researcher to mate two parts of any shape and measure all forces, moments, and displacements during the assembly.

Three features of the PMM make it capable of determining the effects of system parameters on assembly processes. First, the parts to be mated can be offset prior to

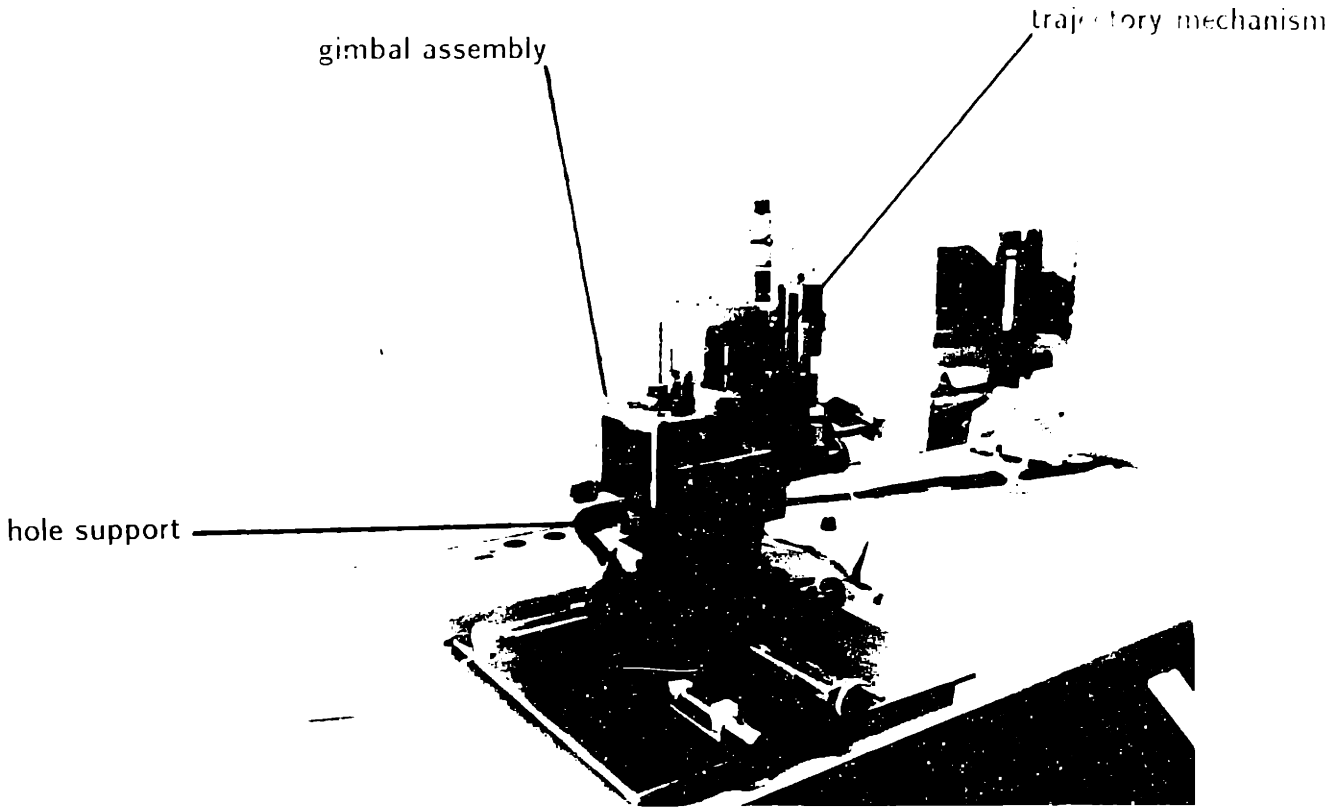

Figure 2.1: Photograph of the parts mating machine.

assembly linearly and angularly in any direction. Therefore, the effects of positional and angular errors can be studied. Second, the stiffness in each of the five dof can be adjusted to any desired value. Using this feature, the effects of changing the stiffness can be analyzed. Third, the location of the center of rotation, which is analogous to the center of compliance in a RCC device, can be changed.

The components of the PMM allow the parts to be mated to move relative to each other in five dof: two linear, and three rotary. The degrees-of-freedom are (see Figure 2.1): (1) linear displacements in X, (2) linear displacements in Y, (3) rotations about X, (4) about Y, and (5) about Z. The stiffness in each of these axes is adjustable. The sixth degree of freedom is along the insertion axis. This DOF is not compliant since the parts are constrained to move in this direction at a constant speed.

During an assembly operation the PMM measures the following: (1) insertion forces, (2) displacements of the parts in X and Y, and (3) rotations of the parts about X, Y, and Z. Insertion forces are measured using strain gages, displacements using linear variable differential transformers (LVDT), and rotations using digital optical encoders. Furthermore, using the measured displacement of the parts and the known linear stiffness, lateral forces during assembly can be calculated. Similarly, using the measured rotation of the parts and preset rotary stiffness, moments can also be calculated.

2.2 Apparatus Description

2.2.1 Components of the PMM

The PMM consists of three main components, shown in Figure 2.1: the hole support, the gimbal assembly, and the trajectory mechanism. Note that the figures show a peg

and a hole being assembled. The machines is not limited to these parts. Any parts that fit inside the gimbal assembly can be studied.

Hole Support

The hole support, shown in Figure 2.2, is a stainless steel block used to position the hole. The support lies below the gimbal assembly, and is mounted atop two orthogonal ball-slides attached to the base plate.

The hole support provides three of the five degrees-of-freedom of the PMM. Because the support is located atop the two slides, it can move in the linear X and Y directions. Therefore, it provides the X and Y linear dof. Also, the hole support can rotate freely about the insertion or Z axis, and thus gives the Z-rotary dof.

The stiffness in each degree-of-freedom is obtained using cantilever beams (see Figure 2.2). The beams, which act like springs, have variable lengths. Therefore, the desired stiffness in each dof can be set by adjusting the length of each beam.

Gimbal Assembly

The gimbal assembly, shown in Figure 2.3, is used to support the peg and to provide two degrees-of-freedom. The gimbal is located above the hole support and in front of the trajectory mechanism.

The gimbal assembly consists of three main parts: an inner yoke, an outer yoke, and a 5/8" shaft. The inner yoke is free to rotate about the outer yoke and holds the peg. The outer yoke is attached to the shaft, which in turn is fixed to the trajectory mechanism. The shaft is attached using bearing blocks, so it can also rotate.

The gimbal assembly provides the remaining two degrees-of-freedom of the PMM: the X-rotary, and the Y-rotary. The X-rotary dof is obtained from the rotation of the

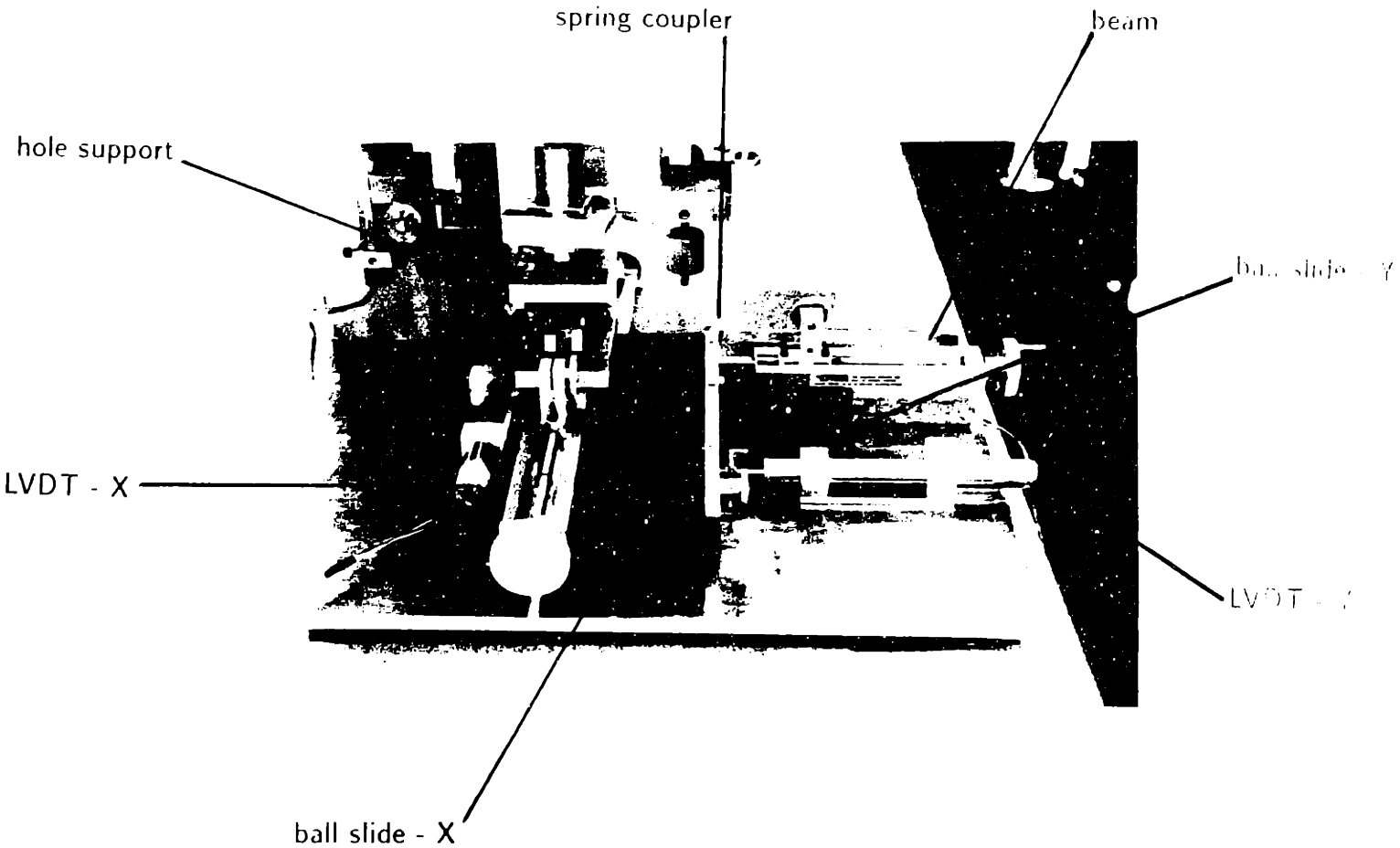

Figure 2.2: Hole support and slides of the parts mating machine.

inner yoke, and the Y-rotary from the rotation of the outer yoke and shaft.

The *center of rotation* (COR) is defined as the point where the axis of rotation of the X-rotary and Y-rotary dof intersect. In other words, in Figure 2.3 the COR is the point where the centerline of the 1/2" shaft and the centerline of the 5/8" shaft intersect. The location of the COR is an important parameter which influences the insertion forces generated during assembly.

The parts mating machine allows the user to move the COR. This effect is achieved by either changing the part length, or by adjusting the slide which supports the yoke. Note that the COR is related to the center of compliance (COC)[1] of a Remote Center of Compliance device, but is not the same. The COR does not have a linear stiffness associated with it, as does the COC. The COR is not compliant in any linear direction, only rotations are allowed. The linear stiffness in the parts mating machine is located with the slides. Both the COR and COC are related in that rotations during assembly occur at these points.

Trajectory Mechanism

The trajectory mechanism, shown in Figure 2.4, causes the cross-roller slide to move up and down. Because the gimbal assembly is attached to the slide, the trajectory mechanism forces the assembly parts to mate.

The trajectory mechanism is composed of: (1) a motor, (2) a lead screw, (3) a strain gage element, and (4) a cross-roller slide. The motor is used to rotate the lead screw, which in turn causes the gage element to move up or down depending on the sense of the rotation of the screw. The second component of the mechanism,

[1] Point at which an applied force results in pure translation and about which an applied torque results in pure rotation.

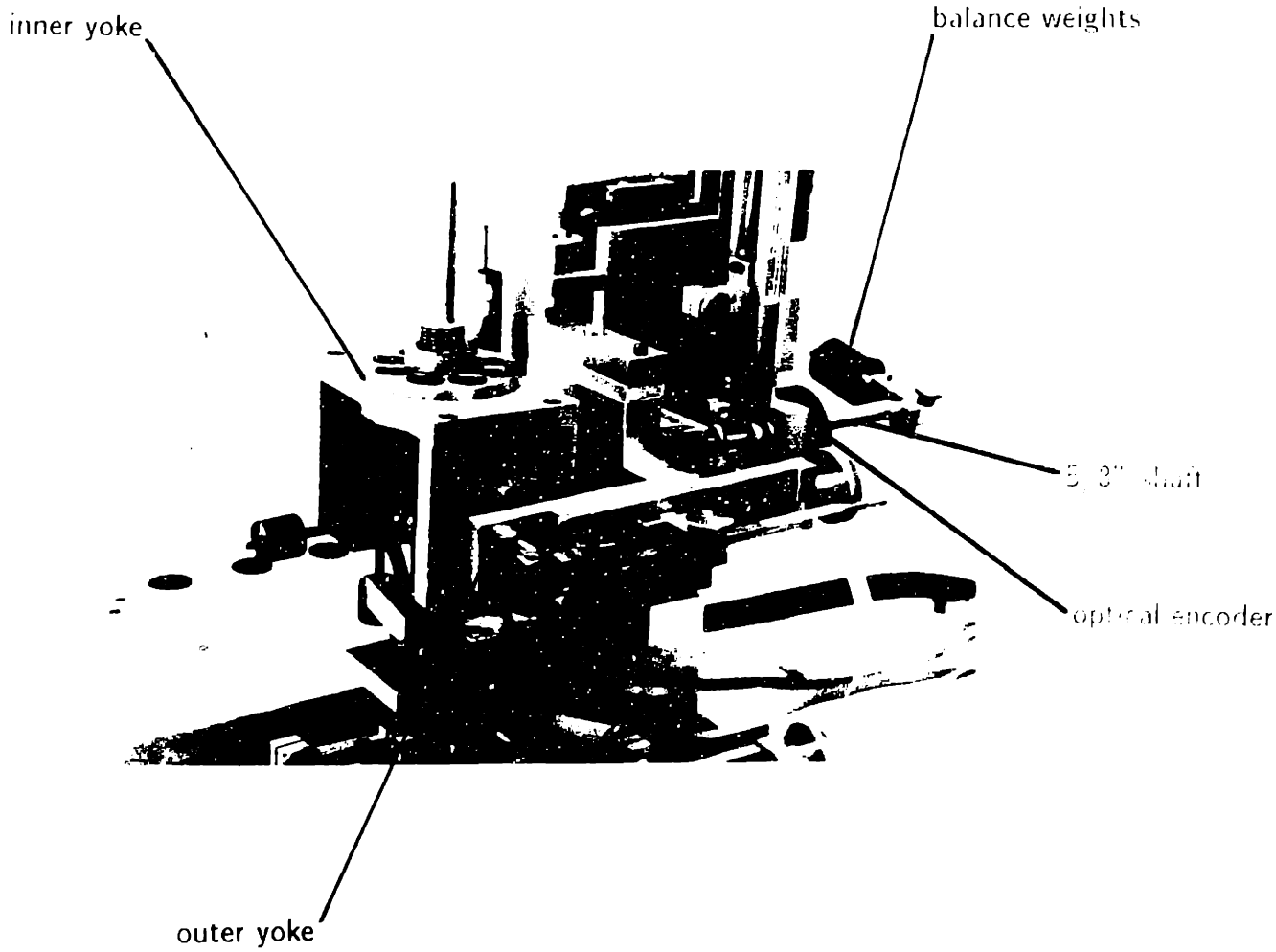

Figure 2.3: Gimbal assembly of the PMM which holds the peg.

the strain gage element, is used to measure insertion forces and is attached to the cross-roller slide. Therefore, by turning the screw the slide to which the gimbal is attached can be lowered or raised. Due to the motor speed the parts are mated very slowly. Thanks to this feature a quasi-static situation is obtained and a force/moment equilibrium analysis can be used. Note the balance weights in Figure 2.4 are again used to balance the apparatus.

2.2.2 Compliance

The compliance on all the degrees of freedom is obtained using springs. Figure 2.5 shows the spring is used to obtain the desired compliance for the case of a rotary dof.. A cantilever beam is attached using a crank to the rotary member, for the case of the rotary dof, or to the slides in the case of the linear dof. By moving the spring clamp using the micro-slide, the lever arm is changed and thus the compliance is adjusted. In the calibration procedure described in a later section the relation between slide position and compliance is determined.

2.2.3 Measurements

In the assembly of two parts, the PMM provides seven channels of data:

1. insertion depth
2. insertion force
3. X-linear displacement
4. Y-linear displacement

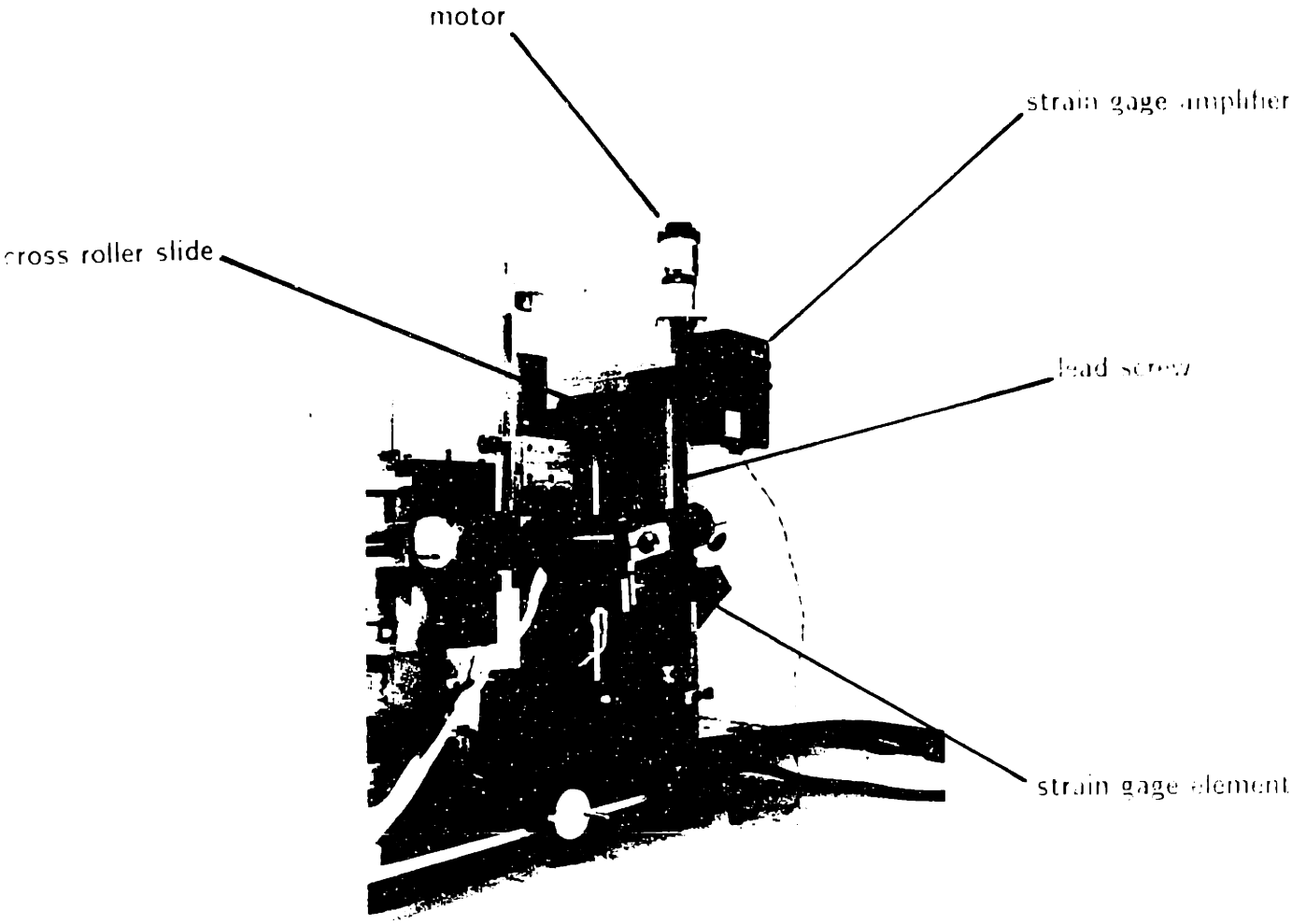

Figure 2.4: Trajectory mechanism of the parts mating machine.

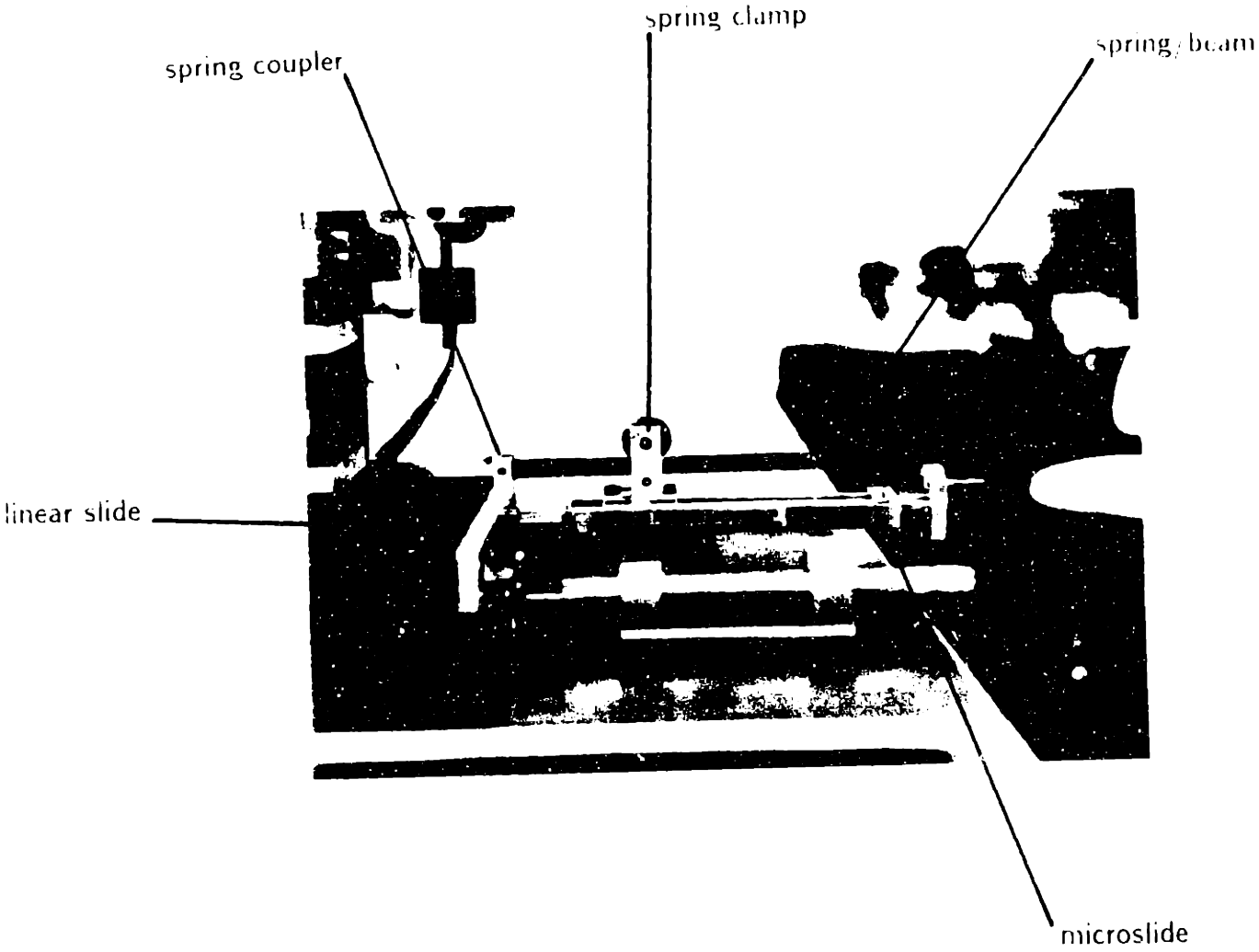

Figure 2.5: Compliance generation using a spring.

5. rotations about X

6. rotations about Y

7. rotations about Z

Insertion depth is obtained using a Linear Variable Differential Transformer (LVDT) attached to the insertion slide as shown in Figure 2.1. Insertion forces are measured using a four-gage Wheatstone bridge located in the gage element shown in Figure 2.4. Linear displacements of the slides are measured using LVDT's (see Figure 2.3 and rotations are obtained using digital optical encoders (see Figure 2.2).

Lateral forces can be obtained from the linear displacements and the known stiffness of the springs. In the same way, moments are determined from the angular displacements of the rotary dof and the stiffness.

Altogether, the parts mating machine provides during the assembly process the following information: insertion depths, insertion forces, linear displacements of the parts, rotations of the parts, lateral forces, and moments.

2.2.4 Specifications

Table 2.1 provides the ranges of motion, stiffness, and sensitivities of the parts mating machine .

2.3 Operation

To study a particular assembly process, one of the parts to be mated is attached to the gimbal and the other to the support block. The stiffness and location of the center of compliance are then set. The parts are mated. Then the reading of the

Table 2.1: Specifications for the parts mating machine.

5 DOF's	
Sensitivity of A/D board	$1.22 \frac{mV}{count}$
Sensitivity - LVDT X-direction	$0.126 \frac{mil}{count}$
Maximum X-displacement	.5 in
Sensitivity - LVDT Y-direction	$0.120 \frac{mil}{counts}$
Maximum Y-displacement	.5 in
Sensitivity - LVDT Z-direction	$0.316 \frac{mil}{count}$
Limitations on Z-displacement	none
Sensitivity - insertion force	$.0347 \frac{ouncef}{count}$
Stiffness Range:	
X-linear	$3 - 82 \frac{lb}{in}$
Y-linear	$3 - 81 \frac{lb}{in}$
X-rotary	$2 - 287 \frac{lb-in}{rad}$
Y-rotary	$9 - 5445 \frac{lb-in}{rad}$
Z-rotary	$4 - 82 \frac{lb-in}{rad}$
Angular Sensitivity	1/4000 rev.

LVDT's is recorded and the encoders are zeroed. These LVDT readings will be used as the zero-offset reference position. The gimbal is raised and the positional errors are introduced by moving the linear LVDT's and noting the LVDT output. The angular errors are obtained by moving the angular dof while noting the encoder output. After the desired initial errors have been introduced, the two parts are mated and all the assembly information is recorded by the PMM.

2.4 Data Acquisition and Processing

The parts mating machine outputs four analog signals (3 from the LVDT's and 1 from the strain gage) and three digital signals (from the optical encoders). The analog signals are fed to an A/D converter and then to a Digital PDP 11/23 computer. The digital signals are fed to Automation's Research encoder counter board, to a DRV-11 board (parallel interface) and then to the PDP 11/23 computer (see Figure 2.6). The encoder counter board has a resolution of 4,000 counts per revolution and outputs a number of counts corresponding to the amount the encoders have rotated.

Program DAT.FOR is used to sample all seven channels and store the data in a file. The sampling rate, name of output file, and the channels to be sampled are inputed by the user. This file calls the following subroutines: ADFAST.FOR, MADC2.MAC, MACD1.MAC, MACD2.MAC, and MACD3.MAC. Once the raw data is in a file, program SCALE.FOR is used to scale the data and convert it to physically meaning units. The conversion factors are presented in the following section. Appendix B contains a listing of the above programs.

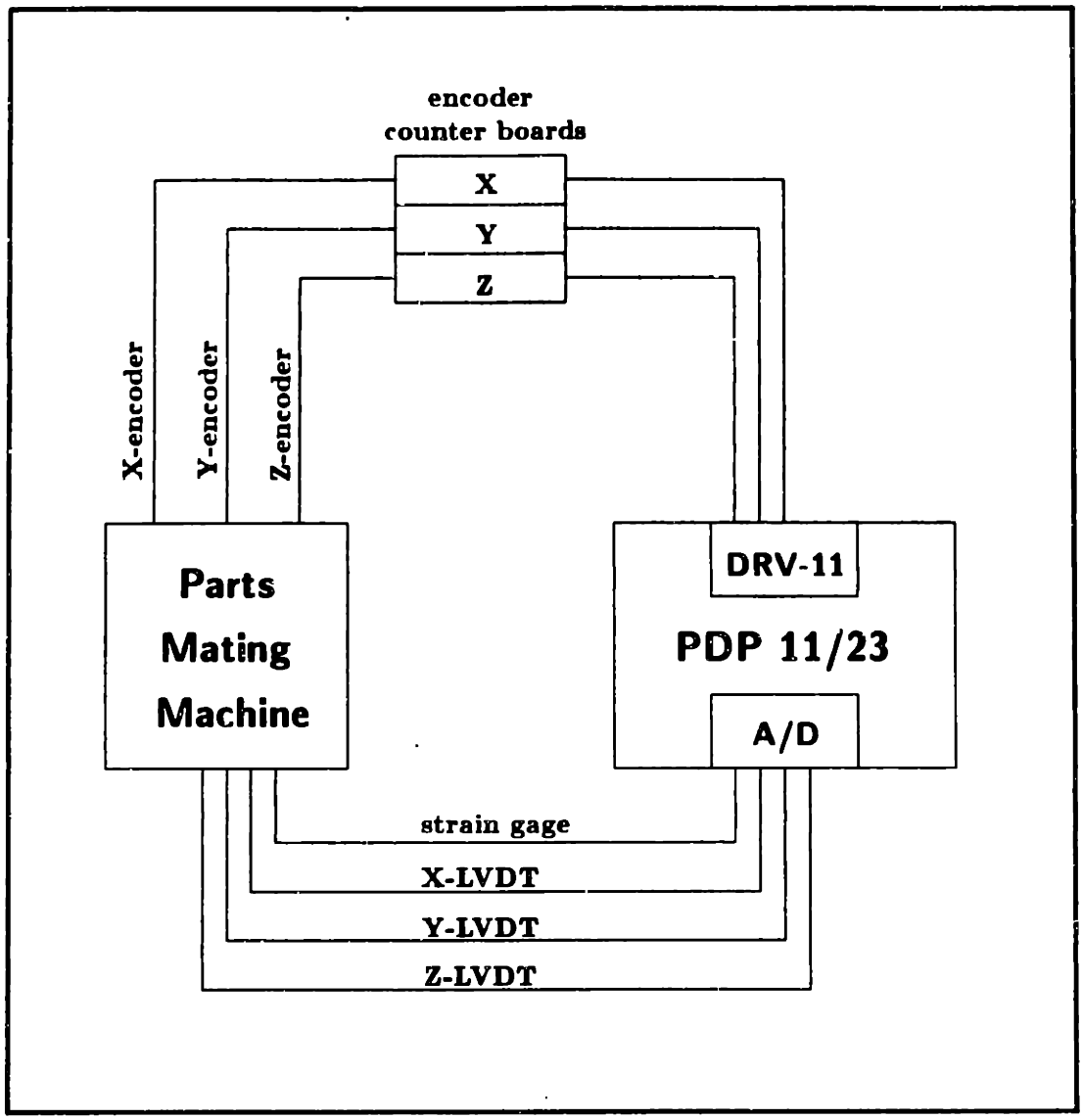

Figure 2.6: Data acquisition hardware.

2.5 Calibration Procedure

This procedure involved calibrating the following:

1. X, Y, and Z LVDT's.
2. strain gage
3. linear springs (X and Y)
4. rotary springs (X, Y, and Z).

Only the digital encoders did not need calibration since they output a constant $4000 \frac{counts}{rev}$ due to the interface cards used. Note that all analog signals are fed into the A/D converter in the computer, which in turn outputs an integer number of counts proportional to the input voltage[2]. This number of counts is then multiplied by a calibration factor to obtain physically meaningful data. Therefore, all the above items will be calibrated in counts. That is, inches per count, ounces per count, and so on.

2.5.1 Calibration of LVDTs

To calibrate the LVDT's, the manufacturers instructions were followed. The initial position in counts was measured. A gage block was then used to move the LVDT an exact amount, and a new reading was obtained. The calibration factor was obtained by dividing the distance moved by the difference in the number of counts. The factors in Table 2.2 were obtained:

[2]The particular A/D converter used outputs ± 2048 counts for an input of ± 2.5 volts

Table 2.2: Calibration factors for LVDT's.

X LVDT	$.126 \frac{mil}{count}$
Y LVDT	$.120 \frac{mil}{count}$
Z LVDT	$.316 \frac{mil}{count}$

2.5.2 Calibration of Strain Gage

The strain gage was first calibrated using a dead weight technique. Several weights were added at the peg location and the corresponding reading in counts was measured. The calibration factor, which equaled $0.0347 \frac{ounces}{count}$, was found from the slope of the weight (force) vs output (counts) curve. This factor was then re-checked using a force gage technique. A push-pull force gage was located under the peg as shown in Figure 2.7. The peg was lowered thus increasing the force exerted. For each gage reading the output in counts was measured. The calibration was again found to equal $.0347 \frac{ounces}{count}$.

2.5.3 Calibration of Linear Springs

The linear and rotary springs were calibrated using a dead weight method, as suggested in the original report for the parts mating machine [3]. Accurate balance scale weights were attached with a thread to the slides and hung using a ball bearing pulley. For each slide reading, the deflection or rotation due to the weight was measured. The

[3]Potter, Ulrich, and Rifai, "A Five Degree of Freedom Compliant Parts Mating Machine", MIT AI Lab, May 1985.

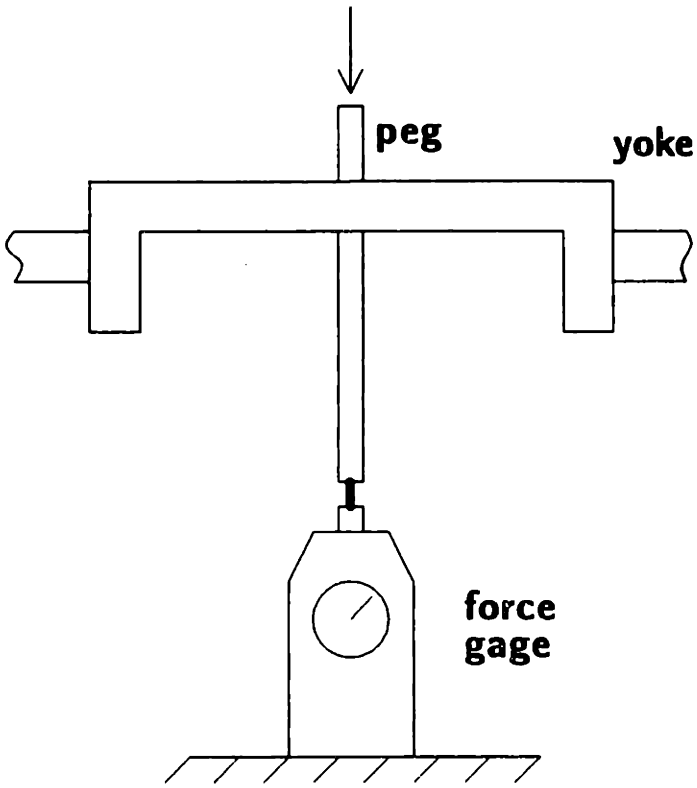

Figure 2.7: Calibration of strain gage using a force gage.

Table 2.3: Calibration factors for linear springs.

X_{lin}	$l_o = 2.134$
	$C = 800$
Y_{lin}	$l_o = 2.147$
	$C = 800$

data obtained was fit to the following general equation:

$$K = \frac{C}{l^3} \tag{2.1}$$

where K is stiffness, C is a constant, and l is the beam length. The useful calibration equation can be put in the form:

$$K = \frac{C}{(l_o + r)^3} \tag{2.2}$$

where r is the slide reading, and l_o a constant. This equation applies for both the linear and the rotary degrees of freedom.

To obtain C and l_o in Equation 2.2 for the linear degrees of freedom, the following procedure was followed (refer to Figure 2.8): for each slide reading, r, a known weight (force) was hung and the slide displacement measured. With this information, the stiffness was calculated and set equal to the right hand side of Equation 2.2. The constants C and l_o were obtained using two different points. Values were obtained using different sets of points and averaged. For the linear degrees of freedom X and Y, the constants in Table 2.3 were found:

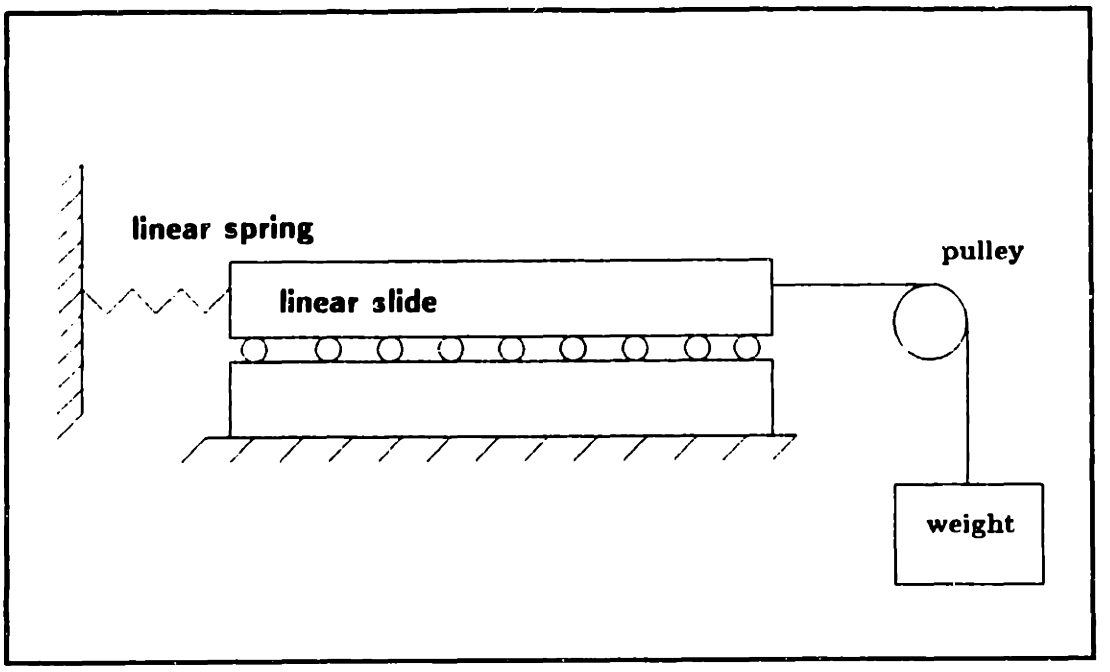

Figure 2.8: Calibration of linear springs.

2.5.4 Calibration of Rotary Springs

For the rotary degrees of freedom a similar procedure was followed. For each slide reading, a weight was hung at a known radius so the moment exerted was known. Using this value and the measured angular displacement, the rotary stiffness was found and set equal to the right hand side of Equation 2.2. The constants were solved for using two points and the results using different sets of points were averaged. For the rotary axes, the calibration constants in Table 2.4 were found:

For applications requiring larger stiffnesses, the slide of the Y-rotary and X-rotary degrees of freedom can be moved to a second position. At this location, the stiffness ranges from 287 $\frac{lb-in}{rad}$ to 7 $\frac{lb-in}{rad}$ for the x-rotary, and 5445 $\frac{lb-in}{rad}$ to 2 $\frac{lb-in}{rad}$ for the y-rotary degrees of freedom . The constants for this case are shown in Table 2.5.

Table 2.4: Calibration factors for rotary springs.

X_{rot}	$l_o = 2.20$
	$C = 714$
Y_{rot}	$l_o = 1.77$
	$C = 727$
Z_{rot}	$l_o = 2.19$
	$C = 863$

Table 2.5: Stiffer calibration factors for rotary springs.

Y_{rot}	$l_o = .538$
	$C = 846$
X_{rot}	$l_o = 1.58$
	$C = 1133$

Table 2.6: Stiffness conversion factors from metric to SI units.

From:	To:	Multiply by:
$\frac{N}{m}$	$\frac{lb}{in}$	0.00571
$\frac{N-m}{rad}$	$\frac{lb-in}{rad}$	8.85075

2.5.5 Dimensions

Using the above constants, and r in $[inches]$, the dimensions for K are $[\frac{lb}{in}]$ and $[\frac{lb-in}{rad}]$ for the linear and rotary degrees of freedom respectively. For those interested in using metric units, please refer to Table 2.6.

2.6 Apparatus Verification

In order to verify the correct functioning of the parts mating machine (calibration, location of center of rotation, offsets, and force/moment information), a test was conducted and compared to that previously performed at The Charles Stark Draper Laboratory (CSDL) in Cambridge, Mass. The results of this experiment appeared in the article "Quasi-Static Assembly of Compliantly Supported Rigid Parts" by Dr. Dan E. Whitney [4].

[4] Journal of System Dynamics, Measurement, and Control, March 1983, Vol. 104

2.6.1 CSDL Experiment

This experiment consisted of mating a hardened and ground peg and hole. The peg was supported by a Remote Center of Compliance (RCC) whose deflections were measured using optical encoders. The RCC was connected to a six degree-of-freedom sensor which measured all forces and moments during the insertion. The force/moment sensor was in turn held in the quill of a milling machine. A linear variable differential transformer was attached to the milling machine and used to measure insertion depths. This experiment, which will be used for comparison and verification of the parts mating machine , consisted of the following parameters:

- $K_{linear} = 39.97 \frac{lb}{in}$
- $K_{rotary} = 469.1 \frac{lb-in}{rad}$
- $hole\ diameter = 0.5002\,in$
- $peg\ diameter = 0.4989\,in$
- $linear\ misalignment = 53.15\,thousands$
- $angular\ misalignment = 0^{\circ}$
- $support\ location$ [5] $= 1.77\,in$

Figures 2.9 and 2.10 show the results of this CSDL experiment. Both of these plots were obtained from Whitney [20]. Figure 2.9 shows a plot of insertion force versus insertion depth for the above experiment, and Figure 2.10 of the lateral force versus insertion depth.

[5] distance from the bottom tip of the peg to the location of the center of compliance

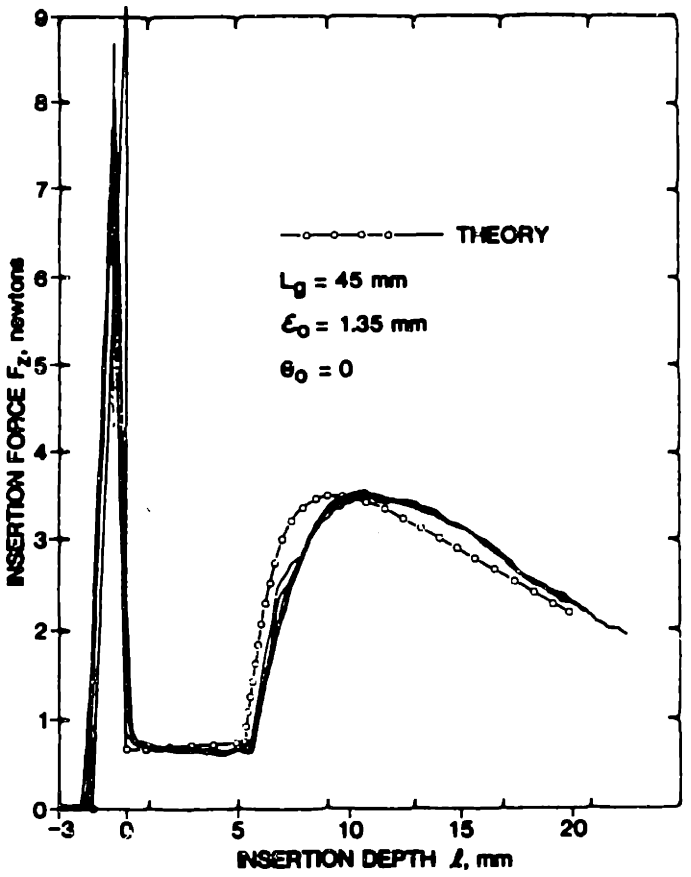

Figure 2.9: Insertion force vs. insertion depth for CSDL experiment: insertion of a 12.672 *mm* peg and a 12.705 *mm* hole; center of compliance 45 *mm* from assembly interface; 1.35 *mm* x-axis offset.

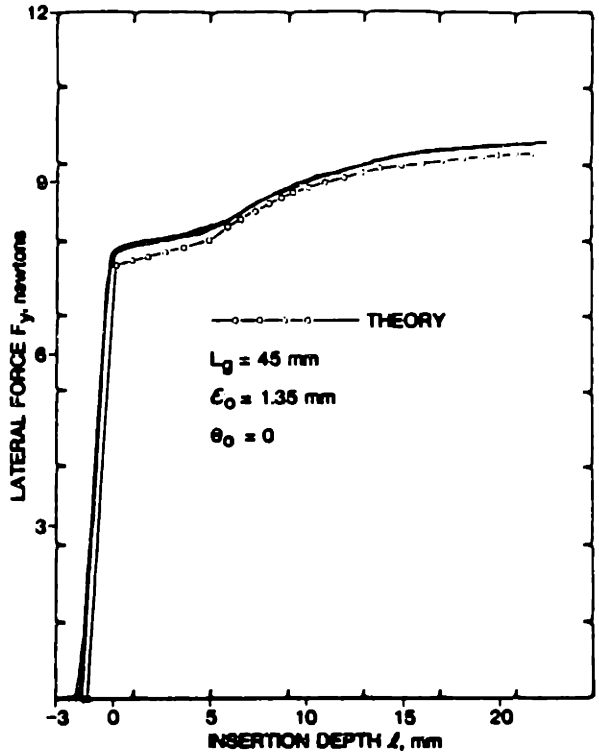

Figure 2.10: Lateral force vs. insertion depth for CSDL experiment.

Governing Equations

The governing equations for the case of a 2-dimensional peg and hole insertion using an RCC as the compliant support were derived in Whitney [20]. The equations are presented in this section since they will be used when comparing and explaining the results obtained using the PMM. The following equations were developed by mathematically representing the RCC by a compliance center where the support's lateral and angular stiffness are located. As can be seen in Figure 2.11, the support consists of a lateral stiffness, K_x, and a rotary stiffness, K_θ. The lateral stiffness acts at, and the rotary stiffness around, the center of compliance (marked in this Figure 2.11 by •). The distance between the center of compliance and the tip of the peg is labeled by L_g, and the radius of the peg by r.

The governing equations for the insertion force, F_z, for the regions of chamfer

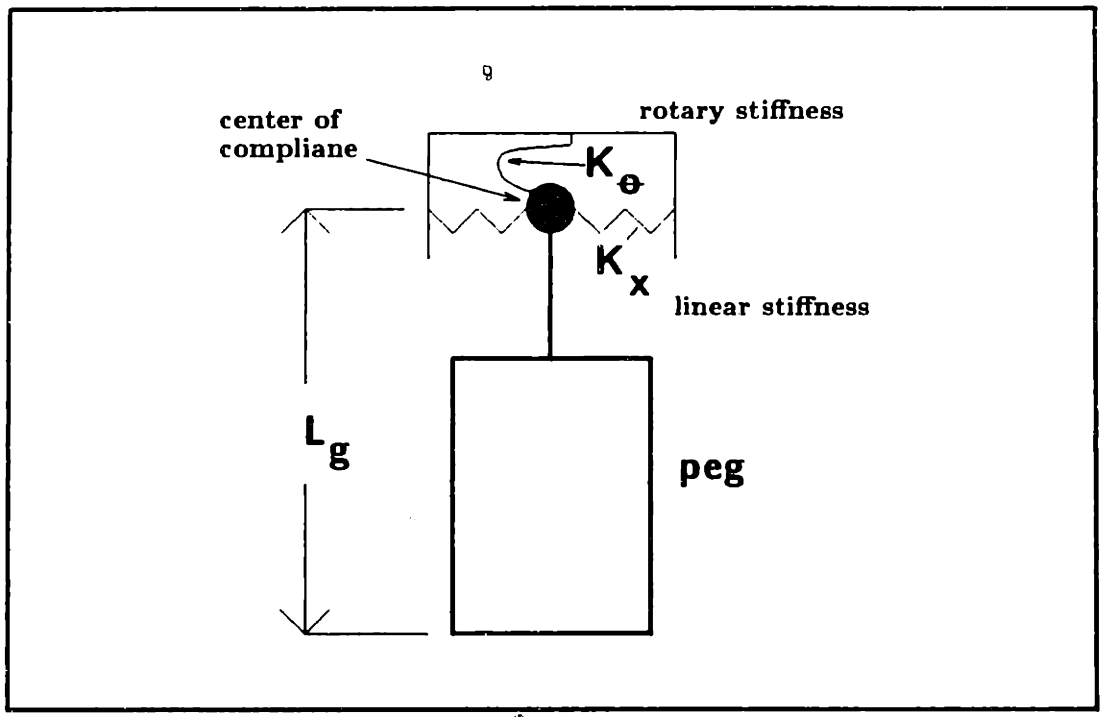

Figure 2.11: Mathematical representation for a compliant support.

crossing, 1-point contact, and 2-point contact are:

- Chamfer crossing:

$$F_z = \frac{K_z K_\theta A(\frac{z}{tan\alpha})}{(K_z L_y^2 + K_\theta)B - K_z L_y r A} \tag{2.3}$$

where:

$$A = \cos(\alpha) + \mu \sin(\alpha) \tag{2.4}$$

$$B = \sin(\alpha) - \mu \cos(\alpha) \tag{2.5}$$

- 1-point contact:

$$F_z = \frac{\mu K_x K_\theta (\acute{\epsilon}_\circ + l\theta_\circ)}{C(L_y - l) + K_\theta} \tag{2.6}$$

where:

$$\acute{\epsilon}_\circ = \epsilon_\circ - cR \tag{2.7}$$

$$c = \frac{R - r}{R} \tag{2.8}$$

$$C = K_x(L_y - l - \mu r) \tag{2.9}$$

- 2-point contact:

$$F_z = \frac{2\mu}{l}[G(\theta_\circ - c\frac{D}{l}) + E] + \mu(1 + \mu\frac{d}{l})[F(\theta_\circ - c\frac{D}{l}) - \frac{E}{L_y}] \tag{2.10}$$

where:

$$G = K_x L_y^2 + K_\theta \tag{2.11}$$

$$E = K_x L_y(\epsilon_\circ + cR) \tag{2.12}$$

$$F = -K_x L_y \tag{2.13}$$

For a description of all the symbols in the above equations refer to Table 2.7.

2.6.2 Results Using the PMM

A peg and hole insertion using the same parameters as the CSDL experiment presented before was conducted using the parts mating machine (an RCC was not used). A hardened (Rockwell C 60) and ground steel hole with a diameter of $0.5004\,in$ was used. A 440 stainless steel peg was ground to a diameter of $0.4991\,in$. Note that

Symbol	Description
K_x	lateral stiffness
K_θ	angular stiffness
μ	coefficient of friction
z	insertion depth during chamfer crossing
α	chamfer angle
L_g	support location (see Fig. 2.11)
r	peg radius
R	hole radius
d	peg diameter
D	hole diameter
l	insertion depth after chamfer crossing
c_o	initial linear offset
θ_o	initial angular offset
c	clearance ratio

Table 2.7: Symbol description.

even though the diameters of the peg and hole were not the same as those of the Draper experiment, the clearance ratio was kept the same (0.0026).

The main difference between an RCC and the parts mating machine lies in the location of the linear stiffness, K_r. As seen in Figure 2.11, for the RCC the linear stiffness is located at the center of compliance with the rotary stiffness. However, a two dimensional model for the parts mating machine (see Figure 2.12) shows that the linear stiffness is located with the hole, and the rotary stiffness with the peg, similar to a RCC. For an RCC the center of compliance moves vertically (insertion direction) and laterally. For the PMM, the location where the rotary stiffness acts around only moves vertically. The effects of this difference in the location of the linear stiffness on the measured results will be discussed at a later time.

A plot of insertion force vs. insertion depth using the parts mating machine is shown in Figure 2.13. As can be seen in the figure, the plot has the same shape as the plot in Figure 2.9. It clearly shows the three main regions of chamfer crossing (cc), 1-point contact, and 2-point contact. The main differences between the two plots lie in the magnitudes of the forces during:

- chamfer crossing
- 1-point contact
- 2-point contact

The difference in the magnitude of the forces in the three regions can be explained by a different coefficient of friction, μ, between the two experiments. In the CSDL experiment the coefficient of friction was found empirically from 1-point contact data to equal roughly 0.1 (see Whitney [20]).

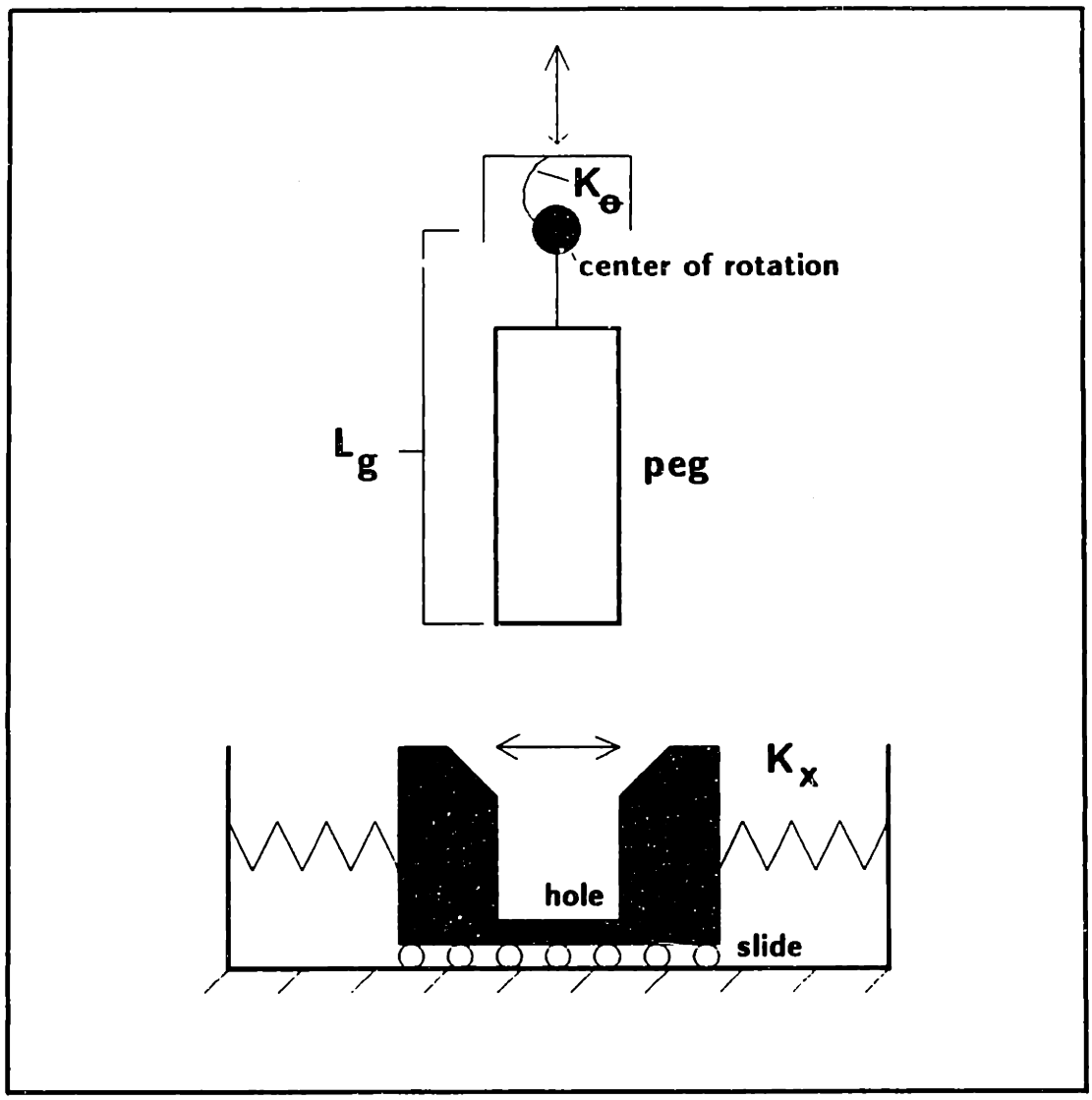

Figure 2.12: A two dimensional model for the parts mating machine .

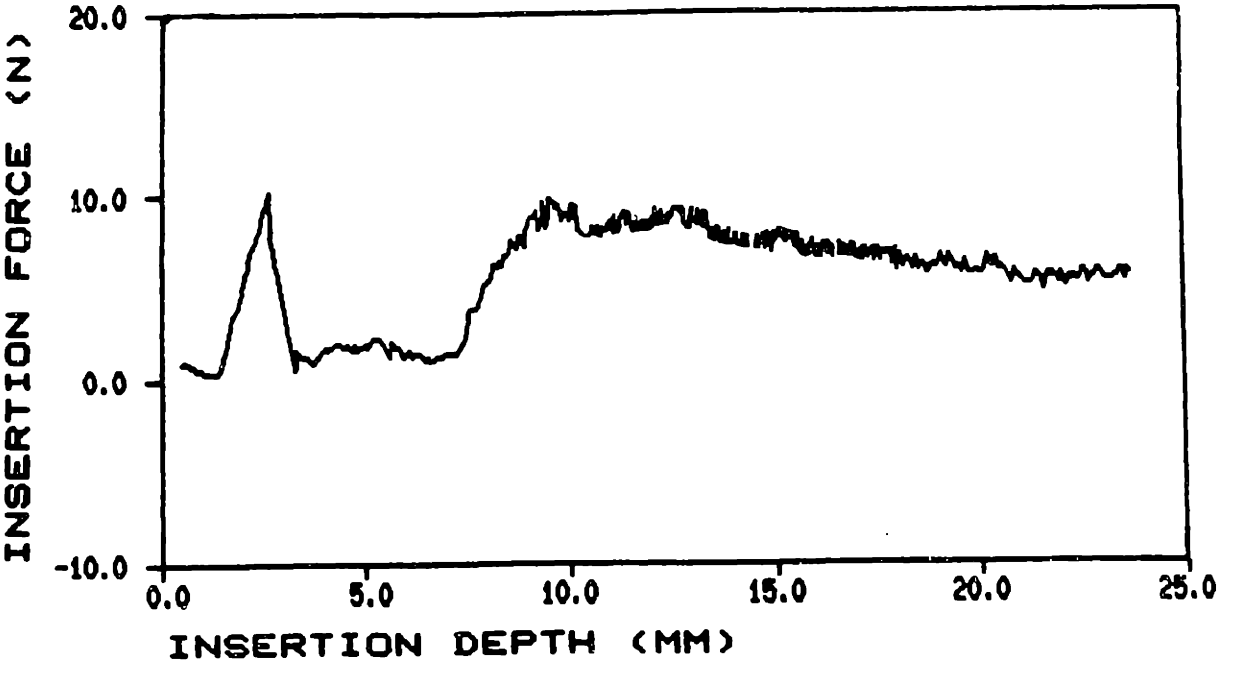

Figure 2.13: Reproduction of CSDL experiment using the PMM: insertion force vs. insertion depth.

For conditions of slip, and for the region of chamfer crossing, the coefficient of friction, μ, can be inferred by measuring the insertion force, F_z, and the lateral force, F_x, and using the following equation (see Appendix A for derivation):

$$\mu = \frac{F_z - F_x}{F_z + F_x} \tag{2.14}$$

Equation 2.14 is for a chamfer of 45°. Note that this equation a way to determine μ empirically, and does not imply that the coefficient of friction is a function of F_z and F_x.

Using the data obtained from the experiment with the parts mating machine , the coefficient of friction was found to be 0.25. Using this value in Equation 2.3, the maximum insertion force is $10.27\,N$ (for $z = 1.06\,mm$ and $\alpha = 45°$). This result close is to $10.15\,N$, which was measured with the PMM.

Using this same coefficient of friction in Equation 2.6, yields an insertion force during 1-point contact of $1.90\,N$ at an insertion length of $2.5\,mm$. Again, this result is close to the one measured using the PMM of $1.82\,N$ (at a length of $2.5\,mm$).

To obtain the coefficient of friction during 2-point contact a simple experiment was conducted (see Figure 2.14). A thin steel peg was inserted at an angle in the hole previously used in the experiment. A known normal force was applied, and the insertion force (which equaled the frictional force) was measured. Using this setup, the coefficient of friction was found to be 0.34 (from $\mu = \frac{F_z}{F_x}$). Using this value for μ in Equation 2.10, yields a maximum insertion force during 2-pt contact of $9.68\,N$ (at a length of $9.03\,mm$). This new value is close to the maximum insertion force measured with the PMM, which equaled $9.97\,N$ (at a length of $9.4\,mm$).

A careful comparison of Figures 2.9 and 2.13 shows that 2-point contact did not start at the same insertion depth. For the Draper experiment two point contact started

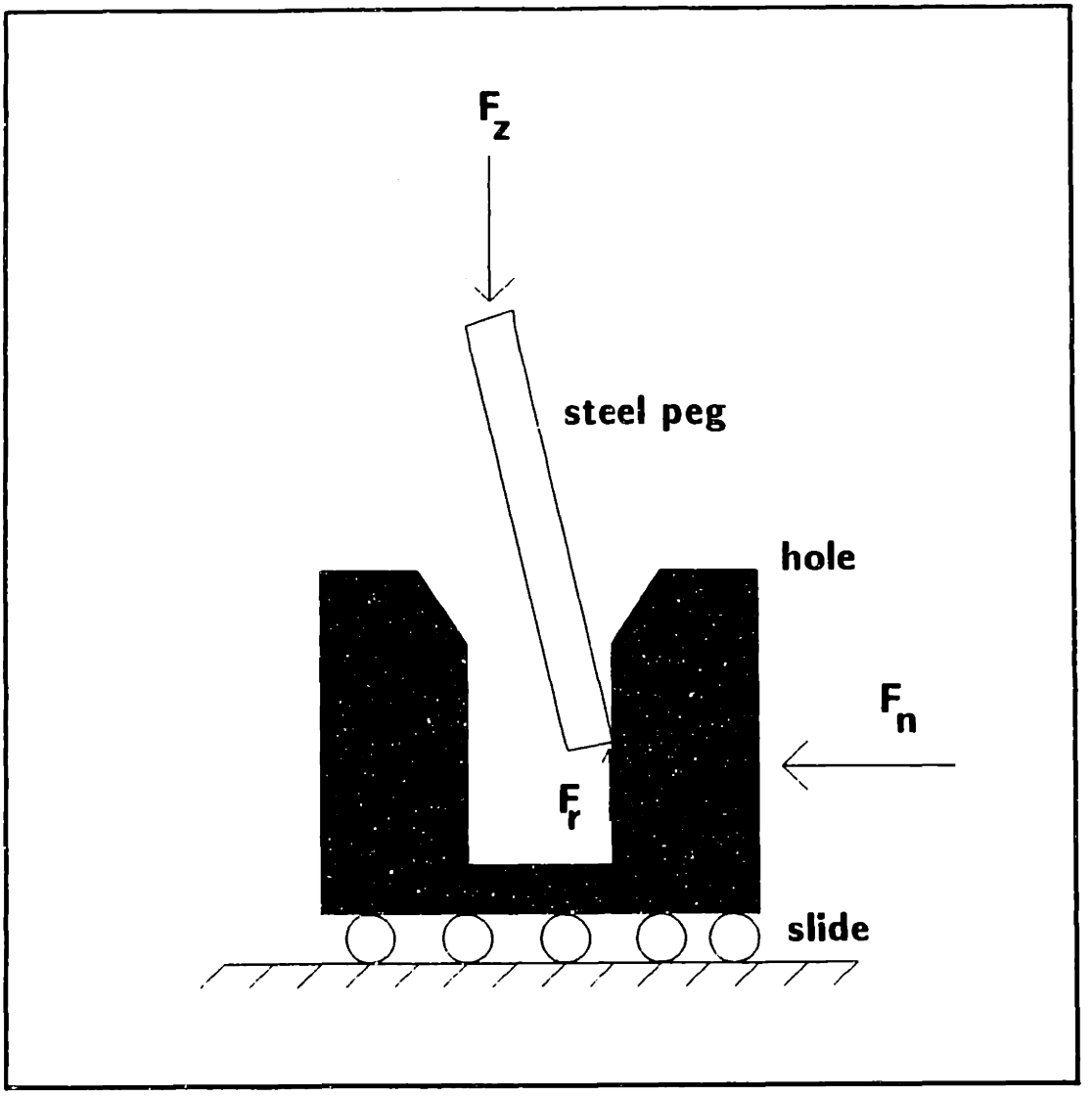

Figure 2.14: Experimental setup used to determine the coefficient of friction.

5% Change in:	Decreases l_2 by [mil]:
L_y	.24
K_x	.26
K_θ	.27
ϵ_o	.32
c	.33

Table 2.8: Effect of some assembly parameters on the location where 2-pt contact starts.

at an insertion length of $5.4\,mm$ (Figure 2.9) and for the PMM it started at $4.18\,mm$ (Figure 2.13). The difference is small, and can be attributed mainly to errors in the different assembly parameters. Refer to Table 2.8 for an example of the effects of some parameters on the location where 2-pt contact starts, labeled as l_2.

Figure 2.15 shows a plot of the lateral force vs. insertion depth using the parts mating machine . The plot shows the same shape as Figure 2.10. Both plots increase rapidly, level out, and then increase slightly. No main differences between the two plots is found.

2.6.3 Conclusion

As seen from the above analysis, the differences between the results of the experiment conducted at Draper Laboratories and that done with the parts mating machine are explained by a different coefficient of friction. That is, the differences were due to an inequality in the parts used, and not due to errors in the PMM. Therefore, it can be concluded that the parts mating machine gives reliable results and that the calibration

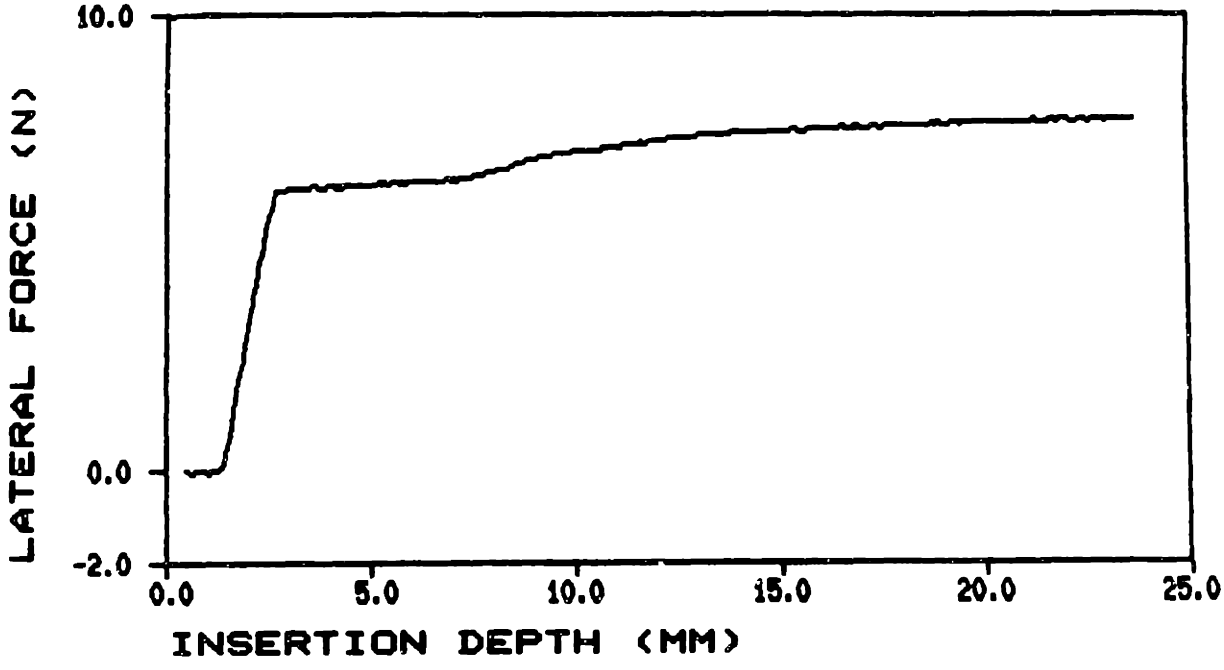

Figure 2.15: Reproduction of CSDL experiment using the PMM: lateral force vs. insertion depth.

procedure was correctly performed.

The equations derived by Whitney [20] for the case of a 2-dimensional peg and hole insertion using a RCC predict the insertion forces obtained using the parts mating machine. This suggests that the location of the linear compliance did not affect the insertion forces observed in the experiment.

Experimental Results

Chapter 3

3.1 Introduction

The following chapter presents experimental results obtained with the parts mating machine. The effects of four parameters were investigated: positional errors, axes stiffness, angular errors, and location of the center of rotation.

It must be pointed out that due to the large amount of information obtained in each experiment (i.e. forces, moments, rotations, and displacements), only results on insertion forces will be presented in this thesis. Data on lateral forces and moments will be left for future analysis. Two groups of insertion forces will be investigated: maximum insertion forces during and after chamfer crossing.

Figure 3.1 shows a typical plot of insertion force vs insertion depth. This plot shows the force behavior during the three ideal assembly stages: chamfer crossing, 1-point contact, and 2-point contact. Figure 3.1 also shows the maximum insertion forces (MIF) during chamfer crossing and after chamfer crossing. This chapter investigates the effects of parameters on these two types of insertion forces.

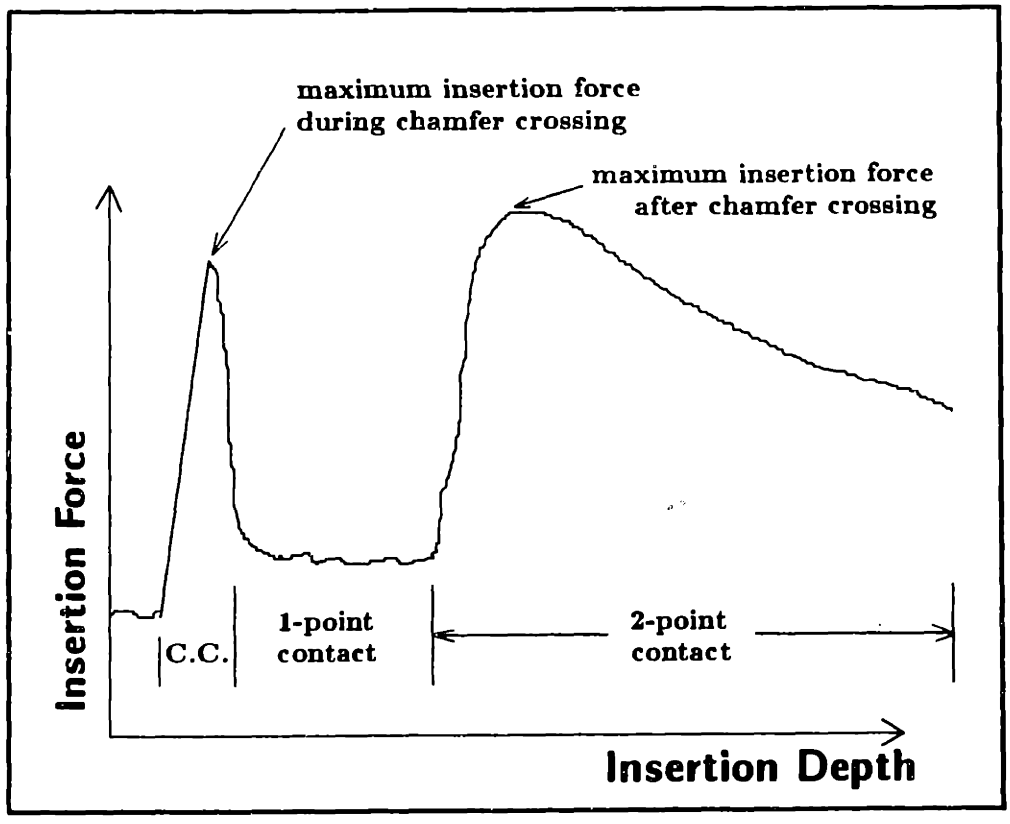

Figure 3.1: Typical insertion force vs insertion depth plot showing maximum insertion forces.

Figure 3.2: Peg and hole used to conduct the experiments.

3.2 Parts Analyzed

The peg and a hole shown in Figure 3.2 were the parts used in all experiments. A ground stainless steel peg with a diameter of 0.4990 in. and stainless steel hole with a diameter of .5020 in. were used. The hole had a 45° straight chamfer.

3.3 Experimental Procedure

3.3.1 Assembly Parameters

Before every experiment was conducted the following assembly parameters had to be specified:

1. positional errors
2. angular errors
3. location of the center of rotation
4. linear stiffness
5. angular stiffness

The initial assembly conditions are determined by the initial positional and angular errors. These initial conditions are added to the value of the stiffnesses (linear and rotary) and to the location of the COR to give all information necessary to characterize each assembly operation. That is, by specifying the above parameters, the assembly state is determined.

3.3.2 Notation

The location of the center of rotation with respect to the assembly parts is an important parameter to be studied. As seen in Figure 3.3, the distance between the center of rotation and the tip of the peg is given by L_y. The center of rotation (COR) was defined in Chapter 2 as the point where the axis of rotation of the yoke and gimbal intercept.

Positional errors in the X and Y linear directions, E_x and E_y, are defined as the distance between the location of the center of rotation and the centerline of the hole (see Figure 3.3). Angular errors about X and Y, θ_x and θ_y, are defined positive for counter clockwise rotations about the COR as shown in Figure 3.3. The axis stiffness in the linear degrees of freedom is labeled by K_x and K_y for the X and Y linear axes respectively. The rotary stiffness in the X, Y, and Z degrees of freedom are labeled

Table 3.1: Notation description.

Symbol	Meaning
K_x, K_y	linear stiffness in X, and Y
$K_{\theta x}$, $K_{\theta y}$	rotary stiffness in X, and Y
L_g	distance from the tip of the peg to the location of the center of rotation
γ	rotary-to-linear stiffness ratio, $\frac{K_y}{K}$
E_x, E_y	positional errors in X, and Y
θ_x, θ_y	angular errors in X, and Y

by $K_{\theta x}$, $K_{\theta y}$, and $K_{\theta z}$ respectively. Another parameter to be used is the ratio of rotary-to-linear stiffness, labeled by γ. Table 3.1 summarizes the notation used.

3.3.3 Procedure

To conduct every experiment, the following procedure was followed: the desired stiffness for each axes was set and the location of the COR adjusted to the desired value. The peg and hole were then mated and a shim was placed between the peg and hole to assure the peg axis was parallel to the hole axis. While the parts were mated the LVDT readings were noted and the encoders were reset to zero. The peg was then raised. The desired positional and angular errors were introduced by noting the LVDT and encoder output. After the errors had been included, the peg and hole were mated, while the data acquisition was taking place. The raw data was then calibrated, the maximum insertion force during assembly was determined from the data, and then plotted.

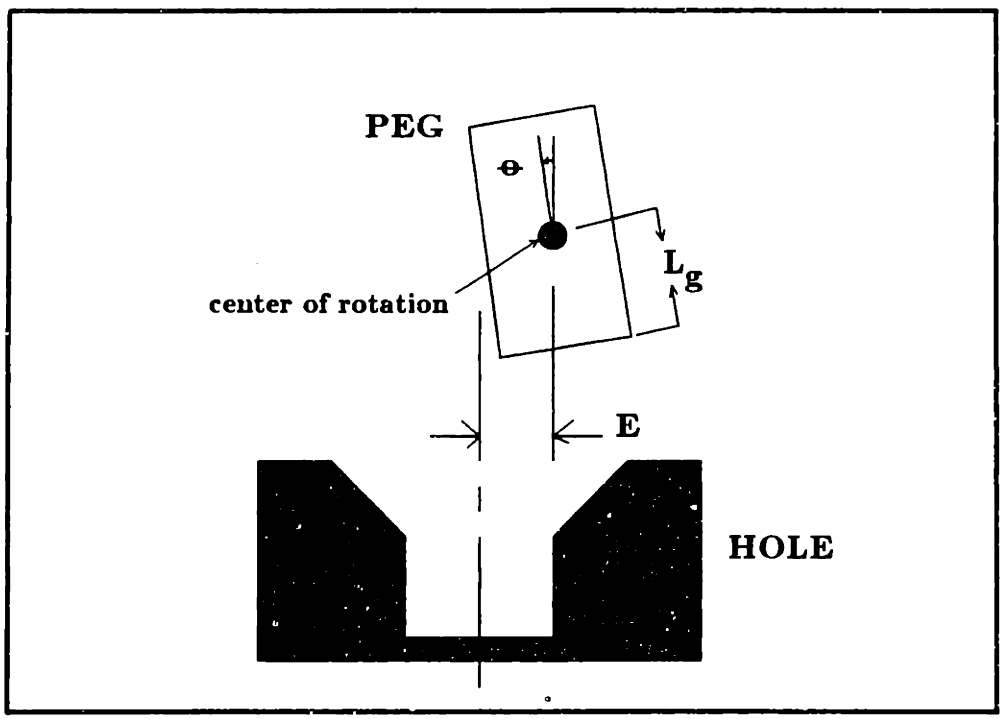

Figure 3.3: Notation used for positional and angular errors.

In setting the stiffnesses and errors, symmetry was assumed. That is, $K_x = K_y$, $E_x = E_y$, $K_{\theta x} = K_{\theta y} = K_{\theta z}$, and so on.

3.3.4 Graphical Techniques

As seen in the following graphs, the effect of different parameters on maximum insertion force during assembly was investigated. To do so, plots of insertion force vs the parameter analyzed were used. The units used are [ounces] for force, [lb/in] for linear stiffnesses, [lb-in/rad] for rotary stiffnesses, [thousanths] for positional errors, and [degrees] for angular errors. In the plots, three points were used most of the time to determine each curve. Preliminary results were conducted and it was determined that using three was sufficient to determine a curve and to investigate the effects of the parameters on assembly. Also, three points per curve had to be used to lower the number of experiments that had to be conducted to a reasonable number.

3.4 Experimental Results and Discussion

The following four sections include graphs showing the effects of positional errors, angular errors, axes stiffness, and location of the center of rotation on MIF. A table is included in each section to summarize the experiments conducted for each parameter.

3.4.1 Effect of Positional Errors

Table 3.2 shows the experiments conducted to investigate the effects of positional errors on MIF.

Figures 3.4 and 3.5 show, for the case of a stiffness ratio of one, the effects on insertion forces of positional errors in X and Y. Figure 3.4 shows peak forces during

Table 3.2: Experiments conducted to investigate the effects of positional errors

Figures	L_g $[inches]$	K_x, K_y $[\frac{lb}{in}]$	$K_{\theta x}, K_{\theta y}, K_{\theta z}$ $[\frac{lb-in}{rad}]$	θ_x, θ_y $[radians]$	E_x, E_y $[thousanths]$	γ
3.5, 3.4	1.25	67	67	0	30,40,50	1
	1.25	50	50	0	30,40,50	1
	1.25	30	30	0	30,40,50	1
3.7, 3.6	1.25	67	67	0	30,40,50	1
	1.25	80	160	0	40,50,70	2
	1.25	60	290	0	70,80,90	4.8

2-point contact and Figure 3.5 shows peak forces during chamfer crossing. Positional errors varied from 30 to 50 thousanths. It is observed that as the stiffness of the structure increases, the insertion forces increase. That is, the stiffer the structure the harder it is to absorb a positional error. However, note that the sensitivity of MIF after chamfer crossing to changes in the stiffness decreases as the positional errors decrease. For example, at an error of 30 thousanths the insertion forces are roughly the same regardless of the stiffness of the structure. From Figure 3.5 it is seen that MIF during chamfer crossing vary linearly as the positional errors are increased.

Figures 3.7 and 3.6 show the effects on MIF of positional errors for different stiffness ratios. Figure 3.6 shows how positional errors affect MIF after chamfer crossing for stiffness ratios of 1, 2, and 4.8. As γ is increased (with no angular errors present) MIF decrease for a given positional error. This is the case because as the ratio increases, the angular errors produced as a side effect of absorbing the initial positional errors are minimized. Therefore, tilt of the peg and the occurrence of

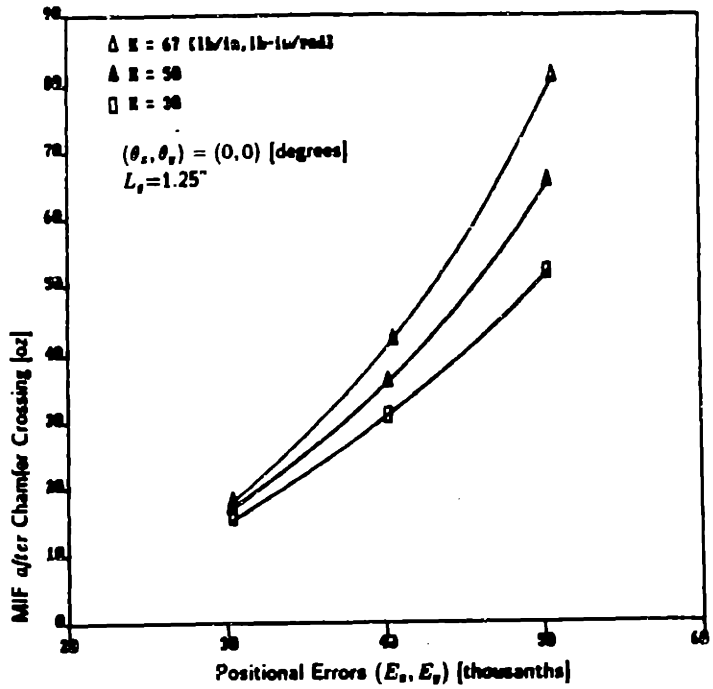

Figure 3.4: Effect of positional errors on maximum insertion forces (MIF) *after* chamfer crossing for a stiffness ratio equal to one.

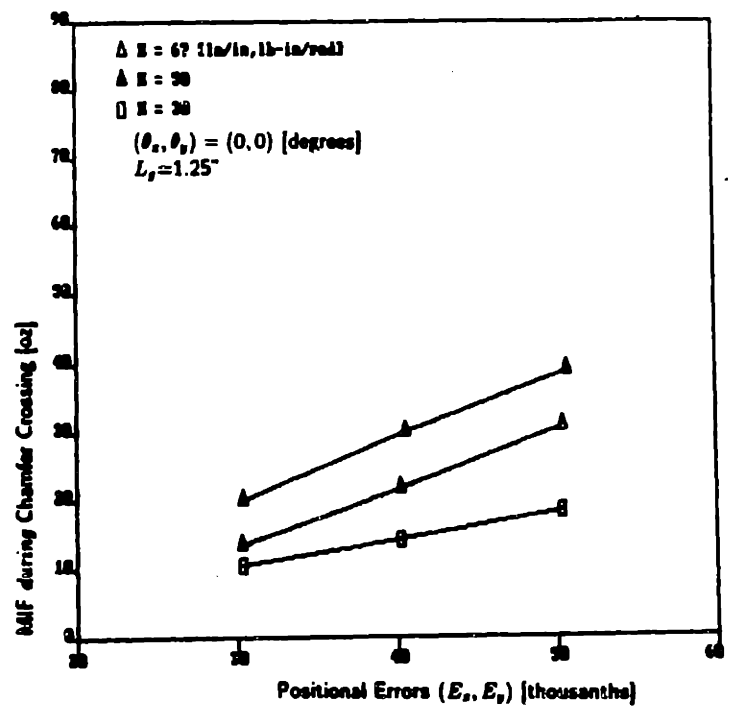

Figure 3.5: Effect of positional errors on maximum insertion forces (MIF) *during* chamfer crossing for a stiffness ratio of one.

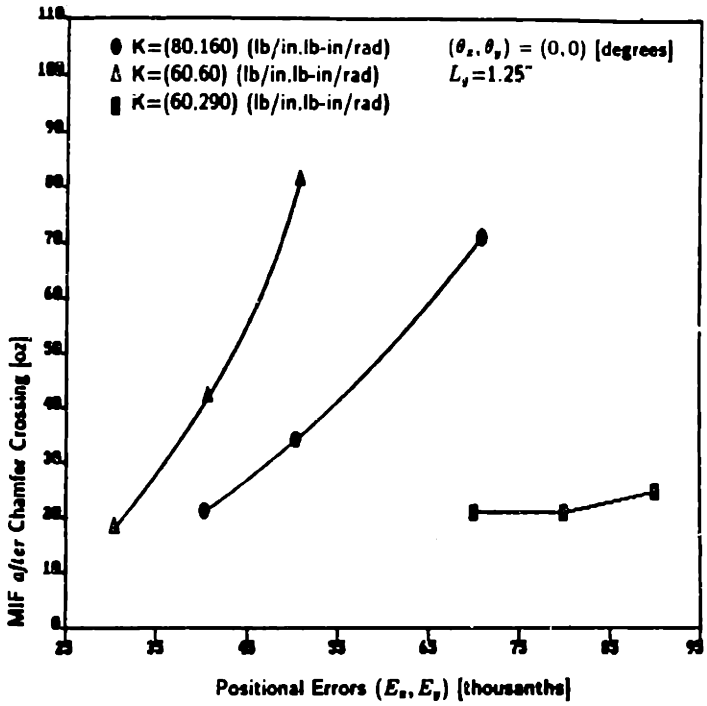

Figure 3.6: Effect of positional errors on MIF after chamfer crossing for stiffness ratios of 1, 2, and 4.8.

two point contact are reduced. As seen from this graph, it is desirable to have high stiffness ratios, when no angular errors are present, to minimize MIF and be able to absorb large positional errors.

The above graphs show that MIF during chamfer crossing vary linearly with positional errors, regardless of the axes stiffness or ratio of rotary to linear stiffness. Also, the graphs show that to absorb positional errors under no angular errors, large γ are desired. This finding explains why most RCC devices commercially available have high ratios (of six and higher).

3.4.2 Effect of Axes Stiffness

Table 3.3 shows the experiments conducted to investigate the effects on MIF of the axes stiffnesses: $K_x, K_y, K_{\theta x}, K_{\theta y}$, and $K_{\theta z}$. That is, the linear and rotary stiffnesses.

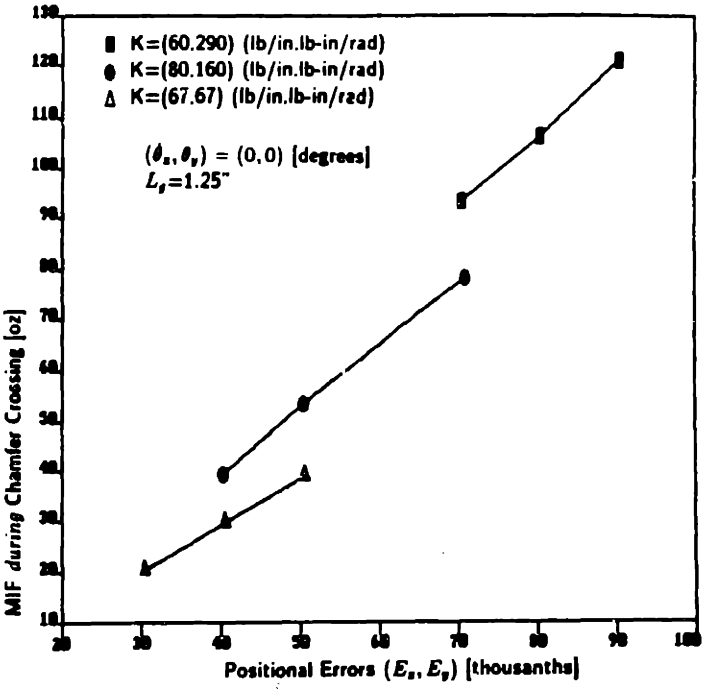

Figure 3.7: Effect of positional errors on MIF during chamfer crossing for stiffness ratios of 1, 2, and 4.8.

Recall that $K_x = K_y$ and so on due to the symmetry assumption.

Figure 3.8 shows the effect of changing the ratio of rotary to linear stiffness for a positional error of 50 thousanths. As the ratio increases from 0.5 to 2.0, forces after chamfer crossing decrease, and forces during chamfer crossing increase. As γ increases, the positional error is mostly absorbed by motion of the hole and not by rotation of the peg. Therefore, angular errors and forces are minimized. This is the same effect observed in Figure 3.6. Note that as the ratio increases, the decrease in MIF after chamfer crossing, is larger than the increase in MIF during chamfer crossing.

Figures 3.9 and 3.10 show the effects of varying the axes stiffness for three positional errors while keeping a γ of 2. MIF during chamfer crossing vary linearly as the stiffness is increased. The stiffer the structure, the larger the forces generated when absorbing a given positional error. Similarly, the larger the positional error, the larger

Table 3.3: Experiments conducted to investigate the effects of the axes stiffness.

Figures	L_y $[inches]$	K_x, K_y $[\frac{lb}{in}]$	$K_{\theta x}, K_{\theta y}, K_{\theta z}$ $[\frac{lb-in}{rad}]$	θ_x, θ_y $[radians]$	E_x, E_y $[thousanths]$	γ
3.8	1.25	80.80.80	40.80.160	0	50	.5.1.2
3.10.3.9	1.25	32.55.80	66.112.161	0	40	2
	1.25	32.55.80	66.112.161	0	50	2
	1.25	32.55.80	66.112.161	0	60	2
3.11	1.25	67.50.30	67.50.30	0	50	1

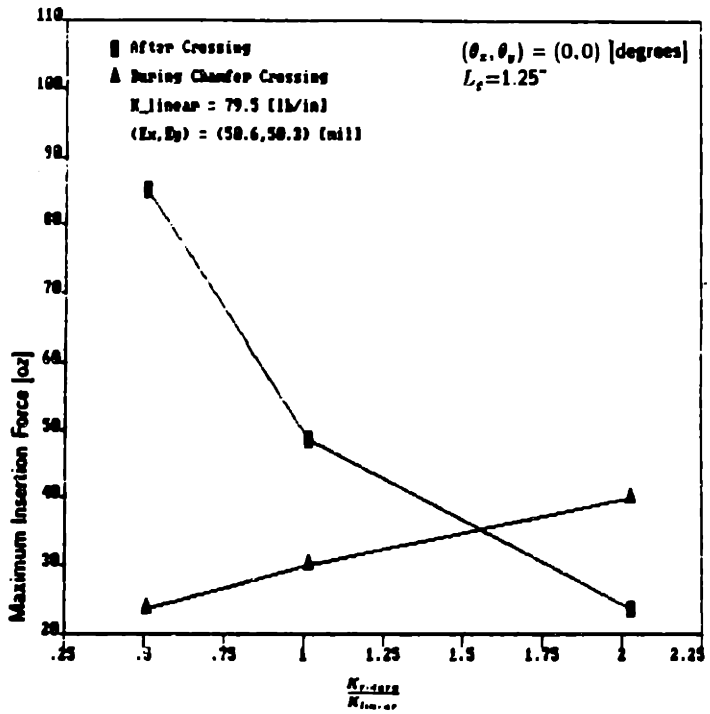

Figure 3.8: Effect of changing the stiffness ratio for a positional error of 50 thousanths.

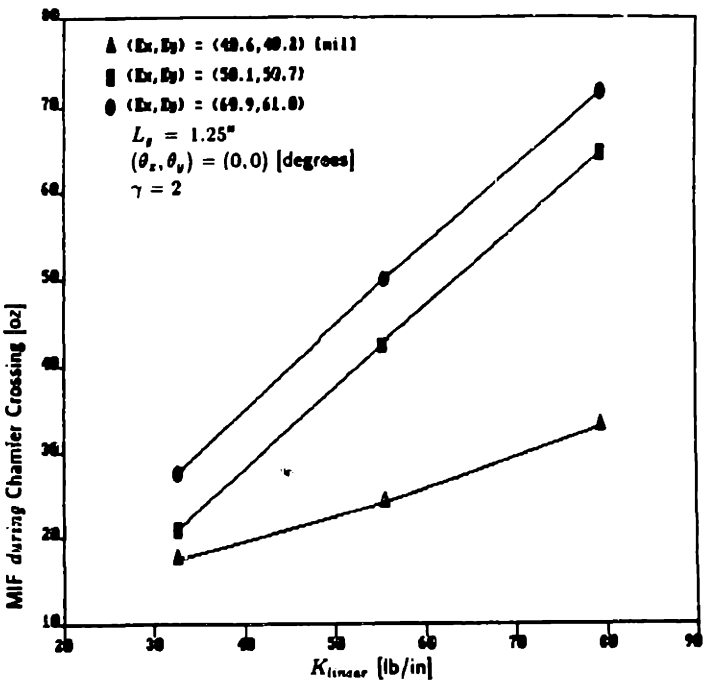

Figure 3.9: Effect of changing the axes stiffness on MIF during chamfer crossing for three positional errors and a γ of 2.

the forces generated for a given stiffness. MIF after chamfer crossing vary linearly with stiffness. Again, it is observed that as the errors increase, the forces also increase. However, the slope of the plots changes. Figure 3.10 suggests that the sensitivity of the assembly to changes in axes stiffness decreases as the positional errors decrease. The same result is observed in Figure 3.4.

Figure 3.11 shows the effects of changing the stiffness for a γ of 1 and a positional error of 50 thousanths. Again, both plots in the figure are linear, as was the case with a γ of 2.

The effects on MIF of two stiffness ratios, 1 and 2, are shown in Figures 3.12 and 3.13. For MIF during chamfer crossing, the forces generated are similar for a γ of 1 and 2. However, for MIF after chamfer crossing the difference in MIF is significant. For a γ of one, MIF can be 50 ounces or more larger than for a γ of 2. This result

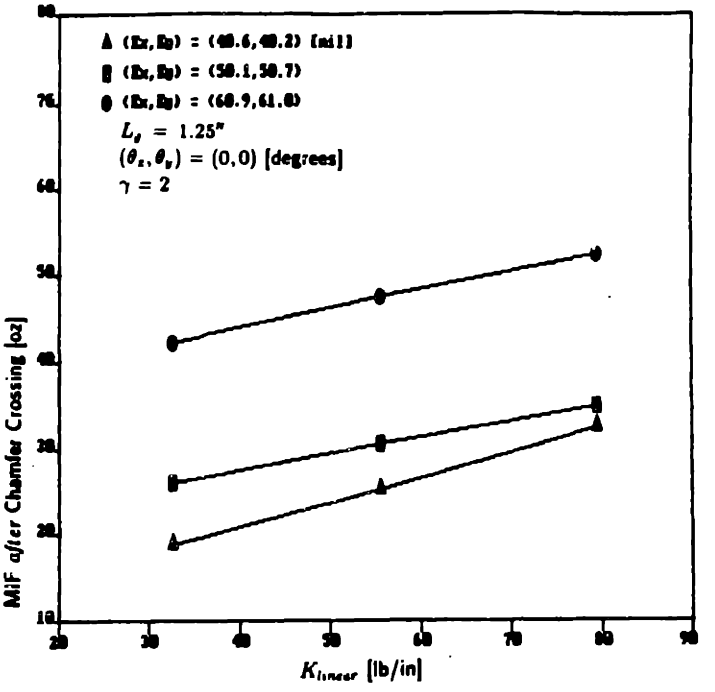

Figure 3.10: Effect of changing the axes stiffness on MIF after chamfer crossing for three positional errors and a γ of 2.

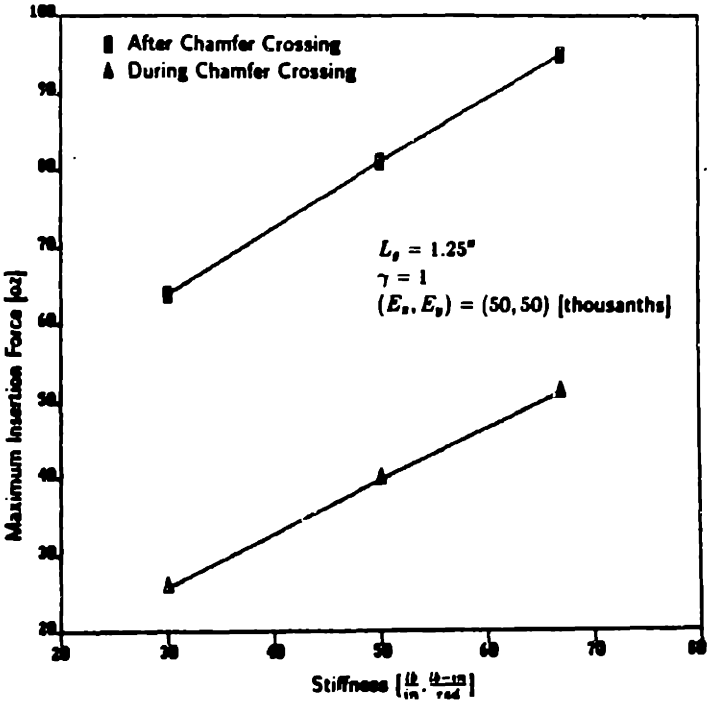

Figure 3.11: Effect of changing the axes stiffness for a γ of 1.

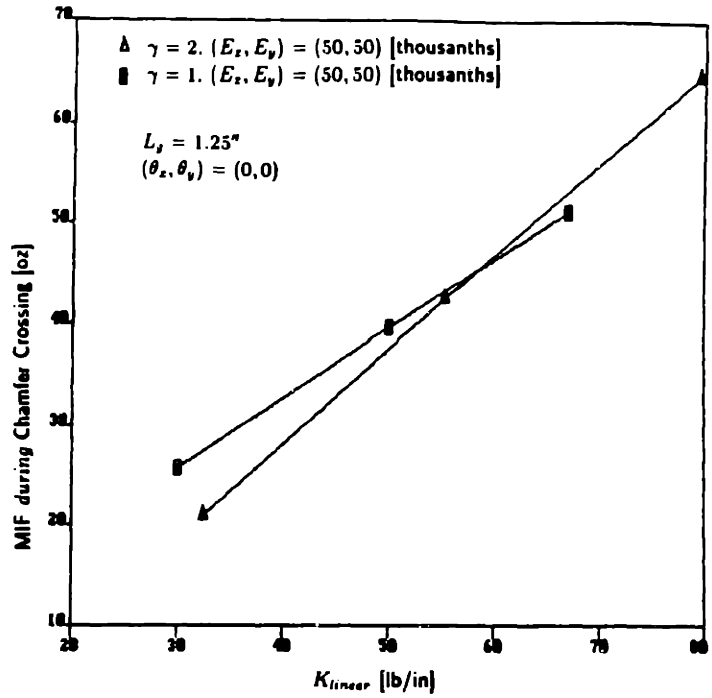

Figure 3.12: Effect of two stiffness ratios of 1 and 2 on MIF during chamfer crossing.

agrees with the previous ones that under no angular errors MIF after chamfer crossing decrease as the stiffness ratio increases.

3.4.3 Effect of Angular Errors

Table 3.4 shows the experiments conducted to investigate the effects of angular errors on MIF.

Figures 3.14 and 3.15 show the effects of angular errors on MIF during chamfer crossing for three positional errors and a stiffness ratio of 1. As seen in Figure 3.14 the forces during chamfer crossing all vary essentially linearly with positional errors for a given angular error. Also, as the errors increase, the forces increase because the peg is pointed more directly towards the chamfer. Figure 3.15 contains the same information as Figure 3.14, but is plotted differently. In this case, MIF during chamfer crossing are plotted versus angular errors. Using Figure 3.15, MIF generated due to a

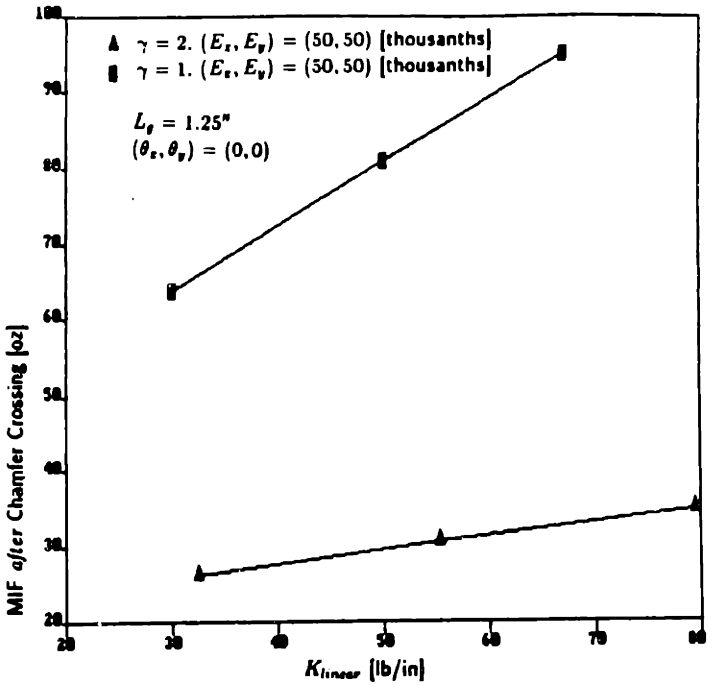

Figure 3.13: Effect of stiffness ratios of 1 and 2 on MIF after chamfer crossing.

Table 3.4: Experiments conducted to investigate the effects of angular errors.

Figures	L_y $[inches]$	K_x, K_y $[\frac{lb}{in}]$	$K_{\theta x}, K_{\theta y}, K_{\theta z}$ $[\frac{lb-in}{rad}]$	θ_x, θ_y $[degrees]$	E_x, E_y $[thousanths]$	γ
3.14,3.15	1.25	67	67	-.99	30,40,50	1
3.16,3.17	1.25	67	67	0	30,40,50	1
	1.25	67	67	.99	30,40,50	1
	1.25	67	67	1.98	30,40,50	1
3.18	1.25	80	160	1.98	30,40,50	2
3.19,3.20	1.25	32,55,80	66,112,161	0	50	2
3.21,3.22	1.25	32,55,80	66,112,161	.99	50	2
	1.25	32,55,80	66,112,161	1.98	50	2
3.23	1.25	30,50,67	30,50,67	1.98	50	1

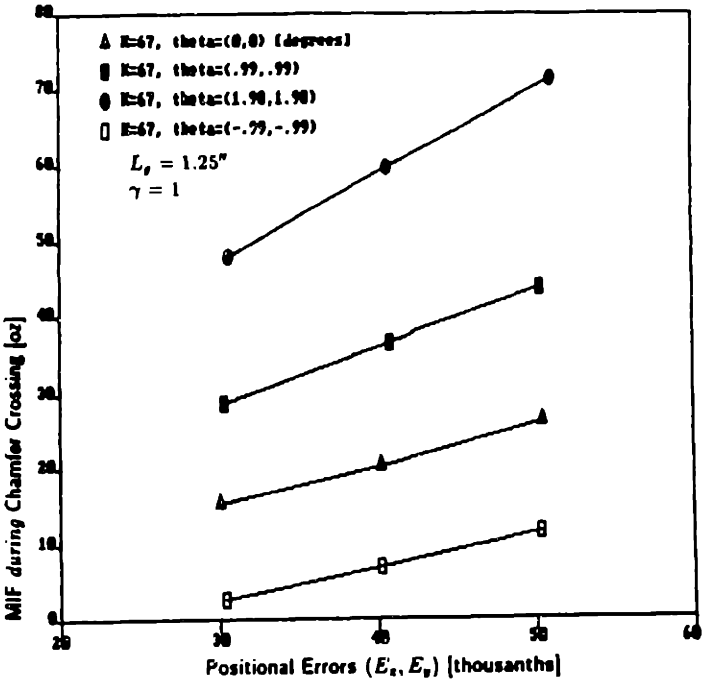

Figure 3.14: Effect of angular errors on MIF during chamfer crossing for a stiffness ratio of one.

determined angular errors can be read directly.

Figures 3.16 and 3.17 show the effects of angular errors on MIF after chamfer crossing. Figure 3.16 shows that as the angular errors increase, forces decrease. This is the case because the initial angular offset counteracts the angular error generated when absorbing the positional offset. For example in Figure 3.17, for a positional error of 30 thousanths, the peg rotates roughly one degree when crossing the chamfer. Therefore, if the initial angular error is close to one degree, the peg would be nearly vertical after chamfer crossing and only one point contact would occur. On the other hand and for the same case, if one starts with a angular error of one degree in the negative direction, the angle of the peg after chamfer crossing would be the initial angular error plus the one degree obtained when crossing the chamfer, or 2 degrees total. In this case, two-point contact occurs. Therefore, we expect higher forces when

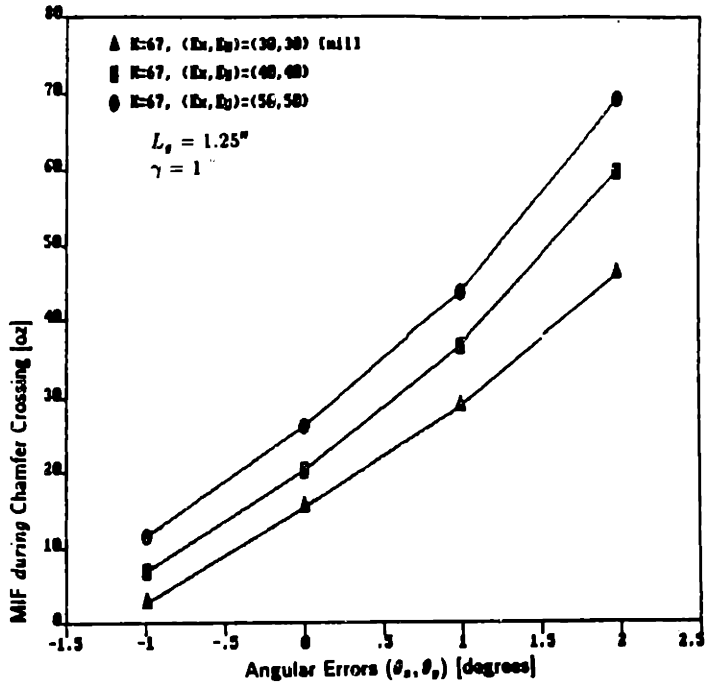

Figure 3.15: Plot of MIF during chamfer crossing vs angular errors in X and Y for a stiffness ratio of one.

we have angular errors in the negative direction. Also note that in Figure 3.17 we would expect the curves to start raising again as the angular errors increase.

Figures 3.18 shows the effects on MIF for a γ of two and a angular error of 1.98°. As before for a γ of one, the forces during chamfer crossing vary linearly with positional errors. MIF after chamfer crossing decrease as the positional errors increase from 30 to 50 thousanths. This is the case for the same reasons as explained before. With no angular errors and a positional error of 50 thousanths, the peg would rotate close to 2 degrees when crossing the chamfer (for the stiffnesses used). Therefore, for an initial angular error of 2 degrees, MIF would decrease as the positional errors approach 50 thousanths since the peg is closer to vertical after crossing the chamfer.

Figures 3.19 and 3.20 show the effects of angular errors for different stiffnesses with a ratio of two. In Figure 3.19 we see that MIF during chamfer crossing increase

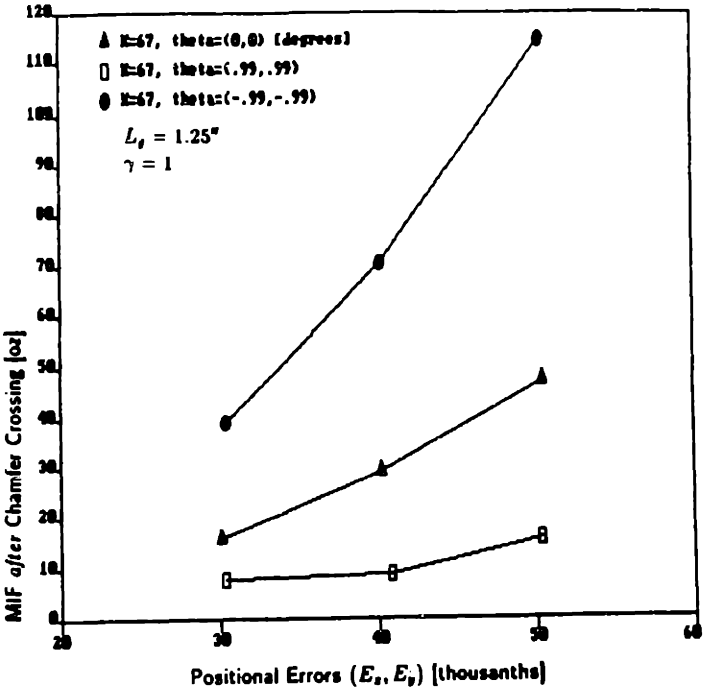

Figure 3.16: Effect on angular errors on MIF after chamfer crossing for a stiffness ratio of one.

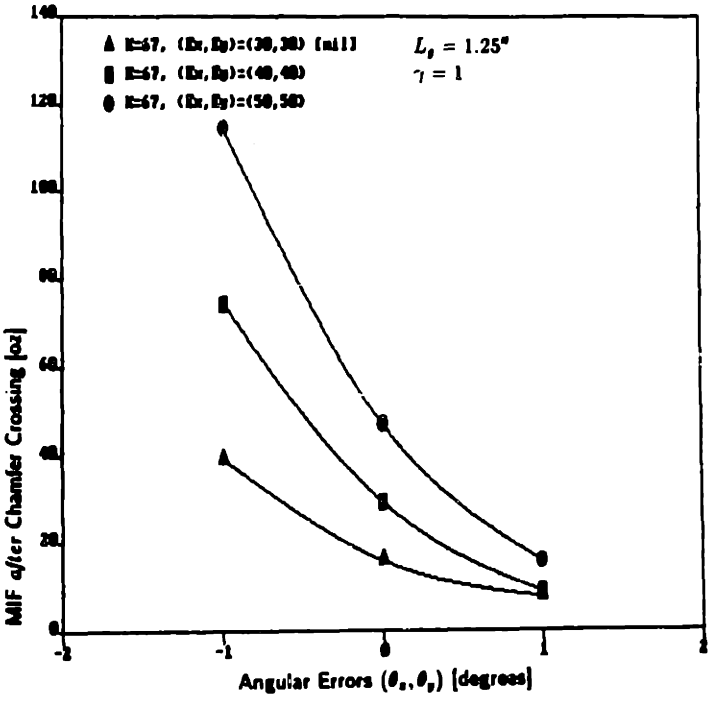

Figure 3.17: Plot of MIF after chamfer crossing vs angular errors in X and Y for a stiffness ratio of one.

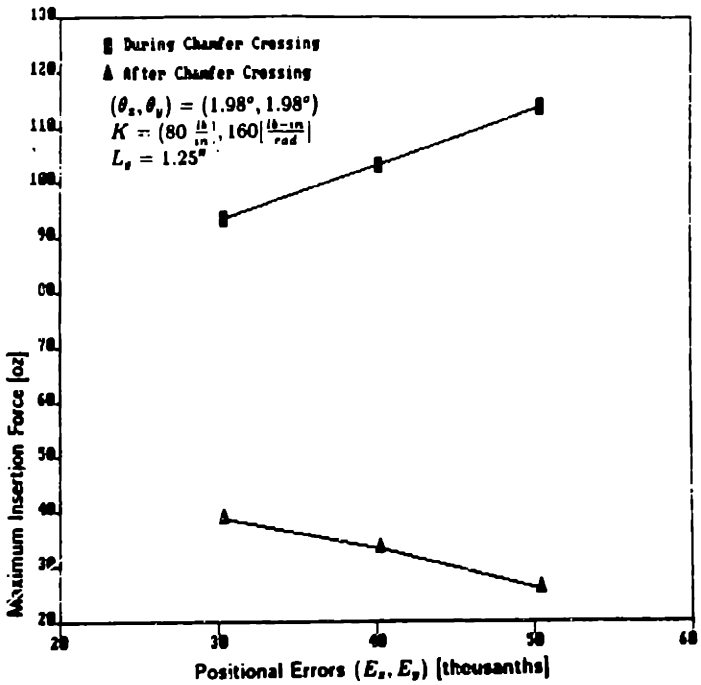

Figure 3.18: Effect of angular errors on MIF for a stiffness ratio of one.

as the angular errors increase for a positional error of 50 thousanths. This is observed because as the angular error increases, the peg is pointed more directly towards the chamfer. From figure 3.19 it is also observed that MIF increase as the stiffness increases and that the relationships are roughly linear. In Figure 3.20 we see that as the stiffness increases, the forces increase for a given angular error. Also, for each stiffness MIF increase as the angular error increases.

Figures 3.21 and 3.22 show the effects of angular errors on MIF after chamfer crossing for different stiffnesses with a ratio of two. MIF after chamfer crossing vary linearly with stiffness for a given angular error as seen in Figure 3.21. In Figure 3.22 we see that MIF increase, for a given positional errors, as the stiffness increases. Again, the curves are downward sloping due to the positional error of 50 thousanths and the counteracting effect of the angular error.

Figure 3.23 shows the effect of stiffness on MIF for a stiffness ratio of one and

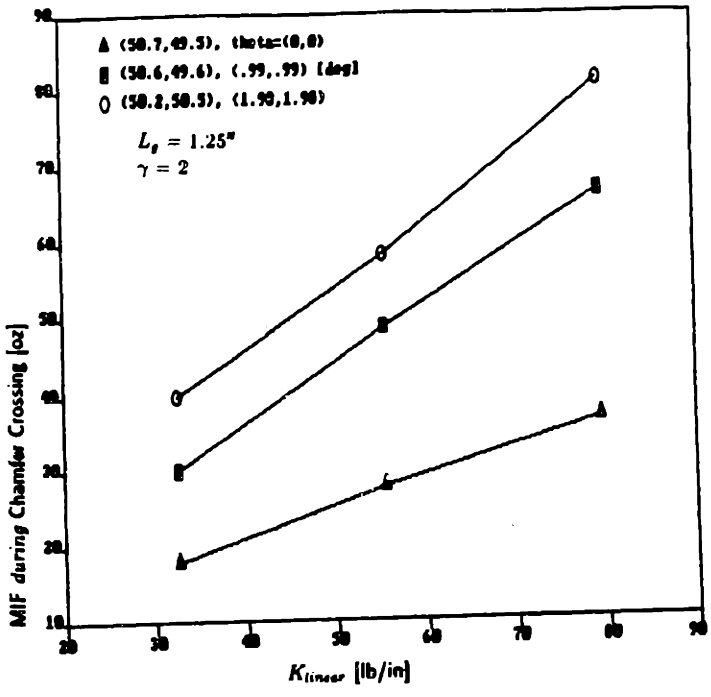

Figure 3.19: Effect of angular errors on MIF during chamfer crossing for different stiffness with a ratio of two.

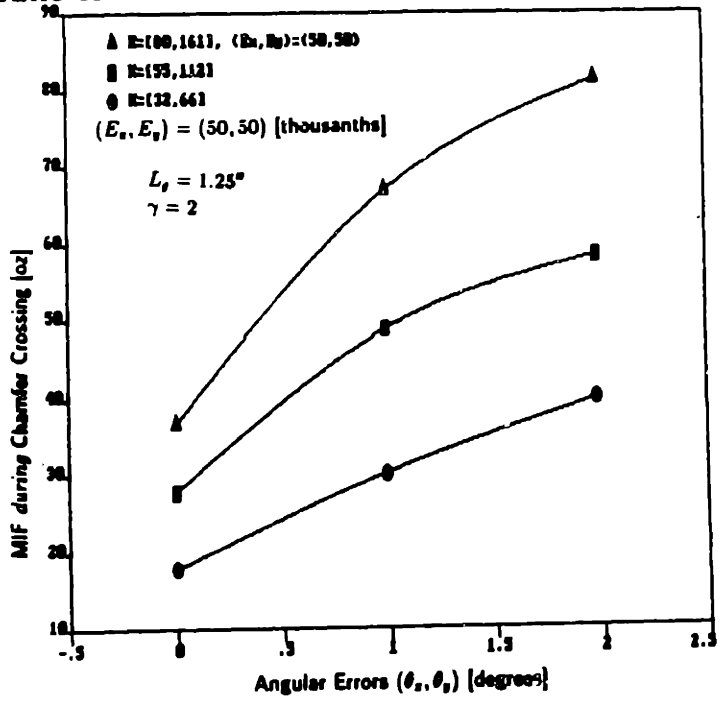

Figure 3.20: MIF during chamfer crossing vs angular errors for different stiffnesses with a ratio of two.

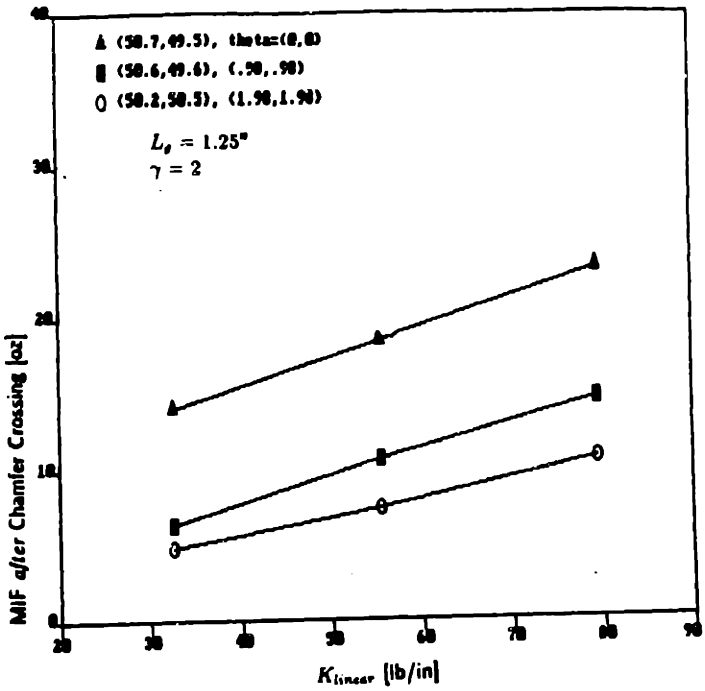

Figure 3.21: Effect of angular errors on MIF after chamfer crossing for different stiffnesses with a ratio of two.

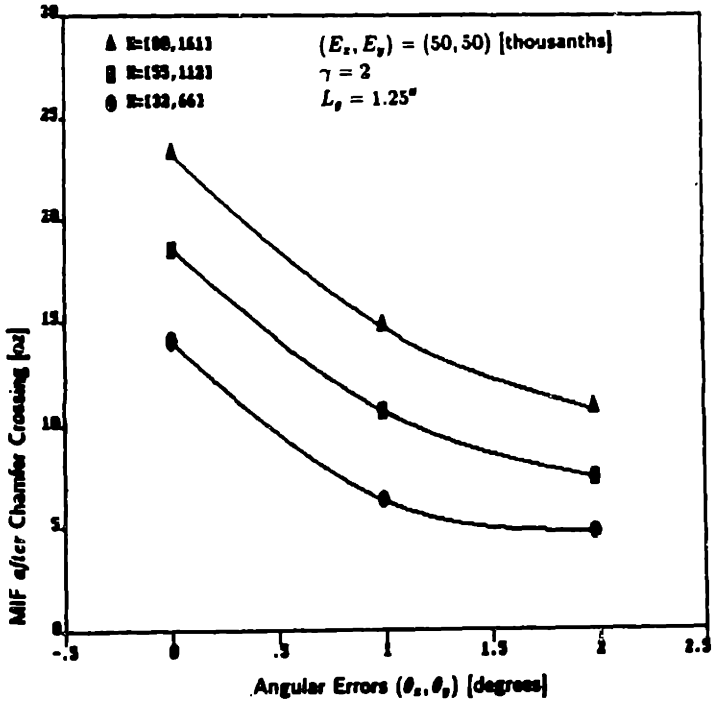

Figure 3.22: MIF after chamfer crossing vs angular errors for different stiffnesses with a ratio of two.

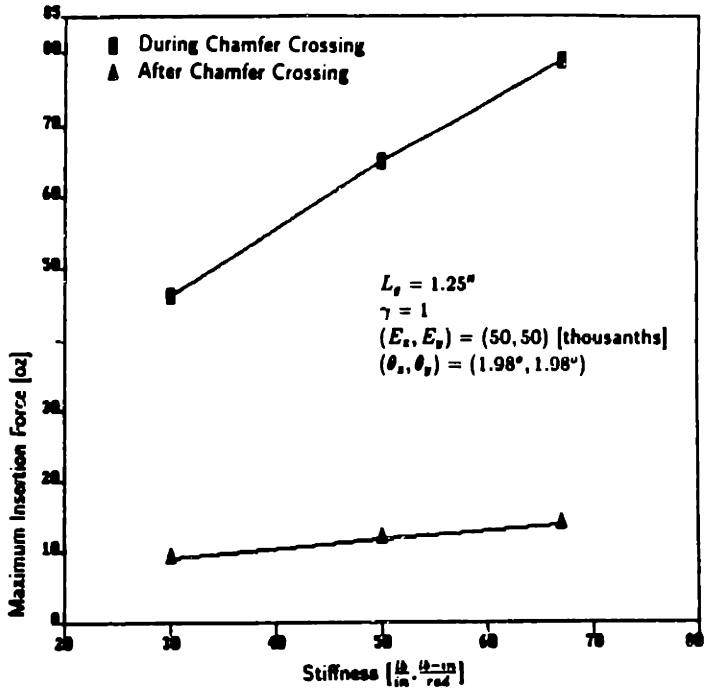

Figure 3.23: Effect of angular errors on MIF for a stiffness ratio of one.

an angular error of 1.98°. In this case, MIF during chamfer crossing vary linearly with axes stiffness. After chamfer crossing, the forces increase as the stiffness increases.

3.4.4 Effect of Location of the Center of Rotation.

The experiments presented so far were all conducted for an L_g of 1.25". Recall that L_g is the distance from the tip of the peg to the location of the center of rotation. This section shows experiments conducted to investigate the effects of different L_g on maximum insertion forces. Table 3.5 summarizes the experiments conducted.

Figures 3.24 and 3.25 show the effect on MIF of changing L_g for a stiffness ratio of one. Again we see that MIF during chamfer crossing vary linearly with positional errors. Also, we note that the the farther the COR is located from the tip of the peg (the greater L_g in the positive and negative direction) the smaller the forces encountered. As the distance from the COR to the tip of the peg increases, the moment generated

Table 3.5: Experiments conducted to investigate the effects of the location of the center of rotation with respect to the tip of the peg (L_y).

Figures	L_y $[inches]$	K_x, K_y $[\frac{lb}{in}]$	$K_{\theta x}, K_{\theta y}, K_{\theta z}$ $[\frac{lb-in}{rad}]$	θ_x, θ_y $[radians]$	E_x, E_y $[thousanths]$	γ
3.24,3.25	-1	67	67	0	30,40,50	1
	0	67	67	0	30,40,50	1
	3	67	67	0	30,40,50	1
3.26,3.27	-1	80	160	0	30,40,50	2
	0	80	160	0	30,40,50	2
	3	80	160	0	30,40,50	2

by the force at the contact point in the chamfer increases since the lever arm increases. Therefore, the moment twisting the peg increases and facilitates chamfer crossing. For the case of MIF after chamfer crossing, the situation is the opposite (see Figure 3.25). The closer the COR is to the tip of the peg, the smaller MIF. This results agrees with those obtained for the two dimensional case (see Whitney[20]). In this case, the closer the COR is to the tip of the peg, the smaller is the moment trying to rotate the peg during chamfer crossing. Therefore, the angular errors produced when absorbing the linear errors decrease. Therefore, MIF and the chances of two point contact also decrease.

Figures 3.26 and 3.27 show the effects of L_y on MIF for a stiffness ratio of two. These experiments were conducted to investigate the effects of the stiffness ratio on the results shown in Figures 3.24 and 3.25. As seen in the graphs, forces during chamfer crossing vary linearly, the larger the absolute value of L_y the smaller the MIF

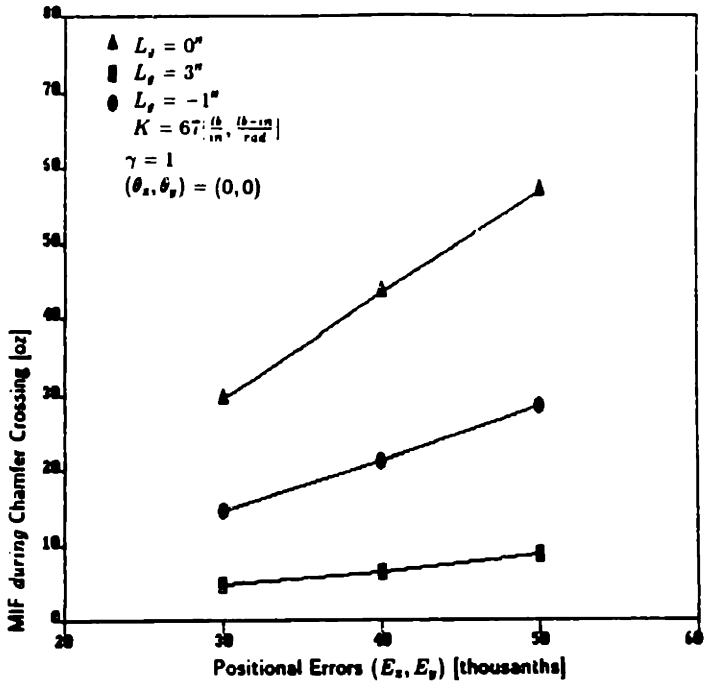

Figure 3.24: Effect of the location of the center of rotation (COR) on MIF during chamfer crossing for stiffnesses with a ratio of one.

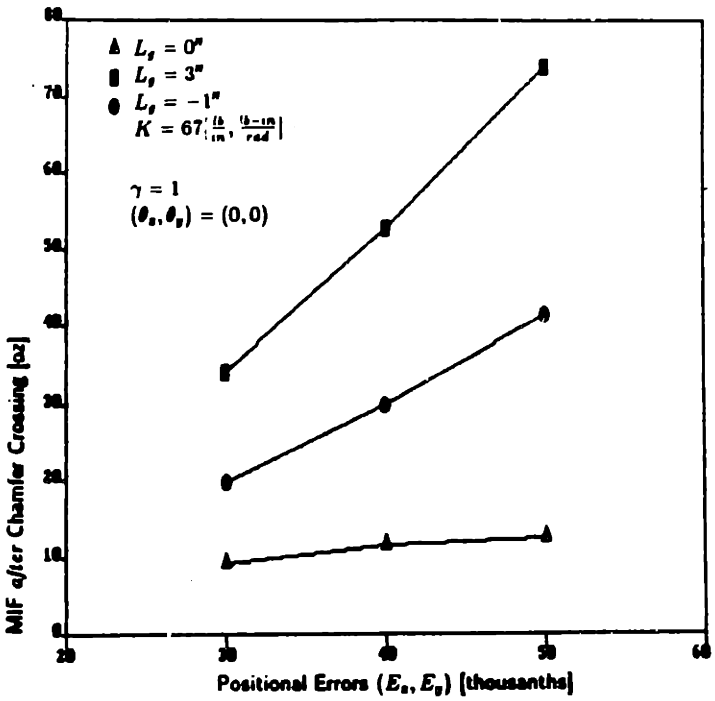

Figure 3.25: Effect of the location of the COR on MIF after chamfer crossing for stiffnesses with a ratio of one.

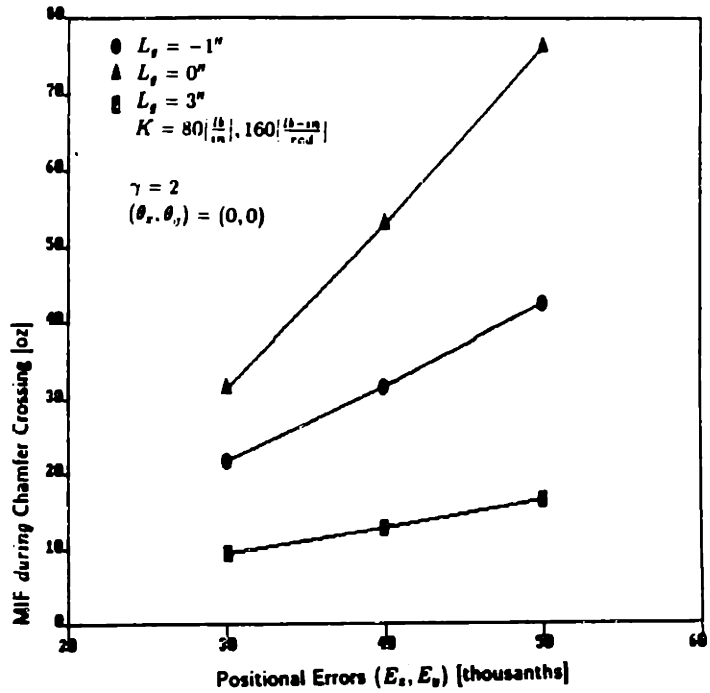

Figure 3.26: Effect of the location of the center of rotation (COR) on MIF during chamfer crossing for stiffnesses with a ratio of two.

during chamfer crossing, and the smaller the absolute value of L_g the smaller the MIF after chamfer crossing. The results obtained are the same for a stiffness ratio of one or two. Clearly, the magnitude of the forces is different, but the trends are the same.

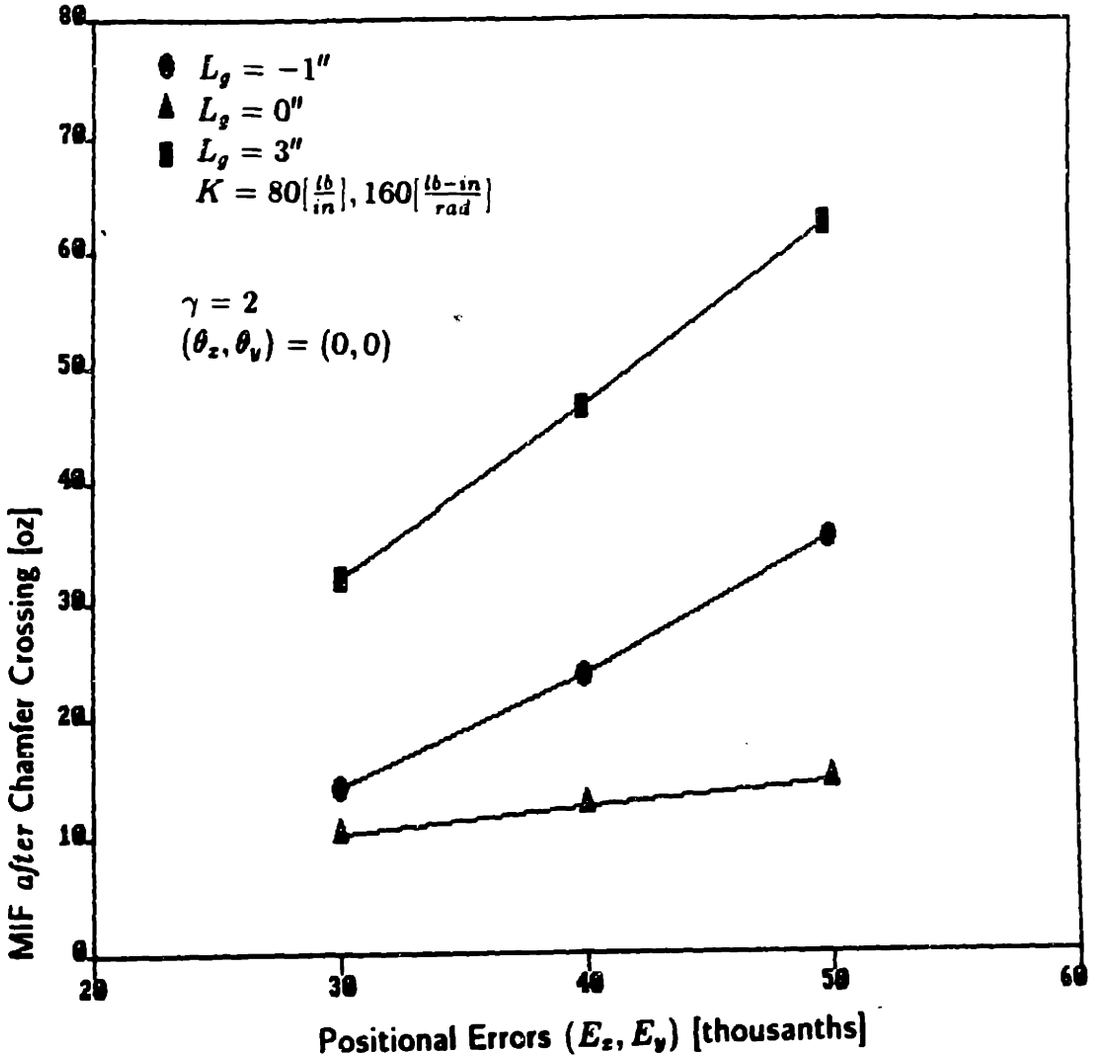

Figure 3.27: Effect of the location of the center of rotation (COR) on MIF after chamfer crossing for stiffnesses with a ratio of two.

3.5 Conclusion

Based on the three dimensional experimental results presented in this chapter, the general conclusions listed below were made. The conclusions describe trends and observations made from the data. For the exact magnitude of the changes and shifts described, the reader is referred to the particular section in this chapter that deals with the question. Recall that MIF means maximum insertion forces, and L_y is the distance form the tip of the peg to the location of the center of rotation.

- For a constant stiffness ratio, MIF after chamfer crossing increase as the positional errors increase. However, the sensitivity to changes in positional errors decreases as the errors decrease (see Figure 3.4). Similarly, MIF after chamfer crossing increase as the stiffness of the structure increases (while keeping the stiffness ratio constant).

- MIF during chamfer crossing vary linearly with positional errors. This result also applies when angular errors are present and is independent of the value of L_y. Furthermore, MIF after chamfer crossing increase as the stiffness of the structure increases, regardless of the stiffness ratio.

- High rotary-to-linear stiffness ratios greatly reduce MIF after chamfer crossing when only positional errors are present. This explains why commercial RCC devices have high stiffness ratios.

- MIF during chamfer crossing increase as the stiffness ratio increases. However, the increase in MIF *during* chamfer crossing is less than the decrease in MIF *after* chamfer crossing.

- For a given positional error and a constant stiffness ratio, MIF during and after crossing vary linearly with axes stiffness. Both of these results apply when angular errors are present. However, the slope of the lines changes for different positional errors.

- MIF during chamfer crossing increase as the angular errors increase.

- MIF after chamfer crossing decrease as the angular error approaches in magnitude the angular error generated when absorbing the positional error. That is, given a determined assembly condition, there is an angular error that minimizes MIF after chamfer crossing. For any other angular error forces are greater.

- MIF after chamfer crossing decrease as the center of rotation is located close to the tip of the peg (L_g small), regardless of the stiffness ratio. This result agrees with the two dimensional case.

Criteria for Determining γ and L_g

Chapter 4

In Chapter 3, the effects of positional errors, axes stiffness and ratio of rotary to linear stiffness, angular errors, and the location of the center of rotation with respect to the tip of the peg were investigated. The effects on maximum insertion forces during and after chamfer crossing were discussed for different sets of assembly parameters. Each set of assembly parameters consisted of values for the following variables:

1. positional errors
2. angular errors
3. axes stiffness and stiffness ratio (γ)
4. L_g (location of COR)

However, in real applications engineers are not capable of adjusting all four of the above parameters to desired values. In general, the positional and angular errors can not be adjusted. That is, these errors depend on the limitations in the accuracy/repeatability of the assembly machine or robot, and on inaccuracies due to tolerance stack up in fixture location and part geometry. Therefore, the engineer only

has two parameters to adjust to minimize MIF during assembly: axes stiffness and stiffness ratio (γ), and the location of the center of rotation with respect to the tip of the peg (L_y).

This chapter provides criteria for determining these two parameters under four different initial conditions. Experimental results are presented and discussed.

4.1 Initial Conditions Considered

Initial conditions here refer to the positional errors, angular errors, or combination of both that are present before the assembly takes place. These initial conditions are important because the choices for the location of the COR and stiffness ratio will depend on the initial assembly conditions.

Clearly, the assembly conditions are not exactly known. If the

assembly device knew what the assembly conditions were, it would simply correct the errors. However, the engineer does have a general idea of the errors present, positional or angular or both, and also has an idea of their magnitude. For the analysis that follows, an exact notion of the initial conditions is not required, only a notion of which errors are present is required.

To select the possible assembly conditions one assumption was made: symmetry. That is, the errors in X (E_x and θ_x) were the same in magnitude and direction as the errors in Y (E_y and θ_y). So, for $E_x = E_y$ and $\theta_x = \theta_y$ there are four possible initial conditions.

The four initial conditions are (shown in Table 4.1): only positional errors (#1), only angular errors (#2), and two combinations of positional and angular errors (#3 and #4). The + sign in Table 4.1 means an error of any magnitude in the positive

Table 4.1: Initial assembly conditions investigated assuming symmetry.

#	E_x and E_y	θ_x and θ_y
1	+	0
2	0	+
3	+	+
4	-	+

direction. Similarly, the - sign means an error of any magnitude in the negative direction. All other initial conditions assuming symmetry are a mirror image of the conditions shown in Table 4.1. For example, having only negative positional errors is the mirror image of condition #1. Figure 4.1 contains a drawing of each condition.

4.2 Selection Criteria

To determine which choice of L_y and stiffness ratio to use given an initial condition, a selection criteria must be determined. In this analysis, the objective was to choose combinations of L_y and γ that would minimize maximum insertion forces after chamfer crossing. This selection criteria was selected because minimizing forces after chamfer crossing translates into lowering the probability of failure and facilitating the assembly. Ideally, the objective is to choose parameters that would only give one-point contact situations during assembly for a wide variety of initial conditions. Having only one-point contact reduces MIF and greatly decreases the probability of failure.

Other selection criteria could have been chosen. For example, in the case of applications in clean-rooms, were particle contamination is critical, it might be desired

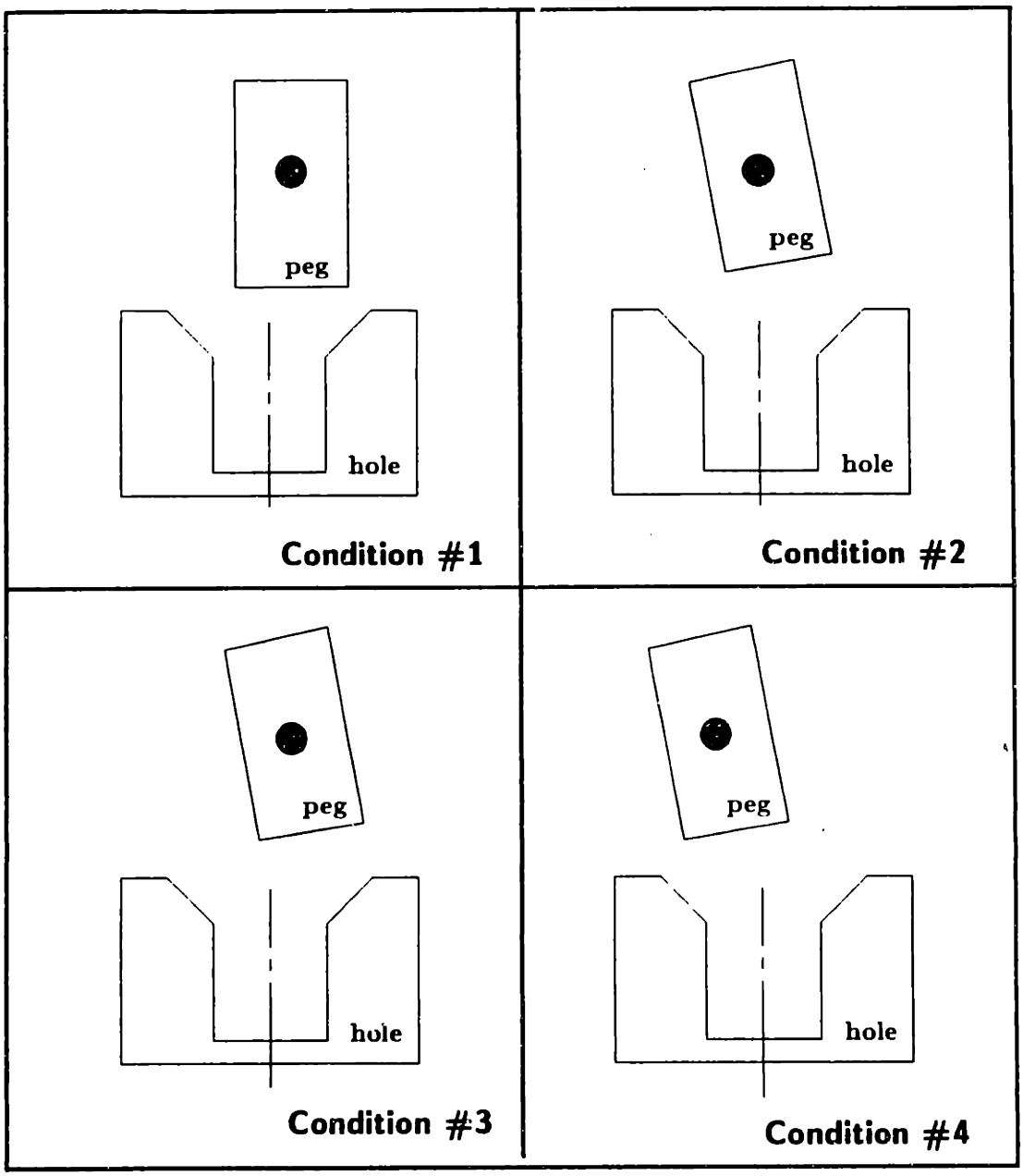

Figure 4.1: Drawing showing, in two dimensions, the four assembly initial conditions considered.

Table 4.2: Experiments conducted to develop criteria for determining γ and L_y.

Figure	Initial Condition	E_x, E_y [thousanths]	θ_x, θ_y [degrees]	L_y [inches]	γ $\frac{K}{K_n}$
4.2	#1	20	0	.5,.04,-.5	6,1,.33
4.3	#1	50	0	1,.5,.04,-.5	6,1,.33
4.4	#2	0	.54	.5,.04,-.5	6,1,.33
4.5	#2	0	1.53	.5,.04,-.5	6,1,.33
4.6	#3	50	.54	.5,.04,-.5	6,1,.33
4.7	#4	-50	.54	.5,.04,-.5	6,1,.33

to minimize forces during chamfer crossing so as to avoid particle generation close to the surface. In any case, the objective of this chapter is to identify combinations of the location of the COR, or L_y, and stiffness ratio, γ, that minimize MIF after chamfer crossing.

4.2.1 Experimental Results and Discussion

Six sets of experiments, shown in Table 4.2, were conducted for the four initial conditions.

Figures 4.2 and 4.3 investigate the effects on MIF after chamfer crossing of L_y and γ when only positional errors are present (initial condition #1). Figure 4.2 is for a positional error of 20 thousanths and Figure 4.3 for an error of 50 thousanths. In both cases, a high stiffness ratio (of six) provides the best results (minimize MIF) for the L_y considered. This result agrees with that presented in Chapter 3: high stiffness

ratios minimize forces in the presence on positional errors only. This result again explains why RCC devices sold off-the-shelf have mostly high stiffness ratios. Note from both figures that for an L_y of .04 the MIF are roughly the same regardless of the stiffness ratio. This result suggests that insertion forces become insensitive to the stiffness ratio when the COR is placed close to the tip of the peg. From Figure 4.2 we see that for a positional error of 20 thousanths, a γ of 6 and 1 yield similar results. A γ of .33 yields high MIF as L_y increases because most of the positional errors are translated into angular errors when the assembly takes place and therefore two point contact occurs. For larger positional errors, of 50 thousanths, a γ of 1 and 6 yield similar results for L_y of .5" and .04". As in Figure 4.2, a γ of .33 yields poor results for L_y other than .04". Overall, a γ of 6 provides the best results by minimizing MIF for the whole range of L_y investigated. Note that using γ of 6, MIF are insensitive to the location of the COR (L_y) in the range of values studied.

Figures 4.4 and 4.5 investigate the effects of L_y and γ on MIF in the presence of angular errors, or condition #2. As expected, high γ ratios yield high MIF because it is difficult for the assembly to absorb the initial angular errors and two point contact occurs. For angular errors of 1.54° the MIF are more than five times greater for a γ of six than for a γ of one or less. Overall, a γ of 0.33 yields the best results because it allows the assembly to accommodate the angular errors easily. A γ of one also yielded favorable results.

Figures 4.4 and 4.5 show that stiffness ratios of six or higher yield high MIF in the presence of angular errors only. These ratios proved to give the best results in the presence of positional errors only, but gave the worst results in the presence of angular errors. Using an intermediate ratio, such as one, and placing the COR close to the tip of the peg would give better results in the presence of both angular and

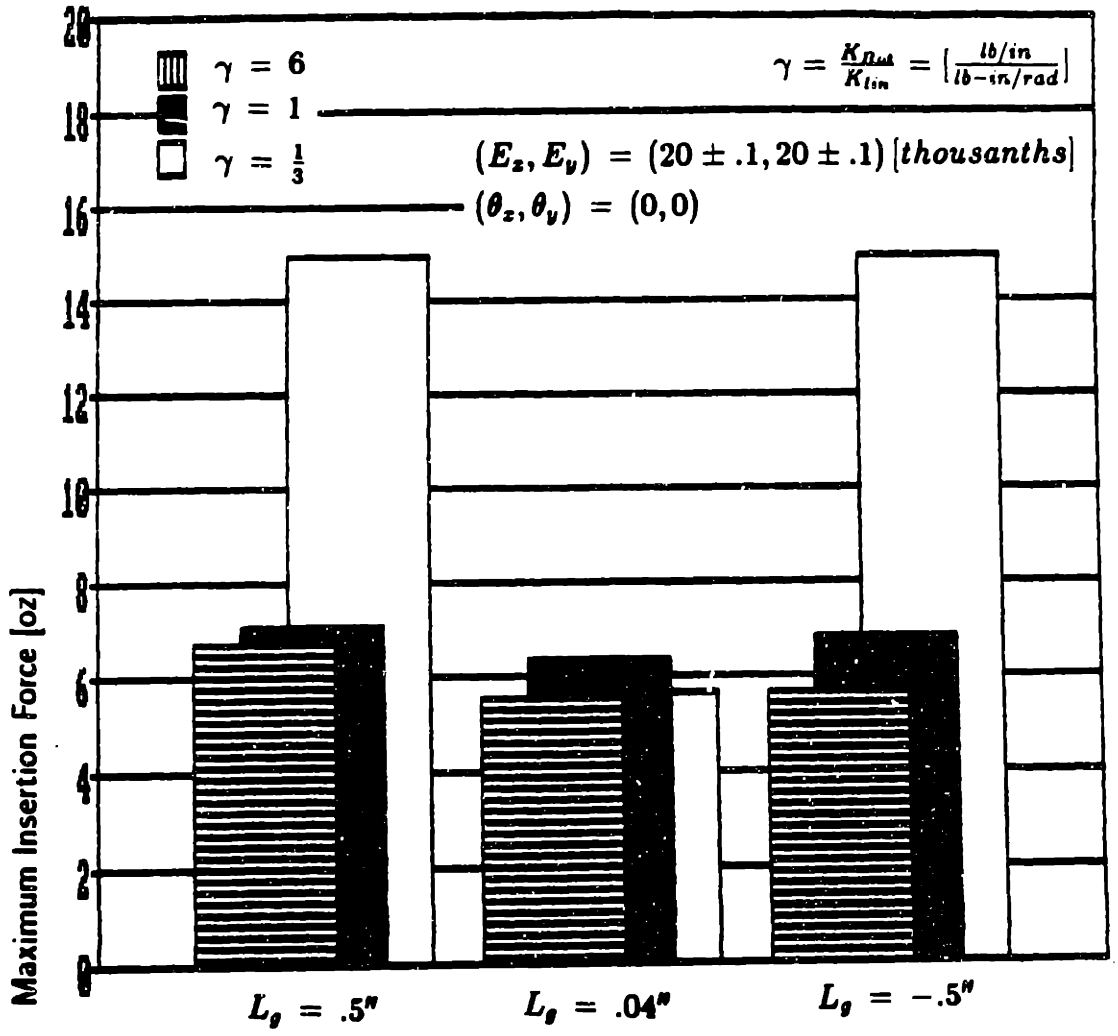

Figure 4.2: Effect of L_g and γ on MIF for a positional error of 20 thousanths.

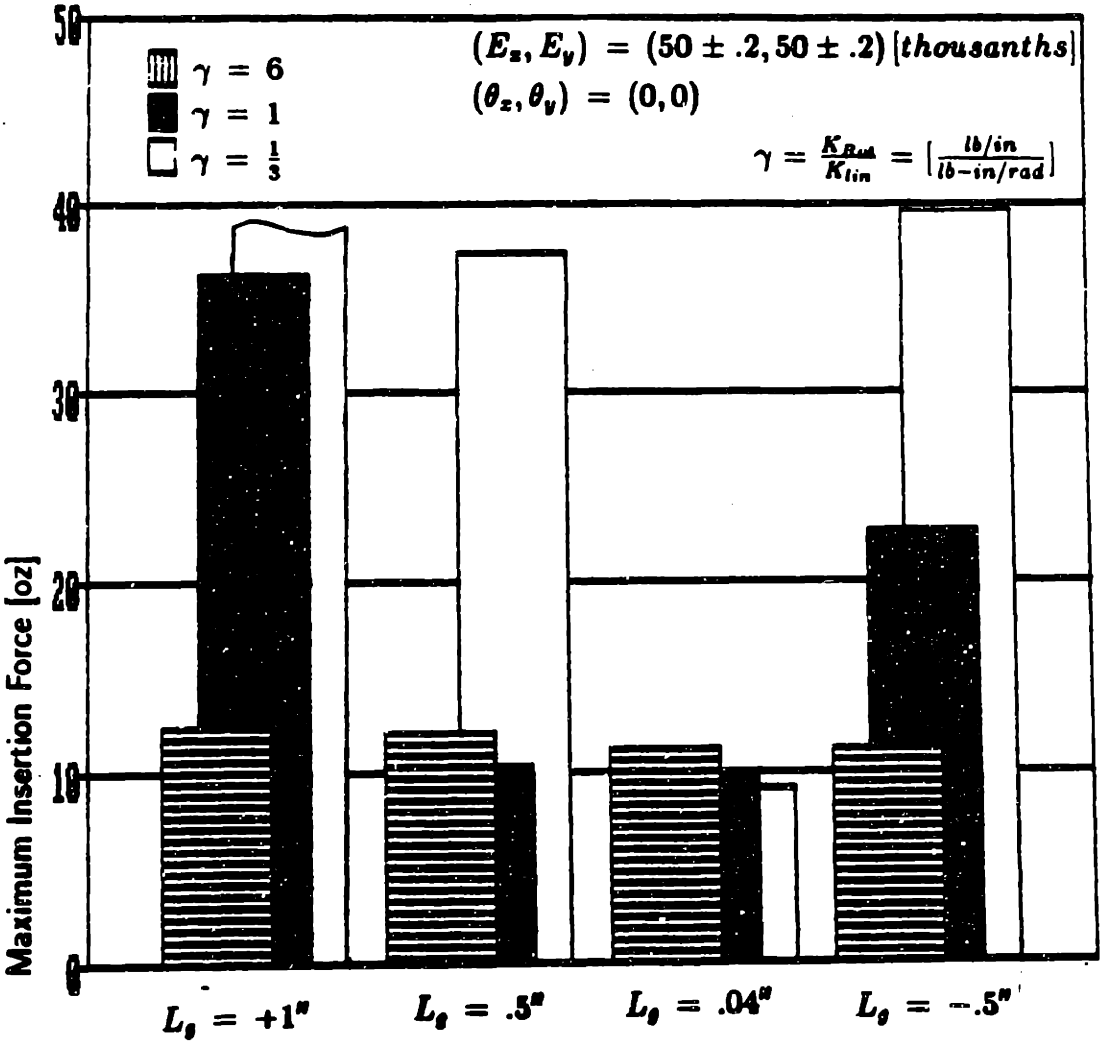

Figure 4.3: Effect of L_y and γ on MIF for a positional error of 50 thousanths.

positional errors.

Also, the poor performance of high stiffness ratios in the presence of angular errors only suggests that RCC devices, which typically have high ratios, should not be used for assembling parts under these conditions.

Figure 4.6 shows the more realistic situation when both positional and angular errors are present (condition #3). An angular error of 0.54° was chosen as appropriate. In this case, a γ of one provides the best results overall. For a L_y of .04", a γ of 1 and .33 provide similar results. Note that in this example, a γ of 6 would have given the best results if no angular errors would have been present. How much larger MIF are with a γ of six depends on the relation between positional and angular error. Recall from Chapter 3 that for particular angular errors and a determined positional errors, MIF are minimized because the initial angular offset cancels the angle created when crossing the chamfer and only one-point contact occurs. Therefore, in Figure 4.5 MIF for a γ of six would have been smaller for a smaller angular error. However, any angular error greater than 0.54° would have given higher MIF.

Overall, in the presence of positive positional and angular errors, the results suggest that a γ of one provide the best results overall. A γ of .33 yields similar results for small L_y, and high γ provides higher forces in general than a γ of one. I say in general, because certain combinations of positional/angular errors would minimize MIF for a particular combination of L_y and γ. For example, there is a combination for a γ of six that provides lower MIF that a γ of 1 for that same combination. However, in general due to the inability of higher ratios to absorb angular errors, a γ of one would prove better results overall.

Figure 4.7 shows the results in the presence of negative positional errors and positive angular errors (condition #4). In this case, all stiffness ratios provide similar

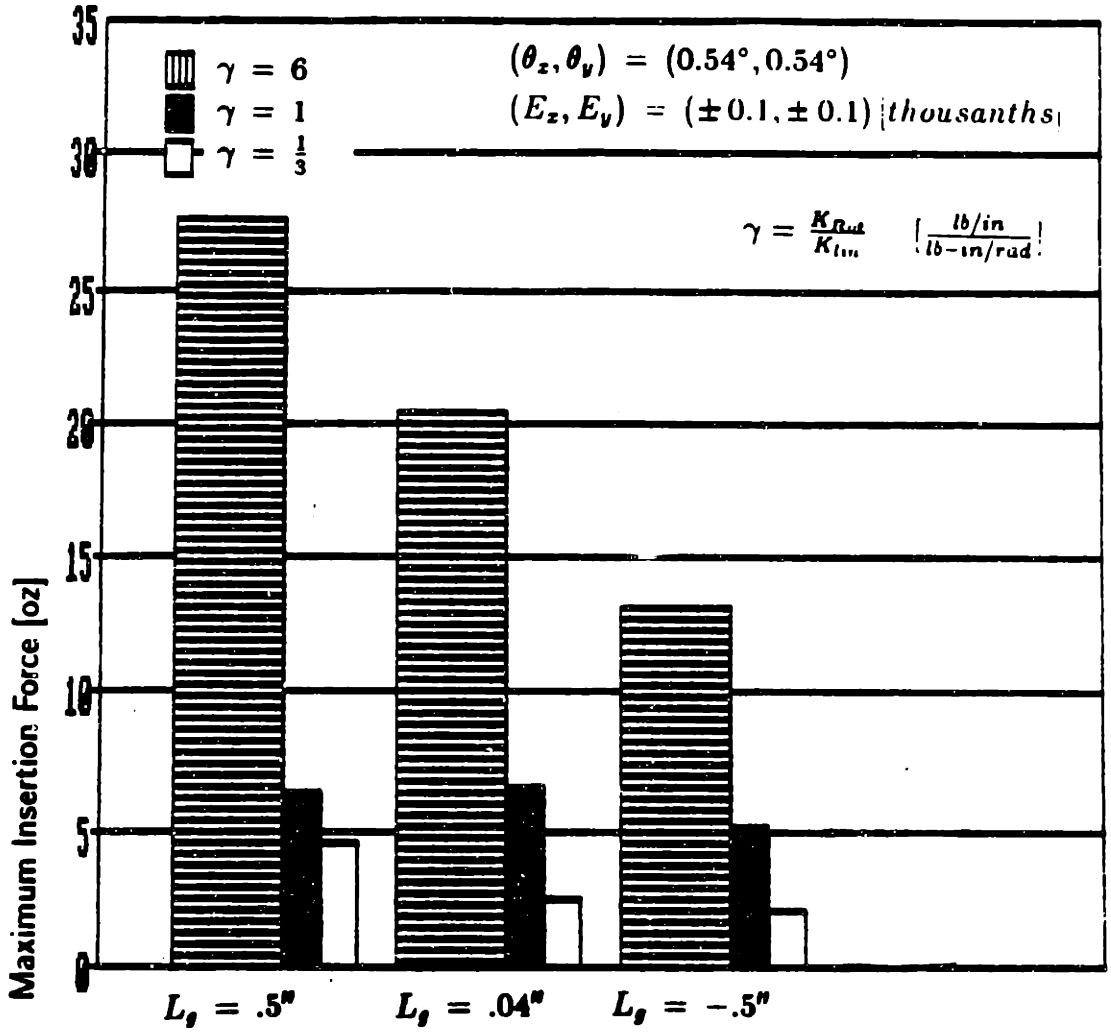

Figure 4.4: Effect of L_y and γ on MIF for an angular error of 0.54°.

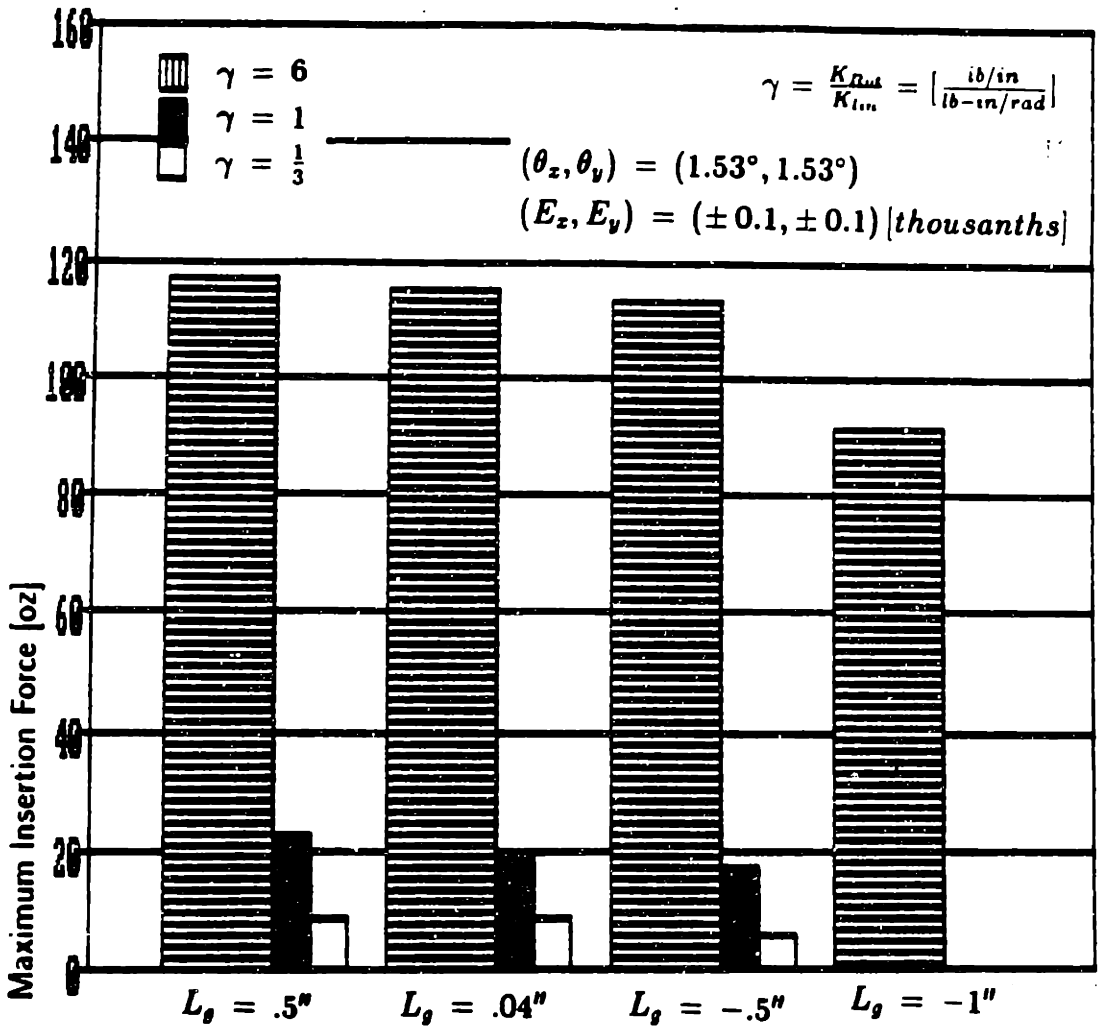

Figure 4.5: Effect of L_y and γ on MIF for an angular error of 1.54°.

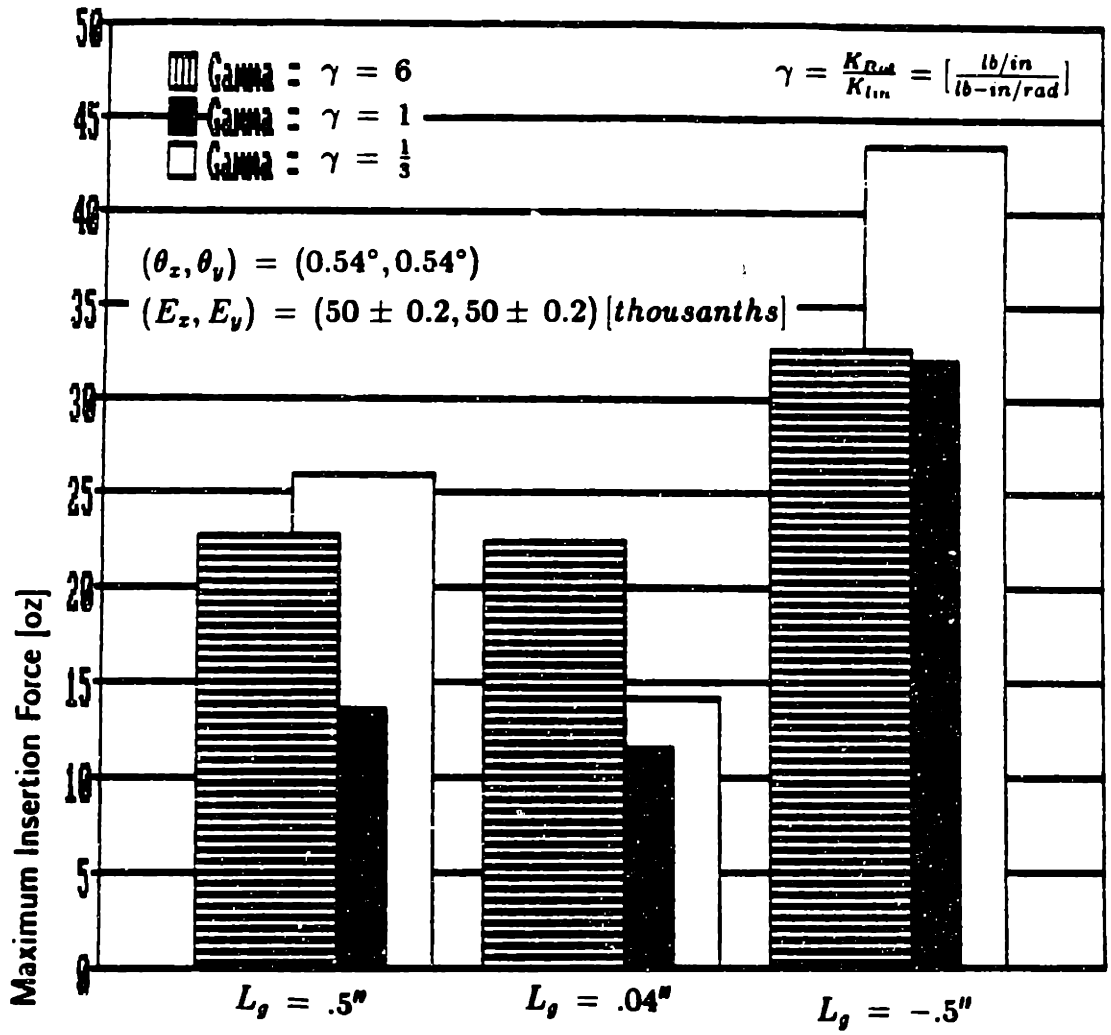

Figure 4.6: Effect of L_g and γ on MIF for a positional error of 50 thousanths and an angular error of 0.54°.

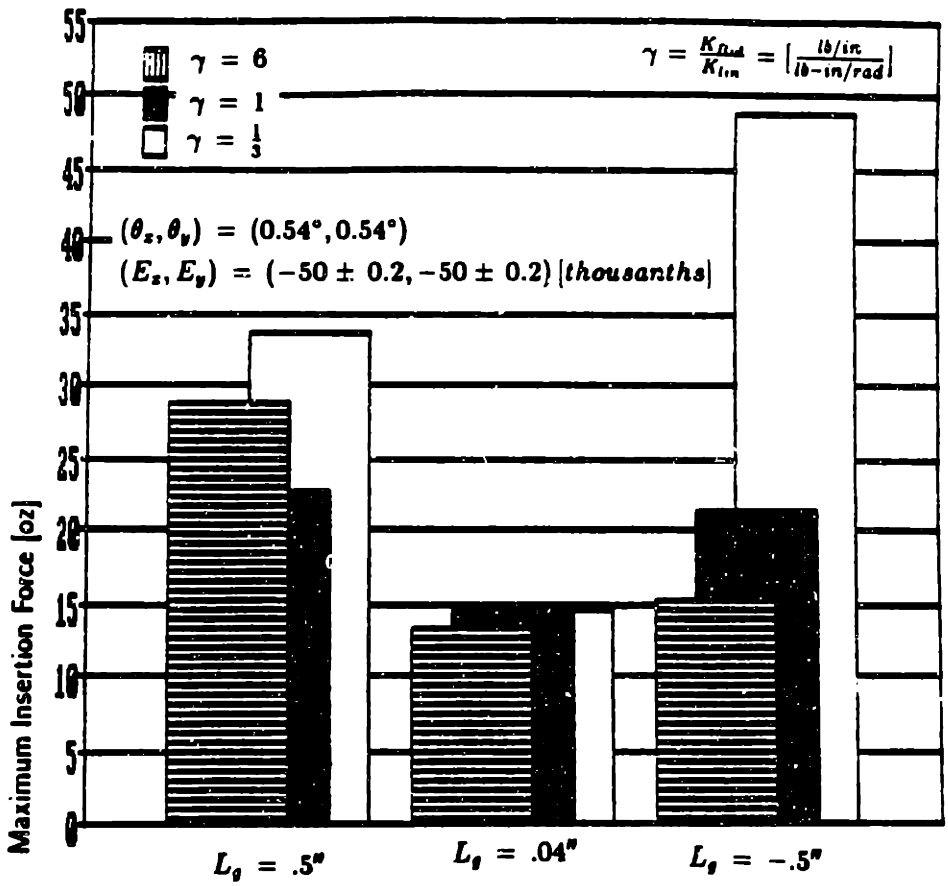

Figure 4.7: Effect of L_y and γ on MIF for a positional error of -50 thousanths and an angular error of 0.54°.

forces for an L_y of 0.04". For other L_y, a γ of 0.33 gives the worst results.

4.3 Conclusion

The general conclusions and summary presented below provide guidelines for determining the location of the center of rotation with respect to the tip of the peg, L_y, and for selecting the ratio of rotary-to-linear stiffness, γ.

- In the presence of positional errors only it is desirable to have high stiffness ratios, where high is considered six or larger. When using high stiffness ratios MIF were minimized for all values of L_y investigated ($-1'' < L_y < 1''$). That is, if high stiffness ratios are used, varying L_y within the one inch limit did not make any difference. Furthermore, for a γ of six only one-point contact situations were observed.

- The above results explain once again why commercial RCC devices have high stiffness ratios. Also see Chapter 3 for more data on this issue.

- When the COR is placed close to the tip of the peg, MIF in the presence of postional errors only become independent of the stiffness ratio. Ratios of .33, 1, and 6 yielded similar results for a L_y of 0.04". This result suggests that the importance of the selection of stiffness ratio decreases as the COR is placed closer to the tip of the peg.

- In the presence of angular errors only and regardless of L_y, it is desirable to have low stiffness ratios. A γ of .33 yielded the lowest MIF (and also one-point contact situations) for $-.5'' < L_y < .5''$. A γ of one also yielded low MIF. However, a γ of six yielded up to five times greater MIF for an error of 1.54" than for a γ of .33.

- This result suggests that RCC devices should not be used for assembling parts in the presence of angular errors only, regardless of L_y.

- In the presence of angular and positional errors there are no straightforward rules to follow to determine the stiffness ratio. In general, the inability of high ratios to absorb angular errors causes high MIF to be generated when these ratios are used. However, this is not always the case. There are certain combinations of errors which also minimize forces for high stiffness ratios.

- In the presence of angular and positional errors, it is desirable to locate the center of rotation close to the tip of the peg. When this was done, MIF were the lowest for all stiffness ratios. Unfortunately, no clear rules are available to determine exactly the effects of larger L_y since the effects depend on the assembly situation.

Conclusion

Chapter 5

5.1 Recommendations

The conclusion sections presented at the end of Chapters 3 and 4 provide a summary of the findings made throughout this research project. Chapter 3 investigated the effects of positional errors, angular errors, axes stiffness and stiffness ratio, and location of the center of rotation on maximum insertion forces during and after chamfer crossing. Chapter 4 presented criteria for determining the stiffness ratio and location of the center of rotation given an initial condition.

To use the results of this research more efficiently to improve a particular assembly operation, the reader should first determine the known assembly parameters. This involves determining, if possible, the errors involved, stiffness, and location of the center of rotation. If the reader is interested in selecting an RCC, for example, he/she should read Chapter 4 to determine γ and L_j. However, if the reader wants to determine the effects of assembly parameters, then he/she should read Chapter 3. For example, it might be desirable to determine how much insertion forces will increase if a cheaper,

but less accurate, robot or fixturing system is used.

The reader is also referred to the article "An Empirical Study of Compliant Assembly in Three Dimensions" which was submitted to the ASME Design Automation Conference in Boston on September 1987 (see references Rivero [15]). This paper presents and summarizes some of the results included in this thesis.

5.2 Suggestions for Future Work

Here are some suggestions for future work in the area of compliant assembly. The suggestions below are not in order of importance.

- Further experimentation with a wider range of parameter values. The experiments presented in Chapters 3 and 4 were conducted for a limited number of parameter values and ranges. Wider ranges of positional errors, angular errors, different stiffness and stiffness ratios, and also other values for L_y should be investigated. The generality of the results presented in this thesis will be determined after more experiments are conducted using wider ranges of parameter values.

- Investigate the effect of surface finish. One important parameter not analyzed in this research was the effect of the surface finish of the parts on insertion forces. The surface finish of the parts will influence the coefficient of friction, and therefore the frictional forces generated during assembly. Frictional forces will have an important effect on MIF.

- This research has concentrated on the effect of parameters on maximum insertion forces during assembly. Future research should be completed to investigate

the effects of parameters on moments and lateral forces also occurring during assembly.

- Evaluation of models available. Several models have already been developed to investigate the three-dimensional assembly of parts. This thesis presents substantial empirical data that can be used to determine the accuracy of these models. The evaluation of the models available will facilitate the improvement and development of better models.

- Different part shapes, not only cylindrical, should be analyzed using the parts mating machine or similar test apparatus. Real applications clearly include parts of many different shapes and sizes. Guidelines for the assembly of parts of different geometries should be developed.

- Generate relationships between initial assembly conditions and failure probability. It would be useful to know the possibility that an assembly operation will fail given the initial positional errors, angular errors, stiffnesses, and L_g.

- Other areas of research include:

  - Extend the above results and areas of research to include "fast" insertions; that is, extend the results to include dynamic assembly considerations.
  - Investigate the assembly of multiple parts at the same time, each with different or similar geometry.
  - At Digital Equipment Corporation in Colorado Springs, particle contamination was an important consideration in their manufacturing facilities. Research could be conducted to investigate the effects of parameters and part shape on particle generation.

Determination of the Coefficient of Friction

Appendix A

Derivation of Equation 2.14

Taking the coefficient of friction, μ, to remain constant during chamfer crossing, the frictional force, F_r, is given by:

$$F_r = \mu F_n \tag{A.1}$$

where F_n in the normal force.

Doing a force equilibrium on the hole in the X-direction (see Figure A.1):

$$\sum F = 0 = F_x - F_n(-\mu \cos\alpha + \sin\alpha) \tag{A.2}$$

where α is the chamfer angle, and F_x is the lateral force.

Doing a force equilibrium on the peg in the Z-direction (see Figure A.2):

$$\sum F = 0 = F_z - F_n(\mu \sin\alpha + \cos\alpha) \tag{A.3}$$

where F_z is the insertion force.

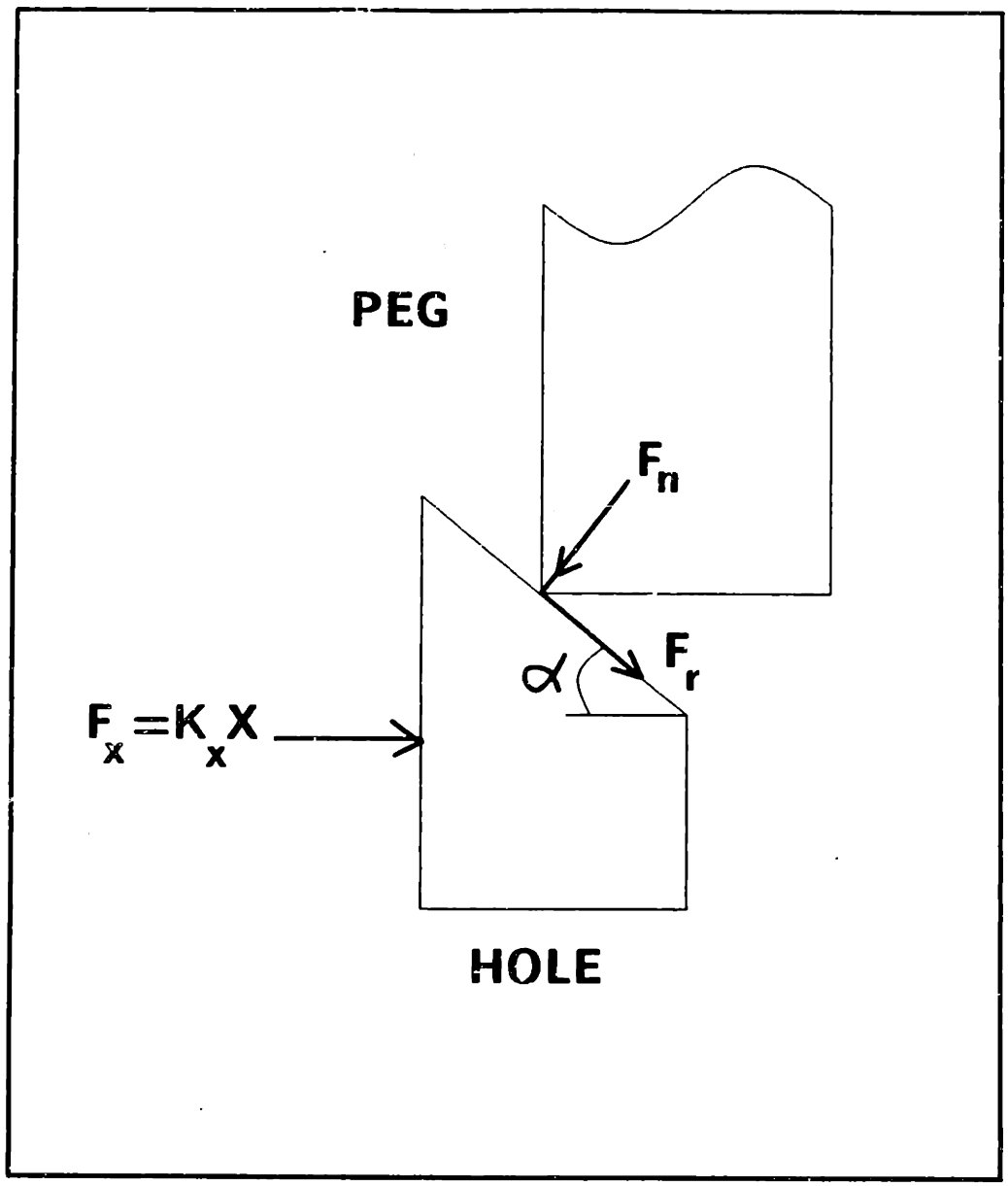

Figure A.1: Forces acting on the hole during chamfer crossing.

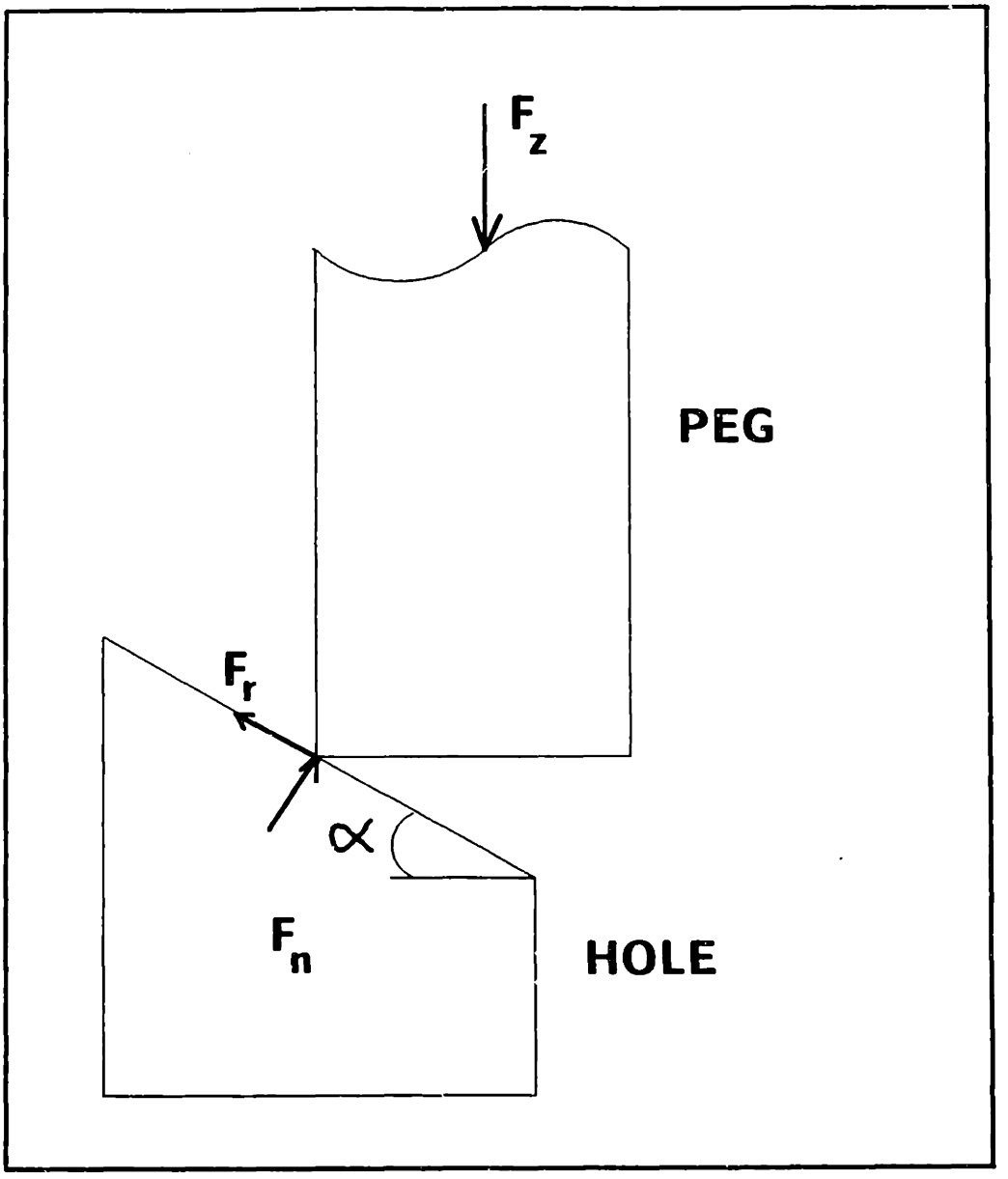

Figure A.2: Forces acting on the peg during chamfer crossing.

Combining Equations A.2 and A.3 and solving for the coefficient of friction, μ:

$$\mu = \frac{F_z \sin\alpha - F_x \cos\alpha}{F_z \cos\alpha + F_x \sin\alpha} \tag{A.4}$$

Data Acquisition Software

Appendix B

This Appendix contains the source listing for most of the programs written for the data acquisition system. These programs run on a PDP 11-23 using the RT-11 operating system. The programs included here are:

1. dat.for (main program for data acquistion)
   (a) adfast.for (A/D subroutine)
   (b) madc2.mac (subroutine to sample A/D board)
   (c) macd1.mac (subroutine to sample A/D board and 1 digital channel)
   (d) macd2.mac (subroutine to sample A/D board and 2 digital channels)
   (e) macd3.mac (subroutine to sample A/D board and 3 digital channels)
2. scale.for (program to calibrate data)

```
**********************************

PROGRAM DAT
C
C PROGRAM TO SAMPLE ANALOG CHANNELS AND UP TO THREE DIGITAL
C CHANNELS. NEEDS SUBROUTINES ADFAST,MADC2,MACD1,MACD2, AND
C MACD3. PROGRAM WRITTEN TO SAMPLE UP TO 14700 POINTS.
C
C Parts Mating Machine Data Acquisition Software
C MIT Artificial Intelligence Laboratory
C Jose A. Rivero, May 1986.
C
COMMON /CM1/ IDVAL(15000)
TYPE 10
10 FORMAT(///'*** WELCOME TO THE PARTS MATING MACHINE DATA
     1 ACQUISITION SOFTWARE PACKAGE ***')
TYPE 20
20 FORMAT(/'                    MIT Artificial Intelligence
     1 Laboratory')
TYPE 30
30 FORMAT(/'                              Version 1.0,
     1 April 1986'/)
40 FORMAT(///' INPUT FILENAME TO STORE DATA (do not include'/
     1 ' file type, program sets it to .DAT):            ',2X,$)
50 FORMAT(A10)
TYPE 40
READ(5,50) FNAME
TYPE 60
60 FORMAT(/' INPUT FIRST ANALOG CHANNEL TO BE SAMPLED: ',2X,$)
ACCEPT*, ICHAN
70 FORMAT(/' INPUT LAST ANALOG CHANNEL TO BE SAMPLED: ',2X,$)
TYPE 70
```

```
ACCEPT*, LCHAN
TYPE 80
80 FORMAT (/' INPUT # OF DIGITAL CHANNELS TO SAMPLE (<=3):',2X,$)
ACCEPT*, IDIG
90 FORMAT(/' INPUT SAMPLING FREQUENCY (HZ) (<=1K) '/' should equal
     1(#points/channel/sec)*(# analog channels): ',2X,$)
TYPE 90
ACCEPT*, FSAMP
TYPE 100
100 FORMAT (/' ENTER DESIRED SAMPLES/SECOND/CHANNEL: ',2X,$)
ACCEPT*, NSSC
TYPE 110
110 FORMAT (/' ENTER DURATION OF DATA ACQUISITION (SECS): ',2X,$)
ACCEPT*,IT
C
C Total number of channels to sample
INPC=(LCHAN-ICHAN+1)+IDIG
C Total number of points
IPTS=NSSC*IT*INPC
IF (IPTS.GT.14700) TYPE*, '  Sorry, program only
     1 samples up to 14700 points.'
IF (IPTS.GT.14700) GOTO 900
C Total number of samples per channel
NPC=IPTS/INPC
130 FORMAT(///' Please Wait ... '//)
TYPE 130
        IGO=1
CALL ADFAST(ICHAN,LCHAN,FSAMP,IGO,IDVAL,DVAL,NPC,IER,IDIG)
IF (IER.EQ.1) GOTO 500
IF (INPC.EQ.1) TYPE 201,(IDVAL(I),I=1,IPTS)
IF (INPC.EQ.2) TYPE 202,(IDVAL(I),I=1,IPTS)
IF (INPC.EQ.3) TYPE 203,(IDVAL(I),I=1,IPTS)
IF (INPC.EQ.4) TYPE 204,(IDVAL(I),I=1,IPTS)
```

```
IF (INPC.EQ.5) TYPE 205,(IDVAL(I),I=1,IPTS)
IF (INPC.EQ.6) TYPE 206,(IDVAL(I),I=1,IPTS)
IF (INPC.EQ.7) TYPE 207,(IDVAL(I),I=1,IPTS)
TYPE 140
140 FORMAT (/' WARNING: If any of the values obtained from the
     1digital ')
TYPE 150
150 FORMAT (' channels was negative then digital convertion
     1failed.'//)
TYPE*, '  '
TYPE*, '***** ACQUISITION COMPLETED ***** STORING DATA *****'
CALL ASSIGN(2,FNAME,0,,,)
IF (INPC.EQ.1) WRITE(2,201) (IDVAL(J),J=1,IPTS)
IF (INPC.EQ.2) WRITE(2,202) (IDVAL(J),J=1,IPTS)
IF (INPC.EQ.3) WRITE(2,203) (IDVAL(J),J=1,IPTS)
IF (INPC.EQ.4) WRITE(2,204) (IDVAL(J),J=1,IPTS)
IF (INPC.EQ.5) WRITE(2,205) (IDVAL(J),J=1,IPTS)
IF (INPC.EQ.6) WRITE(2,206) (IDVAL(J),J=1,IPTS)
IF (INPC.EQ.7) WRITE(2,207) (IDVAL(J),J=1,IPTS)
CALL CLOSE(2)
GO TO 900
500 TYPE 700
201 FORMAT(I9)
202 FORMAT(2I9)
203 FORMAT(3I9)
204 FORMAT(4I9)
205 FORMAT(5I9)
206 FORMAT(6I9)
207 FORMAT(7I9)
700  FORMAT(//' ****** A/D CONVERSION FAILED ******')
900 CONTINUE
TYPE 1000
1000    FORMAT(//' ***** DATA STORED *****'//' Have a good day...'///)
```

```
STOP
END


**************************************

      SUBROUTINE ADFAST(ICHAN,LCHAN,FSAMP,IGO,IDVAL,DVAL,NPC,IER,IDIG)
C
C     CALLS THE MACRO SUBROUTINES THAT PERFORM THE DATA ACQUISITION.
C     TO BE USED WITH PROGRAM **DAT**. ALLOWS TO SAMPLE ALL ANALOG
C     CHANNELS AND THREE DIGITAL.
C
C     Parts Mating Machine Data Acquisition Software.
C     MIT Artificial Intelligence Laboratory.
C     Jose A. Rivero, May 1986.
C
      DIMENSION IDVAL(1)
C     Set clock frequency index
      IBASE=4
      NP=NPC*((LCHAN-ICHAN+1)+IDIG)
      CLRATE=1.0E-03
      FINT=1.0/FSAMP/CLRATE
      INTVL=IFIX(FINT)
C     IDIG is the number of digital channels (<=3)
      IF (IDIG.EQ.0) CALL MADC2(IDVAL,NP,ICHAN,
     1 LCHAN,IBASE,INTVL,IGO,IER)
      IF (IDIG.EQ.1) CALL MACD1(IDVAL,NP,ICHAN,
     1 LCHAN,IBASE,INTVL,IGO,IER)
      IF (IDIG.EQ.2) CALL MACD2(IDVAL,NP,ICHAN,
     1 LCHAN,IBASE,INTVL,IGO,IER)
      IF (IDIG.EQ.3) CALL MACD3(IDVAL,NP,ICHAN,
     1 LCHAN,IBASE,INTVL,IGO,IER)
      RETURN
```

```
      END

**************************************

.TITLE MADC2, MR799B
.IDENT '791025'
.REM \

PURPOSE: CONVERT MULTIPLE ANALOG SIGNALS TO DIGITAL DATA VIA THE PDP
ANALOG TO DIGITAL CONVERTER. ** USES A GAIN OF 4 FOR THE A/D BOARD **.

USAGE: CALL MADC2(IDATA,NPT,ICHAN,LCHAN,IBASE,INTVL,IGO,IER)
  IDATA = INTEGER ARRAY TO WHICH THE DATA IS RETURNED. DATA VALUES
RANGE FROM -2048 TO +2048, REPRESENTING VOLTAGES FROM -5.12V
TO +5.12V. (A FACTOR OF 400.) IF ICHAN=-1, IDATA MUST CONTAIN
THE ADC MULTIPLEXER CHANNELS WHEN MADC2 IS CALLED. (SEE ICHAN
BELOW.)
  NPT = TOTAL NUMBER OF DATA POINTS (SAMPLES) TO BE RECORDED IN IDATA.
(2<=NPT<=32767.)
  ICHAN = N (N>=0): INITIAL ADC CHANNEL FOR A CYCLIC SCAN. THE
CHANNELS ARE NUMBERED 0-11. (THE FIRST 8 ARE SINGLE-ENDED.
THE LAST 4 ARE QUASI-DIFFERENTIAL.)
= -1: WHEN ICHAN=-1, THE ADC CHANNEL NUMBER IS READ FROM
IDATA(K) TO DEFINE THE CHANNEL FOR THE SAMPLE TO BE RETURNED
TO IDATA(K), FOR K=1,2,...,NPT. FOR EXAMPLE, THE IDATA ARRAY
MIGHT BE INITIALIZED TO THE PATTERN
8,9,8,10,8,11,8,9,8,10,8,11,...
TO SAMPLE CHANNEL 8 AT FREQUENCY F AND CHANNELS 9, 10, AND 11
AT FREQUENCY F/3 (WITH SAMPLING RATE 2F).
  LCHAN = LAST ADC CHANNEL FOR A CYCLIC SCAN. (LCHAN IS IGNORED WHEN
ICHAN=-1.) WHEN 0<=ICHAN<=LCHAN<=11, THE ADC MULTIPLEXER IS
CYCLED CONTINUOUSLY FROM CHANNEL ICHAN TO CHANNEL LCHAN UNTIL
```

A TOTAL OF NPT SAMPLES HAVE BEEN RECORDED.

IBASE = CLOCK FREQUENCY INDEX.

= 1: 1 MHZ.

= 2: 100 KHZ.

= 3: 10 KHZ.

= 4: 1 KHZ.

= 5: 100 HZ.

= 6: EXTERNAL.

= 7: LINE FREQUENCY. (60 HZ.)

INTVL = INTERVAL BETWEEN SAMPLES IN CLOCK TICKS AT THE FREQUENCY SELECTED BY IBASE. (32767 MAX.) (EXAMPLE: WITH IBASE=1 AND INTVL=85, A SAMPLE WOULD BE TAKEN EVERY 85 MICROSECONDS.)

IGO = 1: START SAMPLING IMMEDIATELY.

= 2: START WHEN THE CLOCK'S SCHMITT TRIGGER 2 IS FIRED.

IER = ERROR INDICATOR.

= 0: NO ERROR.

= 1: OVERRUN. THE ADC COULD NOT KEEP UP WITH THE CLOCK. (IT IS POSSIBLE FOR AN OVERRUN CONDITION TO OCCUR WITHOUT BEING RECOGNIZED BY THIS PROGRAM.)

TIMING:

THE CONVERSION RATE CAN BE AS HIGH AS 16KHZ. (IBASE=1, INTVL=62.)

THE FIRST SAMPLE IS DELAYED AFTER THE TRIGGER BY A PERIOD EQUAL TO THE INTERVAL BETWEEN SAMPLES.

REMARKS:

THE LINE CLOCK IS STOPPED DURING EXECUTION OF THIS ROUTINE. THE SOFTWARE TIME-OF-DAY CLOCK MAY LOSE SOME TIME.

WE CHOSE NOT TO DISABLE ALL INTERRUPTS SO THAT THIS PROGRAM MIGHT BE INTERRUPTED BY A DOUBLE CTRL/C IN THE EVENT THAT IT HANGS WAITING FOR SCHMITT TRIGGER 2. IT IS UP TO THE USER TO ASSURE THAT NIETHER INTERUPTS NOR NPR(DMA) ACTIVITY INTERFERE WITH THIS ROUTINE.

THE PROGRAMMABLE CLOCK IS USED IN A NON-INTERRUPT MODE.

OTHER CLOCK-DRIVEN ROUTINES CANNOT BE ACTIVE AT THE SAME TIME AS

```
    THIS ROUTINE.
  THIS ROUTINE DOES NOT RETURN UNTIL THE DATA ACQUISITION IS
    COMPLETE.
  REGISTERS ARE NOT SAVED.
SUBPROGRAMS: NONE
PROGRAMMER: NELSON
\
;PARAMETER DEFINITIONS.
ADCSR= 170400 ;MNCAD REGISTERS
ADMUX= ADCSR+1
ADDBR= ADCSR+2
KWCSR= 170420 ;MNCKW REGISTERS
KWBPR= KWCSR+2
LCCSR= 177546 ;LINE CLOCK CSR
;
;GET PARAMETERS AND INITIALIZE.
MADC2:: MOV 2(R5),R0 ;R0 -> IDATA
MOV @4(R5),R1 ;R1=NPT
MOV @6(R5),R2 ;R2=ICHAN
BMI 3$
MOV @10(R5),R3 ;R3=LCHAN
MOV R2,R4 ;R4=CHAN
1$: MOV R4,(R0)+ ;SET UP CYCLIC SCAN
INC R4
CMP R3,R4
BGE 2$
MOV R2,R4
2$: SOB R1,1$
MOV 2(R5),R0 ;RESTORE IDATA PTR
MOV @4(R5),R1 ;  AND NPT
3$: DEC R1 ;R1=NPT-1
MOV @12(R5),R2 ;SET KWCSR BITS
ASH #3,R2
```

```
BIS #2,R2
MOV R2,@#KWCSR
MOV @14(R5),R2 ;SET KWBPR
NEG R2
MOV R2,@#KWBPR
MOV #ADCSR,R2 ;R2 -> ADCSR
MOV #ADMUX,R3 ;R3 -> ADMUX
MOV #ADDBR,R4 ;R4 -> ADDBR
MOVB #50,(R2) ;SET ADCSR BITS; SET GAIN=4
TST (R4) ;CLEAR ADCSR DONE BIT
MOVB (R0),(R3) ;SET FIRST ADC CHANNEL
CLR @#LCCSR ;STOP THE LINE CLOCK
;
;START THE DATA ACQUISITION.
CMP #1,@16(R5) ;IF IGO=1,
BNE 4$
INC @#KWCSR ;  START IMMEDIATELY
BR CVT
4$: MOVB #40,@#KWCSR+1 ;ELSE WAIT FOR ST2
;
;CONVERT THE DATA.
;  LOOP TIME = 36.75 + 8.75*K MICROSECONDS, K>=0. (LSI-11/1.)
;  DEAD TIME < 26.95 MICROSECONDS. (TIME BETWEEN END-OF-CONVERSION
; AND SETTING OF NEXT ADC CHANNEL, INCLUDING TWO PASSES THROUGH
; THE TSTB WAIT LOOP AND THE MOVB INSTRUCTION.)
;  MNCAD CONVERSION TIME = 42 MICROSECONDS.
;  FASTEST MEASURED TIME BETWEEN SAMPLES = 62 MICROSECONDS. (INCLUDES
; 42-MICROSECOND CONVERSION TIME AND ONLY ONE PASS THROUGH THE
; TSTB WAIT LOOP.) ANY PERIOD GREATER THAN 61 MICROSECONDS IS
; OKAY. (THAT 8.75-MICROSECOND WAIT LOOP COULD HAVE CAUSED A
; SLIGHTLY HIGHER RATE TO FAIL.)
CVT: TSTB (R2) ;WAIT FOR NEXT SAMPLE
BPL CVT
```

```
MOVB 2(R0),(R3) ;SET NEXT ADC CHANNEL
MOV (R4),(R0) ;GET SAMPLE
SUB #4000,(R0)+ ;SCALE DATA
SOB R1,CVT ;COUNT POINTS
;
;WAIT FOR THE LAST SAMPLE. THIS WAIT IS SPLIT FROM THE PRECEDING LOOP
;  TO AVOID SETTING THE "NEXT" ADC CHANNEL WHEN THERE ARE NONE LEFT.
;  DOING THAT ONE EXTRA MOVB COULD ENABLE AND CAUSE AN MNCAD ERROR
;  INTERRUPT. WE INSIST ON SETTING THE NEXT ADC CHANNEL IMMEDIATELY
;  AFTER THE PREVIOUS "DONE" IN ORDER TO MINIMIZE DEAD TIME. WE WERE
;  NOT ABLE TO INCREASE THROUGHPUT BY MOVING THE SCALING STEP TO A
;  SEPARATE LOOP, SINCE IT IS OVERLAPPED WITH THE ADC CONVERSION.
1$: TSTB (R2) ;WAIT FOR LAST SAMPLE
BPL 1$
MOV (R4),(R0) ;GET SAMPLE
SUB #4000,(R0) ;SCALE DATA
;
;STOP THE DATA ACQUISITION.
CLR @#KWCSR ;STOP THE MNCKW CLOCK
BIS #100,@#LCCSR ;RESTART THE LINE CLOCK
CLR @20(R5) ;IER=0
TST (R2) ;IF OVERRUN (ON NEXT TO LAST SAMPLE),
BPL 2$
INC @20(R5) ;  SET IER=1
2$: CLR (R2) ;CLEAR ADCSR
RETURN ;RETURN FROM MADC2
.END


;*********************************

.TITLE MACD1, MR799B
.IDENT '791025'
```

```
.REM \

PURPOSE: CONVERT MULTIPLE ANALOG SIGNALS TO DIGITAL DATA VIA THE PDP
  ADC & STORE DIGITAL DATA INTERSPERSED WITH ANALOG
** PROGRAM HARDWIRED FOR ONE DIGITAL CHANNEL **
** A/D BOARD GAIN SET TO 4 **

HACKED BY FRED MARTIN AND JOSE RIVERO;   4-22-86

USAGE: CALL MACD1(IDATA,NPT,ICHAN,LCHAN,IBASE,INTVL,IGO,IER)
  IDATA = INTEGER ARRAY TO WHICH THE DATA IS RETURNED. DATA VALUES
RANGE FROM -2048 TO +2048, REPRESENTING VOLTAGES FROM -5.12V
TO +5.12V. (A FACTOR OF 400.) IF ICHAN=-1, IDATA MUST CONTAIN
THE ADC MULTIPLEXER CHANNELS WHEN MADC2 IS CALLED. (SEE ICHAN
BELOW.)
  NPT = TOTAL NUMBER OF DATA POINTS (SAMPLES) TO BE RECORDED IN IDATA.
(2<=NPT<=32767.)
  ICHAN = N (N>=0): INITIAL ADC CHANNEL FOR A CYCLIC SCAN. THE
CHANNELS ARE NUMBERED 0-11. (THE FIRST 8 ARE SINGLE-ENDED.
THE LAST 4 ARE QUASI-DIFFERENTIAL.)
= -1: WHEN ICHAN=-1, THE ADC CHANNEL NUMBER IS READ FROM
IDATA(K) TO DEFINE THE CHANNEL FOR THE SAMPLE TO BE RETURNED
TO IDATA(K), FOR K=1,2,...,NPT. FOR EXAMPLE, THE IDATA ARRAY
MIGHT BE INITIALIZED TO THE PATTERN
8,9,8,10,8,11,8,9,8,10,8,11,...
TO SAMPLE CHANNEL 8 AT FREQUENCY F AND CHANNELS 9, 10, AND 11
AT FREQUENCY F/3 (WITH SAMPLING RATE 2F).
  LCHAN = LAST ADC CHANNEL FOR A CYCLIC SCAN. (LCHAN IS IGNORED WHEN
ICHAN=-1.) WHEN 0<=ICHAN<=LCHAN<=11, THE ADC MULTIPLEXER IS
CYCLED CONTINUOUSLY FROM CHANNEL ICHAN TO CHANNEL LCHAN UNTIL
A TOTAL OF NPT SAMPLES HAVE BEEN RECORDED.
  IBASE = CLOCK FREQUENCY INDEX.
= 1: 1 MHZ.
```

= 2: 100 KHZ.
= 3: 10 KHZ.
= 4: 1 KHZ.
= 5: 100 HZ.
= 6: EXTERNAL.
= 7: LINE FREQUENCY. (60 HZ.)

INTVL = INTERVAL BETWEEN SAMPLES IN CLOCK TICKS AT THE FREQUENCY SELECTED BY IBASE. (32767 MAX.) (EXAMPLE: WITH IBASE=1 AND INTVL=85, A SAMPLE WOULD BE TAKEN EVERY 85 MICROSECONDS.)

IGO = 1: START SAMPLING IMMEDIATELY.
= 2: START WHEN THE CLOCK'S SCHMITT TRIGGER 2 IS FIRED.

IER = ERROR INDICATOR.
= 0: NO ERROR.
= 1: OVERRUN. THE ADC COULD NOT KEEP UP WITH THE CLOCK. (IT IS POSSIBLE FOR AN OVERRUN CONDITION TO OCCUR WITHOUT BEING RECOGNIZED BY THIS PROGRAM.)

TIMING:

THE CONVERSION RATE CAN BE AS HIGH AS 16KHZ. (IBASE=1, INTVL=62.)

THE FIRST SAMPLE IS DELAYED AFTER THE TRIGGER BY A PERIOD EQUAL TO THE INTERVAL BETWEEN SAMPLES.

REMARKS:

THE LINE CLOCK IS STOPPED DURING EXECUTION OF THIS ROUTINE. THE SOFTWARE TIME-OF-DAY CLOCK MAY LOSE SOME TIME.

WE CHOSE NOT TO DISABLE ALL INTERRUPTS SO THAT THIS PROGRAM MIGHT BE INTERRUPTED BY A DOUBLE CTRL/C IN THE EVENT THAT IT HANGS WAITING FOR SCHMITT TRIGGER 2. IT IS UP TO THE USER TO ASSURE THAT NIETHER INTERUPTS NOR NPR(DMA) ACTIVITY INTERFERE WITH THIS ROUTINE.

THE PROGRAMMABLE CLOCK IS USED IN A NON-INTERRUPT MODE.

OTHER CLOCK-DRIVEN ROUTINES CANNOT BE ACTIVE AT THE SAME TIME AS THIS ROUTINE.

THIS ROUTINE DOES NOT RETURN UNTIL THE DATA ACQUISITION IS COMPLETE.

```
  REGISTERS ARE NOT SAVED.
 SUBPROGRAMS: NONE
 PROGRAMMER: NELSON
 \
 ;PARAMETER DEFINITIONS.
 ADCSR= 170400 ;MNCAD REGISTERS
 ADMUX= ADCSR+1
 ADDBR= ADCSR+2
 KWCSR= 170420 ;MNCKW REGISTERS
 KWBPR= KWCSR+2
 LCCSR= 177546 ;LINE CLOCK CSR
 ; DRV-11 ADDRESSES
 DR1CSR= 167720
 DR1OUT= DR1CSR + 2
 DR1IN=  DR1CSR + 4
 ;
 ;GET PARAMETERS AND INITIALIZE.
MACD1:: MOV 2(R5),R0 ;R0 -> IDATA
MOV @4(R5),R1 ;R1=NPT
MOV @6(R5),R2 ;R2=ICHAN
BMI 3$
MOV @10(R5),R3 ;R3=LCHAN
;
; INITIALIZE DRV11 BOARDS
;
MOV #DR1OUT,R4 ;R4 -> DR1 OUTPUT BUFFER
MOV #2,(R4) ;WRITE '000002'
MOV  #1,(R4) ;WRITE '000001' TO INITIALIZE
;
  MOV R2,R4 ;R4=CHAN
1$: MOV R4,(R0)+ ;SET UP CYCLIC SCAN
INC R4
CMP R3,R4
```

```
BGE 2$ ;BRANCH IF CHANNEL SCAN NOT DONE
;
; LOAD DIGITAL ADDRESSES AFTER CHANNEL SCAN
;
MOV  #DR1IN,(R0)+ ;WRITE DRV11 ADDR TO IDATA ARRAY
DEC R1
BEQ 5$ ;EXIT IF FILLED IDATA ARRAY
;
; MOV #DR2IN,(R0)+
; BEQ 5$
; MOV #DR3IN,(R0)+
; BEQ 5$
;
MOV R2,R4 ;RESET CHANNEL SCAN
2$: SOB R1,1$ ;  CONTINUE SCAN
5$: MOV 2(R5),R0 ;RESTORE IDATA PTR
MOV @4(R5),R1 ;  AND NPT
3$: MOV @12(R5),R2 ;SET KWCSR BITS
ASH #3,R2
BIS #2,R2
MOV R2,@#KWCSR
MOV @14(R5),R2 ;SET KWBPR
NEG R2
MOV R2,@#KWBPR
MOV #ADCSR,R2 ;R2 -> ADCSR
MOV #ADMUX,R3 ;R3 -> ADMUX
MOV #ADDBR,R4 ;R4 -> ADDBR
MOVB #50,(R2) ;SET ADCSR BITS, GAIN=4
TST (R4) ;CLEAR ADCSR DONE BIT
MOVB (R0),(R3) ;SET FIRST ADC CHANNEL
CLR @#LCCSR ;STOP THE LINE CLOCK
;
;START THE DATA ACQUISITION.
```

```
  CMP #1,@16(R5) ;IF IGO=1,
BNE 4$
INC @#KWCSR ;  START IMMEDIATELY
BR CVT
4$: MOVB #40,@#KWCSR+1 ;ELSE WAIT FOR ST2
;
;CONVERT THE DATA.
;  LOOP TIME = 36.75 + 8.75*K MICROSECONDS, K>=0. (LSI-11/1.)
;  DEAD TIME < 26.95 MICROSECONDS. (TIME BETWEEN END-OF-CONVERSION
; AND SETTING OF NEXT ADC CHANNEL, INCLUDING TWO PASSES THROUGH
; THE TSTB WAIT LOOP AND THE MOVB INSTRUCTION.)
;  MNCAD CONVERSION TIME = 42 MICROSECONDS.
;  FASTEST MEASURED TIME BETWEEN SAMPLES = 62 MICROSECONDS. (INCLUDES
; 42-MICROSECOND CONVERSION TIME AND ONLY ONE PASS THROUGH THE
; TSTB WAIT LOOP.) ANY PERIOD GREATER THAN 61 MICROSECONDS IS
; OKAY. (THAT 8.75-MICROSECOND WAIT LOOP COULD HAVE CAUSED A
; SLIGHTLY HIGHER RATE TO FAIL.)
;
; **************************
; NPT MUST BE INTEGRAL MULTIPLE OF NUMBER CHANNELS SAMPLED,
; ANALOG + DIGITAL; THUS LAST CHANNEL SAMPLED IS
; THE LAST DIGITAL CHANNEL.
; **************************
;
;
CVT: TSTB (R2) ;WAIT FOR NEXT SAMPLE
BPL CVT
TSTB 3(R0) ;MSB OF NEXT CHANNEL
BEQ 3$ ;IF ZERO, HAVE ANALOG CHANNEL [6$]
MOV  (R4),(R0) ;LOAD LAST ADC CHANNEL
SUB #4000,(R0)+
DEC R1
BEQ DONE
```

```
MOV  @#DR1IN,(R0)+
; BIC #100000,(R0)+ ;CLEAR HIGH BIT
DEC R1
BEQ DONE
;
; MOV @#DR2IN,(R0)+
; DEC  R1
; BEQ DONE
; MOV @#DR3IN,(R0)+
; DEC R1
; BEQ DONE
;
MOVB (R0),(R3) ;SET FOR CURR ADC CHANNEL [5$:]
BR CVT ;ENTER ANALOG WAIT LOOP
;
;
3$: MOVB 2(R0),(R3) ;SET NEXT ADC CHANNEL [6$:]
MOV (R4),(R0) ;GET SAMPLE
SUB #4000,(R0)+ ;SCALE DATA
SOB R1,CVT ;COUNT POINTS
;
;STOP THE DATA ACQUISITION.
DONE: CLR @#KWCSR ;STOP THE MNCKW CLOCK
BIS #100,@#LCCSR ;RESTART THE LINE CLOCK
CLR @20(R5) ;IER=0
TST (R2) ;IF OVERRUN (ON NEXT TO LAST SAMPLE),
BPL 2$
INC @20(R5) ;  SET IER=1
2$: CLR (R2) ;CLEAR ADCSR
RETURN ;RETURN FROM MADC2
.END
```

```
**********************************


.TITLE MACD2, MR799B
.IDENT '791025'
.REM \

PURPOSE: CONVERT MULTIPLE ANALOG SIGNALS TO DIGITAL DATA VIA THE PDP
  ADC & STORE DIGITAL DATA INTERSPERSED WITH ANALOG
** PROGRAM HARDWIRED FOR TWO DIGITAL CHANNELS **
** A/D BOARD GAIN SET TO 4 **

HACKED BY FRED MARTIN AND JOSE RIVERO;   4-22-86

USAGE: CALL MACD2(IDATA,NPT,ICHAN,LCHAN,IBASE,INTVL,IGO,IER)
  IDATA = INTEGER ARRAY TO WHICH THE DATA IS RETURNED. DATA VALUES
RANGE FROM -2048 TO +2048, REPRESENTING VOLTAGES FROM -5.12V
TO +5.12V. (A FACTOR OF 400.) IF ICHAN=-1, IDATA MUST CONTAIN
THE ADC MULTIPLEXER CHANNELS WHEN MADC2 IS CALLED. (SEE ICHAN
BELOW.)
  NPT = TOTAL NUMBER OF DATA POINTS (SAMPLES) TO BE RECORDED IN IDATA.
(2<=NPT<=32767.) * SEE NOTE CONCERNING NPT AT BOTTOM
  ICHAN = N (N>=0): INITIAL ADC CHANNEL FOR A CYCLIC SCAN. THE
CHANNELS ARE NUMBERED 0-11. (THE FIRST 8 ARE SINGLE-ENDED.
THE LAST 4 ARE QUASI-DIFFERENTIAL.)
= -1: WHEN ICHAN=-1, THE ADC CHANNEL NUMBER IS READ FROM
IDATA(K) TO DEFINE THE CHANNEL FOR THE SAMPLE TO BE RETURNED
TO IDATA(K), FOR K=1,2,...,NPT. FOR EXAMPLE, THE IDATA ARRAY
MIGHT BE INITIALIZED TO THE PATTERN
8,9,8,10,8,11,8,9,8,10,8,11,...
TO SAMPLE CHANNEL 8 AT FREQUENCY F AND CHANNELS 9, 10, AND 11
AT FREQUENCY F/3 (WITH SAMPLING RATE 2F).
```

LCHAN = LAST ADC CHANNEL FOR A CYCLIC SCAN. (LCHAN IS IGNORED WHEN ICHAN=-1.) WHEN 0<=ICHAN<=LCHAN<=11, THE ADC MULTIPLEXER IS CYCLED CONTINUOUSLY FROM CHANNEL ICHAN TO CHANNEL LCHAN UNTIL A TOTAL OF NPT SAMPLES HAVE BEEN RECORDED.

IBASE = CLOCK FREQUENCY INDEX.

= 1: 1 MHZ.

= 2: 100 KHZ.

= 3: 10 KHZ.

= 4: 1 KHZ.

= 5: 100 HZ.

= 6: EXTERNAL.

= 7: LINE FREQUENCY. (60 HZ.)

INTVL = INTERVAL BETWEEN SAMPLES IN CLOCK TICKS AT THE FREQUENCY SELECTED BY IBASE. (32767 MAX.) (EXAMPLE: WITH IBASE=1 AND INTVL=85, A SAMPLE WOULD BE TAKEN EVERY 85 MICROSECONDS.)

IGO = 1: START SAMPLING IMMEDIATELY.

= 2: START WHEN THE CLOCK'S SCHMITT TRIGGER 2 IS FIRED.

IER = ERROR INDICATOR.

= 0: NO ERROR.

= 1: OVERRUN. THE ADC COULD NOT KEEP UP WITH THE CLOCK. (IT IS POSSIBLE FOR AN OVERRUN CONDITION TO OCCUR WITHOUT BEING RECOGNIZED BY THIS PROGRAM.)

TIMING:

THE CONVERSION RATE CAN BE AS HIGH AS 16KHZ. (IBASE=1, INTVL=62.)

THE FIRST SAMPLE IS DELAYED AFTER THE TRIGGER BY A PERIOD EQUAL TO THE INTERVAL BETWEEN SAMPLES.

REMARKS:

THE LINE CLOCK IS STOPPED DURING EXECUTION OF THIS ROUTINE. THE SOFTWARE TIME-OF-DAY CLOCK MAY LOSE SOME TIME.

WE CHOSE NOT TO DISABLE ALL INTERRUPTS SO THAT THIS PROGRAM MIGHT BE INTERRUPTED BY A DOUBLE CTRL/C IN THE EVENT THAT IT HANGS WAITING FOR SCHMITT TRIGGER 2. IT IS UP TO THE USER TO ASSURE THAT NIETHER INTERUPTS NOR NPR(DMA) ACTIVITY INTERFERE WITH

```
    THIS ROUTINE.
  THE PROGRAMMABLE CLOCK IS USED IN A NON-INTERRUPT MODE.
  OTHER CLOCK-DRIVEN ROUTINES CANNOT BE ACTIVE AT THE SAME TIME AS
    THIS ROUTINE.
  THIS ROUTINE DOES NOT RETURN UNTIL THE DATA ACQUISITION IS
    COMPLETE.
  REGISTERS ARE NOT SAVED.
SUBPROGRAMS: NONE
PROGRAMMER: NELSON
\
;PARAMETER DEFINITIONS.
ADCSR= 170400 ;MNCAD REGISTERS
ADMUX= ADCSR+1
ADDBR= ADCSR+2
KWCSR= 170420 ;MNCKW REGISTERS
KWBPR= KWCSR+2
LCCSR= 177546 ;LINE CLOCK CSR
; DRV-11 ADDRESSES
DR1CSR= 167720
DR1OUT= DR1CSR + 2
DR1IN=  DR1CSR + 4
;
DR2CSR= 167760
DR2OUT= DR2CSR + 2
DR2IN=  DR2CSR + 4
;
;GET PARAMETERS AND INITIALIZE.
MACD2:: MOV 2(R5),R0 ;R0 -> IDATA
MOV @4(R5),R1 ;R1=NPT
MOV @6(R5),R2 ;R2=ICHAN
BMI 3$
MOV @10(R5),R3 ;R3=LCHAN
;
```

```
; INITIALIZE DRV11 BOARDS
; DRV #1
MOV #DR1OUT,R4 ;R4 -> DR1 OUTPUT BUFFER
MOV #2,(R4) ;WRITE '000002'
MOV  #1,(R4) ;WRITE '000001' TO INITIALIZE
; DRV #2
MOV #DR2OUT,R4
MOV #2,(R4)
MOV  #1,(R4)
;
  MOV R2,R4 ;R4=CHAN
1$: MOV R4,(R0)+ ;SET UP CYCLIC SCAN
INC R4
CMP R3,R4
BGE 2$ ;BRANCH IF CHANNEL SCAN NOT DONE
;
; LOAD DIGITAL ADDRESSES AFTER ANALOG CHANNEL SCAN
;
MOV  #DR1IN,(R0)+ ;WRITE DRV11 ADDR TO IDATA ARRAY
DEC R1
BEQ 5$ ;EXIT IF FILLED IDATA ARRAY
MOV #DR2IN,(R0)+
DEC  R1
BEQ 5$
;
; MOV #DR3IN,(R0)+
; DEC  R1
; BEQ 5$
;
MOV R2,R4 ;RESET CHANNEL SCAN
2$: SOB R1,1$ ;  CONTINUE SCAN
5$: MOV 2(R5),R0 ;RESTORE IDATA PTR
MOV @4(R5),R1 ;  AND NPT
```

```
3$: MOV @12(R5),R2 ;SET KWCSR BITS
ASH #3,R2
BIS #2,R2
MOV R2,@#KWCSR
MOV @14(R5),R2 ;SET KWBPR
NEG R2
MOV R2,@#KWBPR
MOV #ADCSR,R2 ;R2 -> ADCSR
MOV #ADMUX,R3 ;R3 -> ADMUX
MOV #ADDBR,R4 ;R4 -> ADDBR
MOVB #50,(R2) ;SET ADCSR BITS, *GAIN=4*
TST (R4) ;CLEAR ADCSR DONE BIT
MOVB (R0),(R3) ;SET FIRST ADC CHANNEL
CLR @#LCCSR ;STOP THE LINE CLOCK
;
;START THE DATA ACQUISITION.
  CMP #1,@16(R5) ;IF IGO=1,
BNE 4$
INC @#KWCSR ;  START IMMEDIATELY
BR CVT
4$: MOVB #40,@#KWCSR+1 ;ELSE WAIT FOR ST2
;
;CONVERT THE DATA.
;  LOOP TIME = 36.75 + 8.75*K MICROSECONDS, K>=0. (LSI-11/1.)
;  DEAD TIME < 26.95 MICROSECONDS. (TIME BETWEEN END-OF-CONVERSION
; AND SETTING OF NEXT ADC CHANNEL, INCLUDING TWO PASSES THROUGH
; THE TSTB WAIT LOOP AND THE MOVB INSTRUCTION.)
;  MINCAD CONVERSION TIME = 42 MICROSECONDS.
;  FASTEST MEASURED TIME BETWEEN SAMPLES = 62 MICROSECONDS. (INCLUDES
; 42-MICROSECOND CONVERSION TIME AND ONLY ONE PASS THROUGH THE
; TSTB WAIT LOOP.) ANY PERIOD GREATER THAN 61 MICROSECONDS IS
; OKAY. (THAT 8.75-MICROSECOND WAIT LOOP COULD HAVE CAUSED A
; SLIGHTLY HIGHER RATE TO FAIL.)
```

```
;
; ***************************
; NPT MUST BE INTEGRAL MULTIPLE OF NUMBER CHANNELS SAMPLED,
; ANALOG + DIGITAL; THUS LAST CHANNEL SAMPLED IS
; THE LAST DIGITAL CHANNEL.
; ***************************
;
;
CVT: TSTB (R2) ;WAIT FOR NEXT SAMPLE
BPL CVT
TSTB 3(RO) ;MSB OF NEXT CHANNEL
BEQ 3$ ;IF ZERO, HAVE ANALOG CHANNEL [6$]
MOV  (R4),(RO) ;LOAD LAST ADC CHANNEL
SUB #4000,(RO)+
DEC R1
BEQ DONE
MOV  @#DR1IN,(RO)+
DEC R1
BEQ DONE
MOV @#DR2IN,(RO)+
DEC  R1
BEQ DONE
;
; MOV @#DR3IN,(RO)+
; DEC R1
; BEQ DONE
;
MOVB (RO),(R3) ;SET FOR CURR ADC CHANNEL [5$:]
BR CVT ;ENTER ANALOG WAIT LOOP
;
;
3$: MOVB 2(RO),(R3) ;SET NEXT ADC CHANNEL [6$:]
MOV (R4),(RO) ;GET SAMPLE
```

```
SUB #4000,(R0)+ ;SCALE DATA
SOB R1,CVT ;COUNT POINTS
;
;STOP THE DATA ACQUISITION.
DONE: CLR @#KWCSR ;STOP THE MNCKW CLOCK
BIS #100,@#LCCSR ;RESTART THE LINE CLOCK
CLR @20(R5) ;IER=0
TST (R2) ;IF OVERRUN (ON NEXT TO LAST SAMPLE),
BPL 2$
INC @20(R5) ;  SET IER=1
2$: CLR (R2) ;CLEAR ADCSR
RETURN ;RETURN FROM MADC2
.END
```

****

```
.TITLE MACD3, MR799B
.IDENT '791025'
.REM \

PURPOSE: CONVERT MULTIPLE ANALOG SIGNALS TO DIGITAL DATA VIA THE PDP
  ADC & STORE DIGITAL DATA INTERSPERSED WITH ANALOG
** PROGRAM HARDWIRED FOR THREE DIGITAL CHANNELS **
** A/D BOARD GAIN SET TO 4 **

HACKED BY FRED MARTIN AND JOSE RIVERO;   4-22-86

USAGE: CALL MACD3(IDATA,NPT,ICHAN,LCHAN,IBASE,INTVL,IGO,IER)
  IDATA = INTEGER ARRAY TO WHICH THE DATA IS RETURNED. DATA VALUES
RANGE FROM -2048 TO +2048, REPRESENTING VOLTAGES FROM -5.12V
TO +5.12V. (A FACTOR OF 400.) IF ICHAN=-1, IDATA MUST CONTAIN
```

THE ADC MULTIPLEXER CHANNELS WHEN MADC2 IS CALLED. (SEE ICHAN BELOW.)

NPT = TOTAL NUMBER OF DATA POINTS (SAMPLES) TO BE RECORDED IN IDATA. (2<=NPT<=32767.) * SEE NOTE CONCERNING NPT AT BOTTOM

ICHAN = N (N>=0): INITIAL ADC CHANNEL FOR A CYCLIC SCAN. THE CHANNELS ARE NUMBERED 0-11. (THE FIRST 8 ARE SINGLE-ENDED. THE LAST 4 ARE QUASI-DIFFERENTIAL.)

= -1: WHEN ICHAN=-1, THE ADC CHANNEL NUMBER IS READ FROM IDATA(K) TO DEFINE THE CHANNEL FOR THE SAMPLE TO BE RETURNED TO IDATA(K), FOR K=1,2,...,NPT. FOR EXAMPLE, THE IDATA ARRAY MIGHT BE INITIALIZED TO THE PATTERN

8,9,8,10,8,11,8,9,8,10,8,11,...

TO SAMPLE CHANNEL 8 AT FREQUENCY F AND CHANNELS 9, 10, AND 11 AT FREQUENCY F/3 (WITH SAMPLING RATE 2F).

LCHAN = LAST ADC CHANNEL FOR A CYCLIC SCAN. (LCHAN IS IGNORED WHEN ICHAN=-1.) WHEN 0<=ICHAN<=LCHAN<=11, THE ADC MULTIPLEXER IS CYCLED CONTINUOUSLY FROM CHANNEL ICHAN TO CHANNEL LCHAN UNTIL A TOTAL OF NPT SAMPLES HAVE BEEN RECORDED.

IBASE = CLOCK FREQUENCY INDEX.

= 1: 1 MHZ.

= 2: 100 KHZ.

= 3: 10 KHZ.

= 4: 1 KHZ.

= 5: 100 HZ.

= 6: EXTERNAL.

= 7: LINE FREQUENCY. (60 HZ.)

INTVL = INTERVAL BETWEEN SAMPLES IN CLOCK TICKS AT THE FREQUENCY SELECTED BY IBASE. (32767 MAX.) (EXAMPLE: WITH IBASE=1 AND INTVL=85, A SAMPLE WOULD BE TAKEN EVERY 85 MICROSECONDS.)

IGO = 1: START SAMPLING IMMEDIATELY.

= 2: START WHEN THE CLOCK'S SCHMITT TRIGGER 2 IS FIRED.

IER = ERROR INDICATOR.

= 0: NO ERROR.

```
      = 1: OVERRUN. THE ADC COULD NOT KEEP UP WITH THE CLOCK. (IT IS
POSSIBLE FOR AN OVERRUN CONDITION TO OCCUR WITHOUT BEING
RECOGNIZED BY THIS PROGRAM.)
TIMING:
  THE CONVERSION RATE CAN BE AS HIGH AS 16KHZ. (IBASE=1, INTVL=62.)
  THE FIRST SAMPLE IS DELAYED AFTER THE TRIGGER BY A PERIOD EQUAL TO
    THE INTERVAL BETWEEN SAMPLES.
REMARKS:
  THE LINE CLOCK IS STOPPED DURING EXECUTION OF THIS ROUTINE. THE
    SOFTWARE TIME-OF-DAY CLOCK MAY LOSE SOME TIME.
  WE CHOSE NOT TO DISABLE ALL INTERRUPTS SO THAT THIS PROGRAM MIGHT
    BE INTERRUPTED BY A DOUBLE CTRL/C IN THE EVENT THAT IT HANGS
    WAITING FOR SCHMITT TRIGGER 2.  IT IS UP TO THE USER TO ASSURE
    THAT NIETHER INTERUPTS NOR NPR(DMA) ACTIVITY INTERFERE WITH
    THIS ROUTINE.
  THE PROGRAMMABLE CLOCK IS USED IN A NON-INTERRUPT MODE.
  OTHER CLOCK-DRIVEN ROUTINES CANNOT BE ACTIVE AT THE SAME TIME AS
    THIS ROUTINE.
  THIS ROUTINE DOES NOT RETURN UNTIL THE DATA ACQUISITION IS
    COMPLETE.
  REGISTERS ARE NOT SAVED.
SUBPROGRAMS: NONE
PROGRAMMER: NELSON
\
;PARAMETER DEFINITIONS.
ADCSR= 170400 ;MNCAD REGISTERS
ADMUX= ADCSR+1
ADDBR= ADCSR+2
KWCSR= 170420 ;MNCKW REGISTERS
KWBPR= KWCSR+2
LCCSR= 177546 ;LINE CLOCK CSR
; DRV-11 ADDRESSES
DR1CSR= 167720
```

```
DR1OUT= DR1CSR + 2
DR1IN=  DR1CSR + 4
;
DR2CSR= 167760
DR2OUT= DR2CSR + 2
DR2IN=  DR2CSR + 4
;
DR3CSR= 167750
DR3OUT= DR3CSR + 2
DR3IN=  DR3CSR + 4
;
;GET PARAMETERS AND INITIALIZE.
MACD3:: MOV 2(R5),R0 ;R0 -> IDATA
MOV @4(R5),R1 ;R1=NPT
MOV @6(R5),R2 ;R2=ICHAN
BMI 3$
MOV @10(R5),R3 ;R3=LCHAN
;
; INITIALIZE DRV11 BOARDS
; DRV #1
MOV #DR1OUT,R4 ;R4 -> DR1 OUTPUT BUFFER
MOV #2,(R4) ;WRITE '000002'
MOV  #1,(R4) ;WRITE '000001' TO INITIALIZE
; DRV #2
MOV #DR2OUT,R4
MOV #2,(R4)
MOV  #1,(R4)
;DRV #3
MOV  #DR3OUT,R4
MOV  #2,(R4)
MOV #1,(R4)
;
  MOV R2,R4 ;R4=CHAN
```

```
1$: MOV R4,(RO)+ ;SET UP CYCLIC SCAN
INC R4
CMP R3,R4
BGE 2$ ;BRANCH IF CHANNEL SCAN NOT DONE

;
; LOAD DIGITAL ADDRESSES AFTER ANALOG CHANNEL SCAN
;
MOV  #DR1IN,(RO)+ ;WRITE DRV11 ADDR TO IDATA ARRAY
DEC R1
BEQ 5$ ;EXIT IF FILLED IDATA ARRAY
MOV #DR2IN,(RO)+
DEC  R1
BEQ 5$
MOV #DR3IN,(RO)+
DEC  R1
BEQ 5$
;
MOV R2,R4 ;RESET CHANNEL SCAN
2$: SOB R1,1$ ;  CONTINUE SCAN
5$: MOV 2(R5),RO ;RESTORE IDATA PTR
MOV @4(R5),R1 ;  AND NPT
3$: MOV @12(R5),R2 ;SET KWCSR BITS
ASH #3,R2
BIS #2,R2
MOV R2,@#KWCSR
MOV @14(R5),R2 ;SET KWBPR
NEG R2
MOV R2,@#KWBPR
MOV #ADCSR,R2 ;R2 -> ADCSR
MOV #ADMUX,R3 ;R3 -> ADMUX
MOV #ADDBR,R4 ;R4 -> ADDBR
MOVB #50,(R2) ;SET ADCSR BITS, *GAIN=4*
TST (R4) ;CLEAR ADCSR DONE BIT
```

```
MOVB (R0),(R3) ;SET FIRST ADC CHANNEL
CLR @#LCCSR ;STOP THE LINE CLOCK
;
;START THE DATA ACQUISITION.
  CMP #1,@16(R5) ;IF IGO=1,
BNE 4$
INC @#KWCSR ;  START IMMEDIATELY
BR CVT
4$: MOVB #40,@#KWCSR+1 ;ELSE WAIT FOR ST2
;
;CONVERT THE DATA.
;  LOOP TIME = 36.75 + 8.75*K MICROSECONDS, K>=0. (LSI-11/1.)
;  DEAD TIME < 26.95 MICROSECONDS. (TIME BETWEEN END-OF-CONVERSION
; AND SETTING OF NEXT ADC CHANNEL, INCLUDING TWO PASSES THROUGH
; THE TSTB WAIT LOOP AND THE MOVB INSTRUCTION.)
;  MNCAD CONVERSION TIME = 42 MICROSECONDS.
;  FASTEST MEASURED TIME BETWEEN SAMPLES = 62 MICROSECONDS. (INCLUDES
; 42-MICROSECOND CONVERSION TIME AND ONLY ONE PASS THROUGH THE
; TSTB WAIT LOOP.) ANY PERIOD GREATER THAN 61 MICROSECONDS IS
; OKAY. (THAT 8.75-MICROSECOND WAIT LOOP COULD HAVE CAUSED A
; SLIGHTLY HIGHER RATE TO FAIL.)
;
; **************************
; NPT MUST BE INTEGRAL MULTIPLE OF NUMBER CHANNELS SAMPLED,
; ANALOG + DIGITAL; THUS LAST CHANNEL SAMPLED IS
; THE LAST DIGITAL CHANNEL.
; **************************
;
;
CVT: TSTB (R2) ;WAIT FOR NEXT SAMPLE
BPL CVT
TSTB 3(R0) ;MSB OF NEXT CHANNEL
BEQ 3$ ;IF ZERO, HAVE ANALOG CHANNEL [6$]
```

```
MOV  (R4),(RO) ;LOAD LAST ADC CHANNEL
SUB #4000,(RO)+
DEC R1
BEQ DONE
MOV  @#DR1IN,(RO)+
DEC R1
BEQ DONE
MOV @#DR2IN,(RO)+
DEC  R1
BEQ DONE
MOV @#DR3IN,(RO)+
DEC R1
BEQ DONE
;
MOVB (RO),(R3) ;SET FOR CURR ADC CHANNEL [5$:]
BR CVT ;ENTER ANALOG WAIT LOOP
;
;
3$: MOVB 2(RO),(R3) ;SET NEXT ADC CHANNEL [6$:]
MOV (R4),(RO) ;GET SAMPLE
SUB #4000,(RO)+ ;SCALE DATA
SOB R1,CVT ;COUNT POINTS
;
;STOP THE DATA ACQUISITION.
DONE: CLR @#KWCSR ;STOP THE MNCKW CLOCK
BIS #100,@#LCCSR ;RESTART THE LINE CLOCK
CLR @20(R5) ;IER=0
TST (R2) ;IF OVERRUN (ON NEXT TO LAST SAMPLE),
BPL 2$
INC @20(R5) ;  SET IER=1
2$: CLR (R2) ;CLEAR ADCSR
RETURN ;RETURN FROM MADC2
.END
```

```
**********************************

      PROGRAM SCALE

C
C   Program to scale data files.
C
C   Written by Jose A. Rivero, April 1986, for the Parts Mating
C   Machine Data Acquisition System
C

CHARACTER INAME*20,ONAME*20

WRITE(6,10)
10 FORMAT(/' Welcome to program SCALE '//
     1 ' Program is currently set up for an input file of 7
     2 columns where:'//
     3 '    Column 1 = insertion LVDT'/
     4 '           2 = strain gage output'/
     5 '           3 = y LVDT'/
     6 '           4 = x LVDT'/
     7 '           5 = y-encoder '/
     8 '           6 = z-encoder '/
     9 '           7 = x-encoder '//)

      WRITE (6,100)
100 FORMAT (/' INPUT SCALING FACTOR FOR INSERTION LENGTH (IN/COUNT):',$)
READ (5,*) FCHO

WRITE (6,110)
```

```
110 FORMAT (/' INPUT SCALING FACTOR FOR STRAIN GAGE (LB/COUNT):',$)
READ (5,*) FGAGE

WRITE (6,120)
120 FORMAT (/' INPUT SCALING FACTOR FOR X (AD-CH2) LVDT (IN/COUNT):',$)
READ (5,*) FLVX

WRITE (6,125)
125 FORMAT (/' INPUT SCALING FACTOR FOR Y (AD-CH3) LVDT (IN/COUNT):',$)
READ (5,*) FLVY

WRITE (6,130)
130 FORMAT (/' INPUT SCALING FACTOR FOR PHI AXIS (LB-IN/COUNT):',$)
READ (5,*) FPHI

WRITE (6,133)
133 FORMAT (/' INPUT SCALING FACTOR FOR GAMMA AXIS (LB-IN/COUNT):',$)
READ (5,*) FGAMMA

WRITE (6,136)
136 FORMAT (/' INPUT SCALING FACTOR FOR THETA AXIS (LB-IN/COUNT):',$)
READ (5,*) FTHETA

WRITE (6,140)
140 FORMAT (//' TYPE INPUT FILENAME:',$)
READ (5,210) INAME
210 FORMAT(20A)

WRITE (6,150)
150 FORMAT (//' TYPE OUTPUT FILENAME:',$)
READ (5,210) ONAME

WRITE (6,160)
```

```
160 FORMAT (//' Enter desired number of points for zeroing:',$)
READ (5,*) N

OPEN(UNIT=3,NAME=INAME,STATUS='OLD')
OPEN(UNIT=4,NAME=ONAME,STATUS='NEW')

SUMO=0
SUMG=0
SUMX=0
SUMY=0

DO 200 I=1,N
READ(3,*) CHO,GAGE,VX,VY,PHI,GAMMA,THETA
SUMO=SUMO+CHO
SUMG=SUMG+GAGE
SUMX=SUMX+VX
SUMY=SUMY+VY
200 CONTINUE

CHOZ=SUMO/N
GAGEZ=SUMG/N
XZ=SUMX/N
YZ=SUMY/N

WRITE(6,250) CHOZ
250 FORMAT(' Averaged Zero Values: '/'    Z: ',F15.5)
WRITE(6,260) GAGEZ,XZ,YZ
260 FORMAT(' gage: ',F15.5,/'    X: ',F15.5,/'    Y: ',F15.5)

300     READ (3,*,END=400) CHO,GAGE,VX,VY,PHI,GAMMA,THETA
SCHO=FCHO*(CHO-CHOZ)
        SGAGE=FGAGE*(GAGEZ-GAGE)
SLVX=FLVX*(VX-XZ)
```

```
SLVY=FLVY*(VY-YZ)
IF (PHI.GT.30000) PHI=-(32768-PHI)
SPHI=PHI*FPHI
IF (GAMMA.GT.30000) GAMMA=-(32768-GAMMA)
SGAMMA=GAMMA*FGAMMA
IF (THETA.GT.30000) THETA=-(32768-THETA)
STHETA=THETA*FTHETA
WRITE (4,500) SCHO,SGAGE,SLVX,SLVY,SPHI,SGAMMA,STHETA
GOTO 300

400 CONTINUE
500 FORMAT(1X,F10.5,',',F10.5,',',F10.5,',',F10.5,',',F10.5,',',
     1 F10.5,',',F10.5)

WRITE(6,600)
600 FORMAT(///' ***** SCALING DONE *****'//' Have a good one...'//)

STOP
END


**********************************
```

References

1. **Arai, T., and Kinoshita, N.**

   "The Part Mating Forces that Arise When Using a Worktable with Compliance". Assembly Automation. Vol. 1. No. 4. Aug. 1981.

2. **Baumister, T., Avallone, E.A., Baumister, T. (eds)**

   "Marks' Standard Handbook for Mechanical Engineers". McGraw-Hill. New York. 1978.

3. **Caine, Michael E.**

   "Chamferless Assembly of Rectangular Parts in Two and Three Dimensions". S.M. Thesis. Department of Mechanical Engineering. MIT. Jan. 1985.

4. **Chambers, J.M., Cleveland, W.S., Kleiner, B., and Tukey, P.A.**

   "Graphical Methods for Data Analysis". Duxbury Press. 1983.

5. **Charles Stark Draper Laboratory**

   "Proceedings 3rd Seminar on Assembly Automation". Nov. 1982.

6. **Charles Stark Draper Laboratory**

"Exploratory Research in Industrial Modular Assembly". Sixth Report. #R-1218. August 1978.

7. **Drake, S. H.**

"Using Compliance in Lieu of Sensory Feedback for Automatic Assembly". PhD Thesis. Department of Mechanical Engineering. MIT. Sept. 1977.

8. **Gordon, S.J., and Seering, W.P.**

"Programmable Tools for Flexible Assembly Systems". Porceedings ASME Computers in Engineering. Boston. MA. August 1985.

9. **Gustavson, R. E.**

"A Theory for the Three Dimensional Mating of Chamfered Cylindrical Parts". Journal of Mechanisms. Transmissions. and Automated Design. December. 1984.

10. **Hennesey, Michael P.**

"Compliant Part Mating and Minimum Energy Chamfer Design". M.S. Thesis. Department of Mechanical Engineering. MIT. June 1982.

11. **Ho, C. S., and Boothroyd, G.**

"Design of Chamfers for Ease of Assembly". Proceedings NAMRC-7 Conference. 1979.

12. **LCS Mathlab Group**

"Macsyma Reference Manual". Version 10. Laboratory ofr Computer Science. Masachusetts Institute of Technology. 1983.

13. **Ohwovoriole, M.S., Hill, J.W., and Roth, B.**

"On the Theory of Single and Multiple Insertions in Industrial assemblies". Proceedings 10th International Symposium on Industrial Robots. Milan, Italy. March 1980.

14. **Ohwovoriole, M. S., and Roth, B.**

"A Theory of Parts Mating for Assembly Automation". Proceedings of the Robot and Man Symposium 81. Warsaw. Poland. Sept. 1981.

15. **Rivero, José A., and Seering, Warren P.**

"An Empirical Study of Compliant Assembly in Three Dimensions". Submitted to the ASME Design Automation Conference. Boston. September. 1987.

16. **Simunovic, Sergio N.**

"An Information Approach to Parts Mating". PhD Thesis. Department of Mechanical Engineering. MIT. April 1979.

17. **Simunovic, Sergio N.**

"Parts Mating Theory for Robot Assembly". 9^{th} International Symposium on Industrial Robots. Washington D.C.. March 1979.

18. **Ulrich, K., Rifai, M., and Potter, S.**

"Five Degree-of-Freddom Compliant Parts Mating Machine". MIT Artificial Intelligence Laboratory. May 1985.

19. **Whithey, D.E., and Nevins, J.L.**

"What is the RCC and What Can It Do?". 9^{th} International Symposium on Industrial Robots. 1979.

20. **Whitney, D.E.**

"Quasi-Static Assembly of Compliantly Supported Rigid Parts". Journal of Dynamic Systems, Measurement, and Control. Vol. 104. March 1982.

21. **Whitney D.E., Hennesey M.P., and Gustavson R.E.**

"Designing Chamfers". The International Journal of Robotics Research. Vol. 2. No. 4. Winter 1983.